Upscaling of Coupled Models with Topography-Driven Surface-Water/Groundwater Interactions

by

Andrew P. Snowdon

A thesis
presented to the University of Waterloo
in fulfillment of the
thesis requirement for the degree of
Doctor of Philosophy
in
Civil Engineering

Waterloo, Ontario, Canada, 2015

I hereby declare that I am the sole author of this thesis. This is a true copy of the thesis, including any required final revisions, as accepted by my examiners.

I understand that my thesis may be made electronically available to the public.

Abstract

Since the 1950s, groundwater and surface water models have evolved to better represent complex hydrological and hydrogeological systems. Part of this evolution has been the coupling of surface and subsurface models to properly simulate the transfer of mass between the two systems. While generally robust for simulating phenomena at smaller scales, existing coupled and fully-integrated models are problematic for larger-scale operational use. Fine-scale models are often computationally prohibitive due to the vast amounts of computational data required and because surface and subsurface models are often not discretized the same spatially. Conversely, faster coarse-scale models incorrectly simulate groundwater-surface water exchange fluxes because they neglect the details of subgrid water exchange. The primary goal of this thesis is to develop and test a regional-scale coupled model that may be used in an operational context. The model has two unique features: (1) it uses a novel upscaling formulation for handling groundwater/surface water exchange fluxes and (2) it can operate using unstructured grids (e.g., surface water basin boundaries) as the basic level of discretization for surface water and groundwater systems. The proposed upscaling approach is developed using fine-resolution topography-driven groundwater flow models to generate relationships between vertical water fluxes and average groundwater head. The relationships are used, in coarse-scale models, to represent groundwater-surface water exchange fluxes. These are then implemented in a new groundwater model that is coupled with the surface water model Raven. Comparisons with Modflow and HydroGeosphere are conducted to determine the effectiveness of this new approach.

Acknowledgements

First, I would like to thank my supervisor, James R. Craig. This has been one of the hardest experiences of my life. I will always appreciate your dedication to your craft and students. You have pushed me beyond where I thought I would go and have always made the journey worth it. Thank you.

This research was supported, in part, by the Ontario Graduate Scholarship and the NSERC Industrial Postgraduate Scholarship program. Without that funding, this project would not have been completed.

Thank you to the exceptional professors I've had the fortune to work with in the classroom, on research, and in the Water Institute. They have always encouraged me, challenged me and been excited to share their knowledge with me. In particular I would like to thank Bryan Tolson, Jon Sykes, Dave Rudolph, and Bruce MacVicar. You have all contributed to my experiences and helped me succeed.

To my current and former fellow grads, thank you for being the wonderful supportive people that you are. You have all been sounding boards, shared the pain and made me laugh (a necessity for grad work). Thank you Ben, Pete, Mike, Lorenzo, Richard, and Vicki. Big thanks go out to Nicole for all the collaboration and good times, Vanessa for all the edits and zen time, and Sanders for always having time to solve an equation.

Most importantly, I want to thank my family. Without you, I wouldn't be who I am or becoming who I want to be. Thank you Victoria, Rick, Breanne and Eamon. You always remind me to keep fun in my life.

Lastly, I would to thank my friends who have helped me de-stress, unwind and generally forget about my research (even if it is only for a short time). There are too many of you to list individually, so I will just say thank you to you all!

Dedication

This is dedicated to my mom and dad.

Table of Contents

List of Tables

List of Figures

Chapter 1

Introduction

Some material covered in this chapter is from Snowdon and Craig (2015)

1.1 Motivation

Surface water (SW) hydrology problems involving significant groundwater-surface water (GW-SW) interactions at regional to mega-regional scales (e.g., models of the Laurentian Great Lakes watershed) are difficult to solve with existing hydrological models. These systems generally require the use of high resolution models that are computationally cumbersome due to the large number of parameters needed and the large amounts of physical data necessary to represent the environment (Singh and Woolhiser, 2002). While fine discretization of the model domain may be considered the best way to achieve high spatial accuracy, it is often desirable to understand a problem at the regional scale where fine resolution is infeasible. This poses a problem for many surface water models with significant groundwater contributions since most regional scale surface water models and land surface schemes effectively ignore groundwater (GW) dynamics even in systems where it plays a significant role. For example, the use of simple linear baseflow models is widespread in land surface schemes (LSS) for climate models.

As stated by Loague et al. (2006), many integrated model issues arise from the ability or inability to characterize the boundary value problem and from the extensive information/ data that is required to define the conditions for simulation. This is a limitation of both fully integrated models and of groundwater models with significant treatment of surface water exchange. When used at coarse resolutions, both types of models suffer

from scaling artifacts - an inability to parameterize effective system properties or identify proper relationships to characterize exchange fluxes at the scale of interest. Fine-resolution models of GW-SW exchanges can be difficult to run and calibrate due to computational burden and/or data constraints. In contrast, these scaling issues ensure that naïvely upscaled low resolution models are unable to include the effects of important fine-resolution subgrid details, even if they are much easier to calibrate or apply at the regional scale. The selection of a model and identification of proper model resolution are therefore common issues. Many models sacrifice speed for accuracy by using high resolution discretization (Vermeulen et al., 2006). This ensures that the fine-scale details of a system are represented in a simulation; in addition, the physics of groundwater (GW) flow and surface exchanges are well-characterized at the point scale (Barthel, 2014). However, due to time constraints, computational restrictions and data limitations, it is very common to model hydrological systems at a coarser resolution (e.g., at the watershed or subbasin scale). These models have reduced computational burden when compared to high resolution models. In addition, they typically have fewer parameters and are easier to calibrate. Unfortunately, the validity of physical laws (e.g., Richard's equation, Darcy's equation) derived at the representative elementary area or volume (REA or REV) scale fall apart when the averaging volume is large enough (Wood et al., 1992; Wood, 1995; Blöschl and Sivapalan, 1995). Efforts to rigorously upscale hydrological models to function, at large scales, from first principles (Kavvas et al., 1998, 2013; Kure et al., 2013), has proven a challenging problem (Barthel, 2014). Often, by presuming statistical homogeneity, the upscaled model may insufficiently incorporate all small scale details or fail to properly represent the impact of specific variations in terrain.

Coarse discretization simulations which manage to successfully represent the influence of the subgrid terrain and surface water features would be an advancement for hydrological modelling (Mohanty and Mousli, 2000). Currently, most coarse-resolution models are unable to represent more than a single water feature (e.g., a river channel) within a cell and therefore many details (e.g. wetlands) may be lost at coarse resolutions, resulting in simulations which are poor representations of the actual problem physics (Vermeulen et al., 2006).

The lack of fast and accurate regional scale models that can properly simulate groundwater dynamics is a limitation in hydrology and there is a need to develop models which can appropriately simulate regional scales in more effective ways. The goal of this research is to develop a computationally efficient regional to mega-regional scale basin-discretized coupled groundwater-surface water model that is practical for risk analysis, sensitivity analysis and uncertainty analysis while at the same time properly accounting for groundwater-surface water exchange.

1.2 Research Overview

This research is divided into 4 main objectives:

1. To examine and characterize relationships between terrain physiography and fluxes across the land surface and develop useful relationships between topographic characteristics, upscaled groundwater head, and exchange fluxes (e.g., evaporation, baseflow, and recharge) at multiple scales.

2. To develop, implement and test a novel upscaling method for simulating topography-driven groundwater-surface water-atmospheric exchange fluxes at relatively coarse resolutions.

3. To determine when the upscaling method and the developed relationships can be applied, answering valuable questions about the necessity of fine-resolution models for specific locations/terrain types and whether groundwater-surface water interactions for specific terrains behave in a predictable manner.

4. To develop and test a specialized catchment-discretized finite volume groundwater model that is directly coupled with the basin-scale surface water model, Raven. This novel approach makes use of matching discretization schemes for both the groundwater and surface water systems promoting simplified communication between the groundwater and surface water systems, creating an efficient and accurate upscaled coupled model.

These objectives are expounded upon below:

1.2.1 Objective 1 - Characterize relationships between terrain & groundwater-surface water fluxes

To examine and characterize the relationships between terrain physiography and fluxes across the land surface and develop useful relationships between topography characteristics, upscaled groundwater head, and exchange fluxes (e.g., evaporation, baseflow, and recharge) at multiple scales.

Tetzlaff et al. (2008) have stated that it is necessary to understand how and why a watershed functions in order to be able to properly conceptualize it at large scales. This

suggests that before it is possible to coarsely discretize a model, it is necessary to characterize the entire modelled system including how connections between GW-SW exchange fluxes (ET, baseflow, recharge) and basin-averaged heads are affected as the topography, soil and land cover vary.

When considering a new method for upscaling, care needs to be taken to represent subgrid details (in this case, subgrid topography and/or multiple surface water features). Subgrid topography is considered here as the primary cause of subgrid effects in coarse models of GW-SW exchange. However, despite its importance, few studies have been completed to determine the influences of terrain on water table shape and groundwater-surface water exchange processes (Jencso and McGlynn, 2011). Extensive research into these influences is necessary both to better understand them and to support more accurate upscaled modelling.

It is assumed here that relationships that characterize the relationship between spatially-averaged heads and spatially-averaged exchange flux rates for specific terrains may be identified or presumed under some conditions. These relationships are here referred to as upscaled flux relationships (UFRs), and are presumed to be both terrain- and land-use dependent. Application of the UFRs (rather than their point-scale equivalents) at coarse resolution is intended to circumvent the need for fine resolution models when simulating at regional or mega-regional scales (Saleh et al., 2011).

UFRs are relationships that can be used to estimate averaged exchange fluxes based upon the average head in a location. However, before an UFR can be determined, it is necessary to understand how terrain affects the groundwater-surface water connection at various scales and from this, understand both how the water table responds to spatially distributed exchange fluxes and how these fluxes relate to water table shape. With this information and details about the terrain being examined, the empirical relationships or UFRs may be developed that describe groundwater-surface water interactions. These UFRs may then be used in upscaled models (in support of objective 2) to represent averaged exchange fluxes based upon a given averaged head value.

1.2.2 Objective 2 - Make and test a novel upscaling approach

To develop, implement and test a novel upscaling method for simulating topography-driven groundwater-surface water-atmospheric exchange fluxes at relatively coarse grid mesh resolutions.

As noted by Jana and Mohanty (2012a), there is need for new upscaling methods that enable the use of coarse resolution modeling while still incorporating key information

relating to topography and soils. As scales increase, it is common for bulk parameter values to be applied, decreasing the effective heterogeneity of the simulated area. This reduction in variability limits the ability of coarse resolution models to properly represent the physical processes occurring at a location, because the relationships between state variables and fluxes can change with scale. For example, many coarsely resolved conjunctive models are actually fine-resolution models being operated at a coarse scale and they cannot therefore be used reliably for coarse resolution simulations (Beven, 2013).

Unfortunately, many models sacrifice speed for accuracy by using high resolution discretization (Vermeulen et al., 2006). While this ensures that all the details of the environment (e.g., hydraulic conductivity distributions, surface water features, topographic details) can be represented in the simulation (provided they can be characterized), these high resolution models are often over-parameterized making them a challenge to use for meaningful analyses (e.g., uncertainty analysis). Therefore, it is desirable to simulate problems using a coarse discretization while managing to represent the diversity of the landscape and surface water features within a low resolution discretization (Mohanty and Mousli, 2000). Since most upscaled or low resolution models are unable to represent more than a single water feature (e.g., a river channel) within a cell, many details (e.g. wetlands) are lost at coarse resolutions resulting in the simulation being a poor representation of the actual problem physics (Vermeulen et al., 2006).

An upscaling method for topography-driven flow which is based upon the characterization of the relationships between cell-averaged heads and exchange fluxes at large (1-10 km2) scales is here developed. The upscaled flux relationships are determined via the application of fine-scale models, then generalized via observation of simulated GW-SW interactions on multiple terrain types.

The new upscaling method is intended to enable surface water models to more appropriately treat the groundwater component without the need to use a fully conjunctive approach. This may make it possible to solve hydrological simulations at the regional to mega-regional scale with relatively low data resolution while maintaining a higher level of physical appropriateness than would be otherwise attainable using standard reservoir models or naïve upscaling of point-scale physics. In locations where groundwater heads strongly influence surface water fluxes and cannot be ignored (i.e., places with shallow water tables or locations where the GW and SW are in contact such as connected rivers), this approach may improve understanding of both regional water balances and regional groundwater dynamics.

1.2.3 Objective 3 - Applicability of the novel upscaling approach

To determine when the upscaling method and the developed relationships can be applied answering valuable questions about the necessity of fine-resolution models for specific locations/terrain types and if groundwater-surface water interactions for specific terrains behave in a predictable manner.

Verification of the method developed in objective 2, based upon the UFRs identified in objective 1, requires determining when, where and how they should be applied. This includes determining which terrains (e.g., mountainous areas) and locations (e.g., locations with shallow water tables) are able to be successfully simulated with the new upscaling method. Salvucci and Entekhabi (1995), Sanford (2002) and Liang et al. (2003) suggested that ideal locations for assessing hydrologic process performance are locations with topographies that are not steep, locations with shallow water tables and locations with deep soil profiles.

1.2.4 Objective 4 - Develop and test a catchment control volume finite difference groundwater model that can couple with Raven

To develop and test a specialized catchment-discretized finite volume groundwater model that can be directly coupled with the basin-scale surface water model, Raven.

Many surface water models are discretized using natural watershed, basin or hydrological response unit boundaries, whereas groundwater models are typically discretized using regular blocks or elements that are much smaller than the cells of surface water models. In general, there are three options for coupling groundwater and surface water models; (1) a 1:1 GW-SW fine resolution discretization, (2) a 1:1 GW-SW basin discretization, and (3) a M:N GW-SW exchange. The first approach is the most common approach in coupled groundwater-surface water modelling and integrated models. Shrinking the size of the surface water cells to match the groundwater cell size increases the accuracy of the simulation through increased spatial discretization, while also increasing the computational burden. The second approach requires that the groundwater cell discretization be upscaled to match the natural or basin scale discretization often applied in surface water models (Sivapalan, 2005). This simplifies communication between the surface water system and groundwater system, and respects the typically well-known delineation of the landscape into catchments. This approach is useful when coupling to a surface water model that is specifically designed to use watershed boundaries such as Raven (Craig and the Raven Developement Team,

2013). However, the use of coarse cell-based discretization on a Cartesian grid for surface water modelling ignores key information, such as the basin boundaries, making the representation of subgrid features a challenge (Van Nieuwenhuyse et al., 2011). The third method is similar to option 2 in that it upscales the groundwater cells but not to match the discretization of the surface water cells 1:1 (i.e., the surface water and groundwater cells will overlap, but their cell edges may not line up). Two implementations of this method can be conceptualized. The first method is used in MODBRANCH (Swain and Wexler, 1996) where a GW cell can connect to multiple reaches of a river. The second method, used in this research, involves the use of Voronoi polygons as GW cells (i.e, pseudo basin discretization). The overlap of SW basins and the GW Voronoi polygons creates the M:N discretization. This approach makes communication between the two systems more complex but can improve model speed by reducing the number of groundwater cells in the simulation.

Following the verification of the relationships developed in objectives 1 and the methods determined in objective 2, the novel upscaling approach is here incorporated into the existing surface water model, Raven. Testing of the new coupled model involved simulating a real world location (Postling, UK) to show that integrating the new upscaling method with an existing surface water model (with accurate exchange fluxes) will accurately and efficiently solve regional scale problems. The upscaled groundwater component has been coupled with Raven, an open source surface water model. This coupling improves the capabilities of Raven, enabling mega-regional groundwater modelling with SW exchange dynamics.

Previously, Raven's groundwater component was a simplified representation of a groundwater system with the ability to represent multiple soil layers and a general aquifer unit. Raven had the ability to simulate basic hydrological processes (e.g., infiltration, percolation, baseflow) but lacked the ability to calculate lateral groundwater flow that was spatially discretized. While the simplified approach is often effective, the addition of the upscaled groundwater component increases Raven's capabilities so that it can represent groundwater system storage, processes and heads. The upscaled groundwater component, which was designed to improve simulation runtimes, is ideal for coupling with Raven, which was designed to be a fast and efficient surface water model.

1.3 Outline of Contents

This dissertation is structured as follows.

1.3.1 Chapter 1 (Introduction)

This chapter provides an overview of the proposed research plan including the intended objectives and an outline of the thesis sections.

1.3.2 Chapter 2 (Background)

The sections within this chapter include a comprehensive literature review and the mathematical baseline necessary for the advancement of this research. The literature review contains information on hydrological modelling, including surface water, groundwater and coupled models. It also describes exchange fluxes, upscaling, and gives an overview of the math necessary to understand the research contained in this thesis.

1.3.3 Chapter 3 (Methods)

Chapter 3 explains the methodology used to conduct the research presented in chapters 4 and 5. An overview of the surface water model, Raven, is provided and the proposed upscaling approach are explained. The structure of the new coupled groundwater-surface water version of Raven is also detailed.

1.3.4 Chapter 4 (Results and Discussion)

All tests used to validate the model and to verify the proposed upscaling approach are explained here. This chapter provides the results for the benchmarking, testing and verification of the tests as outlined in chapter 3. Chapter 4 also discusses the results from all testing, highlighting their significance to hydrological modelling and ties the study objectives into the interpretation of the results.

1.3.5 Chapter 5 (Conclusion)

This section summarizes the entire study and concludes the thesis and includes recommendations for future research.

Chapter 2

Background

Some material covered in this chapter is from Snowdon and Craig (2015)

In order to properly understand how issues of scale impact the effectiveness of GW-SW models, it is necessary to first understand what hydrological models are, how groundwater and surface water models are traditionally coupled, how coupled models interact, and the strengths and limitations of current GW-SW upscaling techniques. The following sections discuss these issues and contain an overview of the numerical background needed to understand this research.

2.1 Literature Review

2.1.1 Modeling

2.1.1.1 Hydrological Models

Hydrological simulation models are numerical representations of the hydrological cycle which describe how, when and where mass and energy are redistributed within watersheds. These models are quantitative representations of hydrological regimes developed through the establishment of continuous mathematical relationships between the various components (Crawford and Linsley, 1966; Singh and Woolhiser, 2002). The components of the hydrological cycle are typically represented by 1-dimensional water balance equations that govern the change in storage of water (or energy) within a given unit (e.g., soil, canopy, snowpack), where multiple units are associated with a specific location. These

zero-dimensional water balance equations are often treated as collections of ordinary differential equations (ODEs) that each represent a process (e.g., infiltration, runoff, percolation) within the water balance equation.

Appropriate simulation of a watershed system requires that the model (1) be able to simulate all the important processes and relationships, (2) represents the physical makeup of the system and (3) replicates the system spatially and temporally so that it can be applied over a wide range of hydrologic and geographic conditions (Freeze and Harlan, 1969).

To meet the first requirement, it is necessary to sufficiently understand the location being simulated so that the model can incorporate all relevant hydrological processes. The second requirement states that the model be able to represent the physical makeup of the system including characteristics such as hydraulic conductivity, soil characteristics and topography. Without the ability to incorporate the physical characteristics of the system, a model would not be capable of simulating the movement of mass (or energy) within the system with any level of accuracy.

The spatial and temporal discretization of a model, as stated in the third requirement, can have significant impact on the ability of the model to represent a real world location. Both of these discretization choices impact the ability of the model to provide accurate simulation results at scales that may be of interest, whether in relation to a specific location or a moment in time.

Models typically divide a watershed into smaller parts to allow for increased detail and higher accuracy. When the resolution is fine, a model is able to resolve more detailed features of the landscape but the computational burden is high, slowing down simulations. When the resolution is low, a simulation may not incorporate the important heterogeneity within a watershed or represent all of the hydrological processes (e.g., evapotranspiration, runoff, baseflow) at an appropriate scale.

If a model's capabilities meet the requirements as set out by Freeze and Harlan (1969), it is then possible to place the model into one of several categories based loosely upon which system the model is intended to simulate. For the purposes of this dissertation, the system models of interest include surface water models, groundwater models and coupled GW-SW models.

2.1.1.2 Surface Water Models

The term 'surface water model' is used to refer to models which simulate the water cycle above the topographic surface, typically with a simplified groundwater component and a

basic atmospheric flux representation. These models attempt to represent the physical processes that move water between surface water bodies (e.g., lakes, rivers) as well as the exchange fluxes (e.g., infiltration, evapotranspiration) that transfer water between the surface, the subsurface and the atmosphere. The parameters within the model describe the physical characteristics of the watershed including the surface water features that store water and the processes that transfer water between the storage locations (Gupta et al., 1999). In many cases, the primary goal of a SW model is to predict the magnitude and timing of stream/river flows at a watershed outlet or gauge.

Surface water models are often categorized as lumped, semi-distributed or distributed. A lumped model can be thought of as a 'bucket' model where there is no spatial discretization of any input data or the model parameters (Clarke, 1973). Unlike lumped models, distributed models are spatially discretized and each cell represents a particular location in the real world (Kampf and Burges, 2007). These models allow for advanced understanding of the inner workings of an area by determining the change in mass and/or energy throughout a collection of cells. Semi-distributed models are essentially a crossover of lumped and distributed models, providing some spatial discretization while being less explicit about position than a distributed model in their implementation. Since this research intends to use a semi-distributed surface water model, it is necessary to have some understanding of spatial discretization conventions.

The spatial units often used in a semi-distributed hydrological model are basins/ watersheds, subbasins and hydrological response units (HRUs). Basins/watersheds typically refer to a large area (i.e., $\approx$100 sq. km) consisting of an entire river system, often delineated using the natural catchment boundaries that exist in the real world. Subbasins are subsets of basins and can contain a tributary or main channel that is a part of the larger basin. HRUs are a spatial unit where the physical characteristics and parameters are considered uniform, as is the hydrologic response to external forcing. The physical characteristics/parameters used to characterize HRUs can include soil properties, land use and vegetation. The selection of the discretization method varies between models and can be impacted by the desired simulation output accuracy.

Surface water models, particularly semi-distributed models, are often discretized using the boundaries of HRUs, subbasins, basins or, in some cases, political boundaries. However, some distributed surface water models (Rigon et al., 2005; Koren et al., 2006; Kampf and Burges, 2007; Dutta and Nakayama, 2009) use a Cartesian-grid or regular mesh that is appropriately suited to the mathematical solver being implemented within the model. In general, the finer the resolution, the more surface water features and surface heterogeneity can be represented, resulting in a more physically accurate solution to the problem. As the resolution is decreased, subgrid details are lost, but simulation run time is improved. Both

high and low resolution models have limitations that need to be considered when selecting an appropriate model for a simulation. High spatial resolution can be a limitation due to computational burden and potential stability issues, whereas low spatial resolution can be a limitation due to the loss of less relevant physical detail and inadequate descriptions of physical processes at larger scales. The choice of model should be based on the end goal of the simulation (e.g., high spatial accuracy versus ability to calibrate and/or apply uncertainty analyses).

Current surface water models are designed for a variety of purposes including river flow forecasting, mass balance prediction and/or sediment/nutrient transport simulation. Most surface water models represent groundwater using a simplified approach (e.g., treating it as a linear reservoir) which does not explicitly represent groundwater head and storage (Morita and Yen, 2000). To simulate systems with a significant groundwater component, more advanced surface water models have been loosely coupled with independent groundwater models of varying complexity (Morita and Yen, 2000; Panday and Huyakorn, 2004; Sulis et al., 2010) and included as a component of a fully integrated groundwater-surface water model (Freeze, 1972; Morita and Yen, 2000) such as PARFLOW (Kollet and Maxwell, 2006) or HydroGeoSphere (Therrien et al., 2006). Standalone surface water models with no groundwater representations are often used to simulate channel flows and storm events. In many cases, these models can adequately replicate hydrographs, but may poorly estimate recharge to groundwater or other components of the hydrological cycle. However, surface water models with simplified groundwater systems are commonly applied for basic mass balance estimation or hydrograph prediction. These basic representations are often sufficient when the subsurface and interactions with the subsurface do not need to be represented in a precise manner. Of course, in systems with significant GW-SW interactions, these simplified relations fall short.

2.1.1.3 Groundwater Models

Groundwater models are used to predict the movement of water and contaminants in the subsurface. Specifically, they are often used to calculate changes in water table elevation or to determine the amount of GW flow between areas of interest (e.g., subbasin to subbasin). As such, groundwater models are often finely resolved spatially so that it is possible to map the elevation contours of the water table while also accurately reflecting the system mass balance. A fine resolution groundwater model can be discretized in many ways, depending on the solver being implemented in the model. Typically, a finite difference approach (e.g., Modflow (Harbaugh, 2005)) requires a Cartesian grid and a finite element approach (e.g., FEFLOW (Diersch, 2005)) uses a triangular mesh. If a control volume approach is applied,

then grids, meshes and other discretization options can be used. The size of the individual grid cells, elements or other discretization units is dependent on the model, the level of accuracy required and/or the problem being solved (usually formed as a 2-dimensional or 3-dimensional mass balance solution to a discrete form of partial differential equations).

Like surface water models, groundwater models have similar limitations linked to spatial resolution. When the discretization is fine, the computational burden is increased, and when the discretization is coarse, the model may fail to account for subgrid heterogeneity in properties, variability in head elevation, or exchange fluxes.

2.1.1.3.1 Groundwater Fluxes Through System Boundaries

Generally, saturated groundwater models simulate the input and output of water from an aquifer along four pathways; through direct surface water connection (i.e., baseflow) and through the topographic surface (e.g., recharge, evapotranspiration), through pumping wells, and through connections to adjacent aquifer systems (see figure 2.1). The first two pathways represent the groundwater-surface water connection, with the latter mediated by the physics of the vadose zone. Models characterize these exchange fluxes using a variety of methods. For interactions with rivers, it is common for a river to be represented by a constant head boundary condition, adding or removing as much water as is necessary to maintain the head constraint. Drain conditions (e.g., seepage faces) are often applied at the topographic surface, where groundwater that exceeds the surface elevation is transferred across the GW-SW interface into the surface water system, effectively treating the surface water system as a sink. Evapotranspiration is handled as an extraction of water from the shallow groundwater to the atmosphere and recharge is considered to be the amount of water that reaches the GW saturated zone from the surface water system (i.e., is some fraction of infiltration) (Jyrkama et al., 2002; Jyrkama and Sykes, 2006). The unsaturated zone (i.e., vadose zone or root zone) is an area that lies between the surface and the water table or aquifer. This is often where the bulk of transpiration occurs.

For stand-alone GW models, it is common to determine GW-SW exchange fluxes from boundary conditions. Solving for these terms generally requires prior knowledge of the exchange flux, or a mechanism by which to estimate fluxes from groundwater head, the dependent variable. Typically this is achieved by first solving a (often very simplified) surface water model prior to the operation of the groundwater model in order to determine the net recharge to the groundwater system, or using the groundwater model prior to the surface water model for calculating evapotranspiration and drain fluxes. Coupled and fully integrated models allow for the determination of exchange fluxes to be resolved during each timestep as opposed to determining exchange fluxes using independent models (for entire

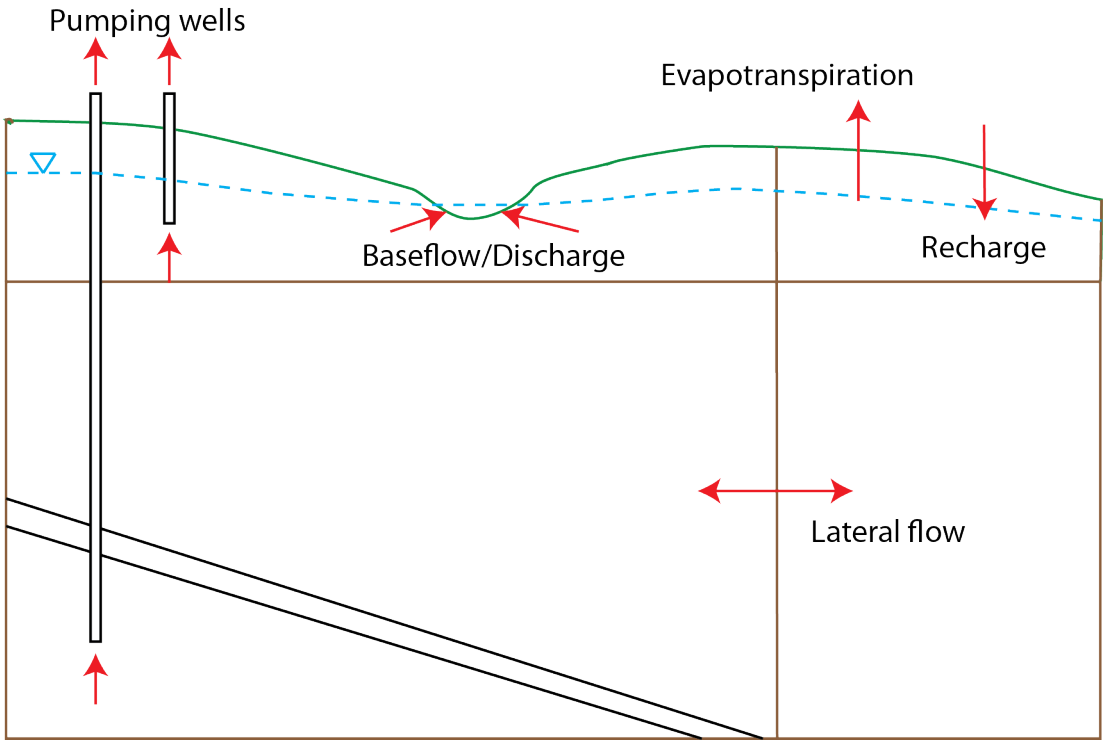

Figure 2.1: Pathways for water flow to and from aquifers

simulations) which are then used as input forcings for the opposite systems model. While this is not unique to coupled models, it is one of the characteristics of coupled models that make them a suitable choice for the implementation of the proposed upscaling method.

2.1.1.4 Coupled Models

Surface water models are generally not equipped to handle problems where the more nuanced interactions with groundwater systems need to be respected (e.g., wetland exchange, groundwater discharge). Models that are coupled or fully integrated, however, can solve problems that require simulation of the complex interactions and processes that occur in the surface and subsurface systems as well as the two-way exchange fluxes between the two systems (Morita and Yen, 2000; Furman, 2008). Over the last 20 years, many integrated GW-SW models have been designed with the intention of simulating both surface-water and groundwater systems in a seamless fashion. Models such as InHM (VanderKwaak and Sudicky, 1999), ParFlow (Kollet and Maxwell, 2006) or HydroGeoSphere (Jones et al., 2006), focus on the coupled solution of Richards' equation and the overland flow equations, particularly at the relatively small scales where Richards' equation may be deemed appropriate. Simpler, more loosely coupled models such as MODBRANCH (Swain, 1992; Swain and Wexler, 1996) link standalone groundwater and a surface water models (i.e., MODFLOW and BRANCH for MODBRANCH) with feedback from each contributing to the other. Exchange via baseflow or net recharge calculated in each model is treated as input to the other creating a coupled model.

Integrated models that fully couple surface water and groundwater systems (as opposed to loosely coupled methods) are deployed to simulate large, complex problems which may require significant computational resources in order to be solved. The data needs of such models may be considerable and these models are often unable to be properly calibrated or applied in uncertainty analysis due to computational cost. Some fully conjunctive simulations can take days or months for a single run, making analysis requiring many runs impractical (Vermeulen et al., 2006). Ideally, low resolution methods which still provide for adequate simulation of two-way groundwater-surface water interaction in an appropriate manner are desirable. As stated earlier, while low resolution approaches have some limitations, they are beneficial if methods are employed that can overcome the loss of subgrid heterogeneity.

2.1.2 Exchange Fluxes

It is common for surface and subsurface models to be created and operated independently even though surface and subsurface systems often behave in a coupled manner (Winter, 2001; Sophocleous, 2002; Kollet and Maxwell, 2006). Groundwater-surface water interactions typically occur via subsurface lateral flow in dominantly unsaturated systems and by infiltration/discharge in saturated systems (Sophocleous, 2002). Where the surface and subsurface systems connect, such as when the water table is in direct contact with a surface water feature (e.g., a river) or seepage face, water is able to easily move from the surface to the subsurface and vice versa. The amount of water transferred between an aquifer and a river is important as it affects both the flow patterns within the aquifer and the magnitude of the flow within the river (Rushton and Tomlinson, 1979; Osman and Bruen, 2002). The magnitude and significance of the connections between the groundwater and surface water systems are determined in part by the shape and nature of the water table (Fan et al., 2007; Maxwell and Kollet, 2008; Gleeson and Manning, 2008). Additionally, the transferrable amount of water is strongly dependent upon local GW head and SW stage. Flows between rivers and aquifers are typically estimated with a function of permeability and head difference (based on Darcy's law) which is similar to the mechanism that controls flows through low permeable strata into aquifers (Walton, 1970). Elsewhere in a coupled system, water infiltrates downward through the land surface and, if it reaches a saturated zone, is considered recharge. Recharge, often hard to quantify, is considered to be the sum of all inflows to the groundwater system or aquifer (Jyrkama and Sykes, 2006; Kollet and Maxwell, 2006; Racz et al., 2012), though the term often neglects surface water contributions. Unfortunately, many groundwater and surface water modellers limit or ignore surface-subsurface interactions due to their complexity (Saleh et al., 2011). When the interactions are included in models, it is typical to couple the surface-water and groundwater components using a flux term representing the sources and/or sinks for the surface water and groundwater systems (Kollet and Maxwell, 2006). The explicit representation of these exchange fluxes in the coupling with a surface water system model enable coupled models to simulate more complex problems.

When designing a regional scale GW-SW model, it is necessary to be able to represent all of the connecting processes. Given a lack of understanding of hydrological processes such as evapotranspiration or infiltration at large scales, it is common to use point-scale representations to estimate the magnitude of exchange fluxes. Point-scale representations are equations that have been defined to represent a process and have been empirically or analytically shown to accurately determine exchange fluxes at a very small spatial scale (i.e., at one point but not necessarily areally). Many models can fail to simulate exchange

fluxes well because they are being used at scales that don't allow for the inclusion of the relevant topographic and soil heterogeneity in an area (Salvucci and Entekhabi, 1995).

Alternative approaches commonly used in surface water modelling avoid these resolution issues by applying simple conceptual models of the relationships between bulk aquifer storage and fluxes - for example the commonly used assumption of a linear relation between groundwater storage and baseflow. The common justification is one of empirical fit, typically of modelled to observed hydrographs. These simpler models enable practitioners to adequately fit the key features hydrographs without trying to fully characterize the physics of GW-SW exchange at the sub-watershed scale. Some approaches, such as that of TOPMODEL (Beven and Kirkby, 1979; Lamb et al., 1997; Iorgulescu and Musy, 1997) arrive at simple power law relations via the extension of simplified conceptual models to problems of baseflow and runoff generation. Many previous studies have used simple linear and power law relationships to represent relationships between groundwater storage, groundwater infiltration and surface water-groundwater (SW-GW) exchange fluxes such as evapotranspiration, discharge to rivers or discharge from hillslopes (Beven, 1984; Selker et al., 1999; Rupp and Selker, 2005; Cardenas, 2008; Troch et al., 2008; Harman et al., 2009; Kambhammettu et al., 2011, 2013). These are rarely justified via the application of fine-resolution physically-based models.

Here we consider subgrid topography as the primary cause of subgrid effects in coarse models of GW-SW exchange. Topography is known to be a controlling factor in GW-SW exchange. Topographic lows typically correspond to GW discharge areas and act as basins for surface water collection and conveyance. Likewise, the interaction of the water table and topographic surface impacts evapotranspiration (ET), with plants having greater access to water when a shallow water table is present. There is evidence, as supplied by Kollet and Maxwell (2008), Rihani et al. (2010) and Condon and Maxwell (2015), to suggest that a strong link exists between water table depth, groundwater dynamics, exchange fluxes and the mass/energy balance of the surface water system. In standard GW models, ET is treated as a function of water table (WT) depth, which can vary significantly within a large grid cell. This is further expounded upon in section 2.2.3.

There are several macroscale changes of exchange fluxes that may occur with a change in the average head in a coupled system. For example, low recharge systems may have less discharge/baseflow and potentially lower ET rates as the water table is less likely to be shallow, and therefore less accessible to plants. High recharge systems will often have a higher water table which can result in higher discharge, higher ET, higher baseflow and a larger percentage of the topographic surface being saturated or near-saturated. This relationship is illustrated in figure 2.2.

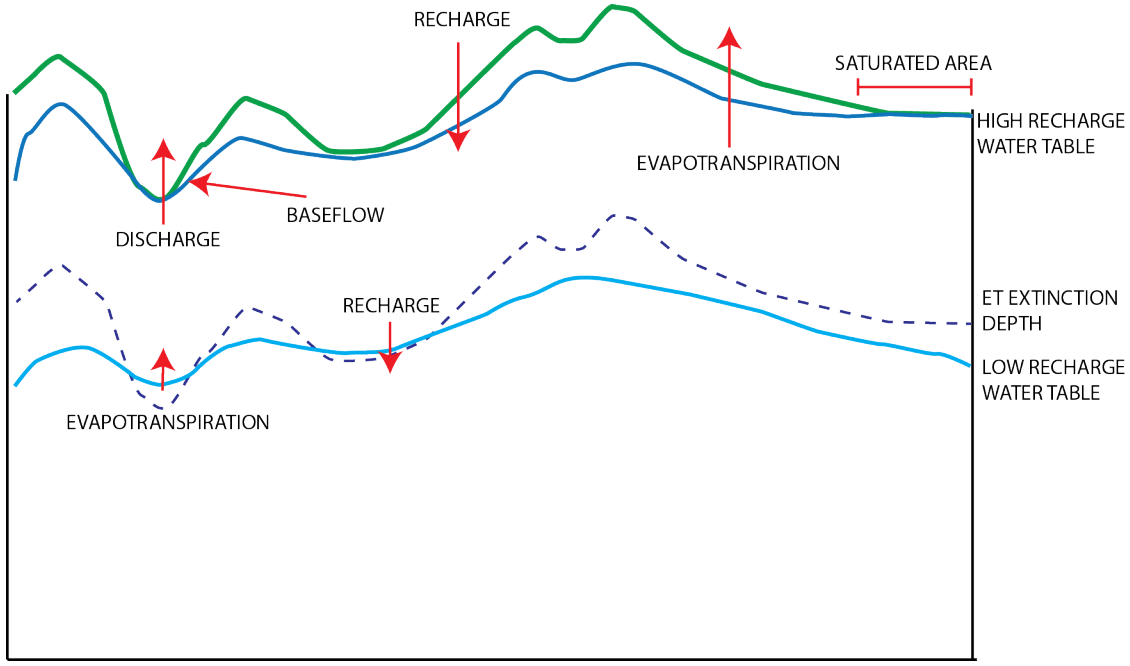

Figure 2.2: Macroscale changes in exchange fluxes due to changes in hydraulic head

2.1.3 Upscaling

A 'scale' is a level of spatial resolution. The size of the smallest computational unit, for instance, often determines the model scale. 'Upscaling' can then be used to refer to a change in computational resolution from a finer to a coarser scale (Gupta et al., 1986). This research will define scales approximately as follows using a surface water convention; local (or point) scale ≈1 sq. metre; hillslope scale ≈10 000 sq. metres; catchment scale ≈100 sq. kilometres; and regional scale ≈1 000 000 sq. kilometres (Dooge, 1982, 1986). Upscaling takes information from the small scale to inform the simulation of a given hydrological process at the large scale (Blöschl and Sivapalan, 1995; Troch et al., 2008). Upscaling of a model domain is intended to make simulations over large areas, which would normally be solved with fine resolution models, less cumbersome to solve (Vermeulen et al., 2006). However, upscaling can create new concerns as high resolution details are necessarily lost during parameter upscaling due to smoothing and averaging (Jana and Mohanty, 2012b).

Many upscaling techniques exist, such as using effective parameters (Jana and Mohanty, 2012a), designing new process algorithms that function at larger scales (e.g., the non-linear, threshold-type responses of hillslope drainage networks of Tetzlaff et al. (2008)), the use

of statistical operations such as ensemble averaging (Kavvas et al., 1998; Kavvas, 1999), or the use of "rating curves" (e.g., functional stage-discharge relationships extracted from 1D St. Venant approach to upscale stream-aquifer interactions as shown by Saleh et al. (2011)). These methods approach upscaling in different ways in order to account for the loss of subgrid information as cell sizes increase.

Effective parameters make use of point-scale methods with a scaling factor applied to parameters to ostensibly account for the change in cell size - for example, to reduce recharge to account for surface water features which are not explicitly included in the model. It is recognized that if a computational unit has significant subgrid heterogeneity, it will not behave the same as a homogeneous unit with effective parameters (Kavvas et al., 2013). The use of effective parameters is therefore not ideal for upscaling heterogeneous cells. Designing new process algorithms that function at larger scales attempts to step away from the point-scale approach and develop new and meaningful algorithms that are effective for solving problems at the decreased resolution. For example, McGuire et al. (2005), Tetzlaff et al. (2007) and Tetzlaff et al. (2008) show how understanding the role of topography as a controlling factor for groundwater flow behaviour can be used to improve new process conceptualizations. Kavvas et al. (1998) and Kavvas (1999) show that the use of statistical operations such as the areal averaging of hydrological processes can transform processes from non-stationarity to stationarity allowing a valid representation of the flux rates at larger scales. "Rating curves" are generated by relating the response of a variable defined at the averaging scale (e.g., head) to an exchange flux rate (e.g., baseflow). The resulting curve, which may be generated explicitly via a rigorous averaging scheme or empirically, can be used to represent the change in a process rate in response to the variable. Although "rating curves" have only been applied in a few cases (Saleh et al., 2011), they have shown promising results when simulating river flows, and will be used here. This upscaling concept has the potential to be applied to more complex upscaling goals.

Unfortunately, it is a common approach in modelling to apply appropriate descriptions of hydrological processes at smaller scales to describe processes averaged over larger scales (Troch et al., 2008). As discussed above, this simple "effective parameter" scaling approach is generally not effective. Hydrological models depend on lateral catchment structure and heterogeneity, yet physically-based models often approach scaling using aggregation in "an unsophisticated" way (Beven, 1995). For example, some models (e.g., BATS (Dickinson et al., 1993), SiB (Sellers et al., 1986)) apply local (i.e., point-scale) processes at the regional scale with little or no accounting for the scale change (Beven, 1995). Scale changes affect parameters, processes and even boundary conditions. Investigations by Gelhar (1986), Wheatcraft and Tyler (1988), Dagan (1989), Neuman (1990), Desbarats (1992) and Durlofsky (1992) indicated that effective parameters for heterogeneity in hy-

draulic conductivity and for the dispersion coefficient should not be used at any scale and may be considered scale-dependent for saturated systems. Some alternative parameter upscaling approaches that have been developed include power averaging (Wiener, 1912; Matheron, 2011), Darcian methods (Warren and Price, 1961), homogenization (Bensoussan et al., 1978), and the local-global method (Chen et al., 2003). These approaches are specific to the hydraulic parameter that they upscale and are not general approaches (i.e., power averaging upscales the hydraulic permeability for flow parallel to the strata, Darcian methods upscale hydraulic transmissivities).

Little work has been done to examine the impact of scaling upon calculations of GW-SW exchange, and even less work has addressed how best to upscale (Kavvas, 1999; Wallender and Grismer, 2002; Soulsby et al., 2008; Tetzlaff et al., 2010). Effectively, no one has attempted upscaling of groundwater-surface water exchange fluxes.

2.2 Mathematical Background

2.2.1 Groundwater Flow

The 3-dimensional transient groundwater flow governing equation is:

$$\frac{\partial}{\partial x}\left(K_x h\frac{\partial h}{\partial x}\right)+\frac{\partial}{\partial y}\left(K_y h\frac{\partial h}{\partial y}\right)+\frac{\partial}{\partial z}\left(K_z h\frac{\partial h}{\partial z}\right)=S\frac{\partial h}{\partial t}-W^{*} \tag{2.1}$$

where K is the hydraulic conductivity of the aquifer $[LT^{-1}]$, h is the hydraulic head measured from the aquifer base $[L]$, S is the aquifer storativity [-] and $W*$ is representative of the sinks/sources to the system $[LT^{-1}]$. Here, we focus on regional scale systems where head variation in the vertical direction is of secondary importance, and therefore invoke the Dupuit-Forchheimer approximation to simplify this equation.

A common approach to simulate groundwater flow problems was developed by Dupuit (1863). He simplified groundwater systems by ignoring vertical flow, allowing 3-dimensional systems to be approached as 1- or 2-dimensional problems (Haitjema and Mitchell-Bruker, 2005). In 1886, Forchheimer developed a differential equation to explain water table elevations in unconfined aquifers based upon an integrated flow approximation. Both Dupuit (1863) and Forchheimer (1886) ignored vertical water flow at the regional scale. This primary focus on lateral flow simplifies the problem making the simulation of groundwater heads easier to predict. The use of the Dupuit-Forchheimer approximation in this research reduces the complexity of the unconfined GW system, permitting it to be solved as a

2-dimensional problem instead of a 3-dimensional one. Note that the modern use of the Dupuit-Forchheimer approximation (Strack, 1984) presumes zero resistance to flow in the vertical direction, not that there is no flow in the vertical direction. In this case, the Dupuit-Forchheimer governing equation may be considered simply a vertical integrated form of the fully 3-dimensional governing equation. The governing equation used to describe 2-dimensional saturated unconfined groundwater flow which invokes the Dupuit-Forchheimer approximation (Dupuit, 1863; Forchheimer, 1886) is:

$$\frac{\partial}{\partial x}\left(K_x h \frac{\partial h}{\partial x}\right) + \frac{\partial}{\partial y}\left(K_y h \frac{\partial h}{\partial y}\right) = S\frac{\partial h}{\partial t} + \begin{cases} ET(x,y,h) - R(x,y,h) & \text{if } h < h_t \\ ET(x,y,h) + D(x,y,h) & \text{if } h \geq h_t \end{cases} \tag{2.2}$$

where $ET(x,y,h)$ is the evapotranspiration rate $[LT^{-1}]$, $R(x,y,h)$ is the recharge rate $[LT^{-1}]$, $D(x,y,h)$ is the discharge rate $[LT^{-1}]$, and h_t is the topographic surface elevation measured from the aquifer base $[L]$. In this equation, the aquifer is assumed to be unconfined and has a base at 0 datum.

Both recharge and ET are dependent on head in equation 2.2. In this formulation, recharge can only enter the aquifer if the head is at or below the topographic surface. Likewise, ET can only be extracted from the GW system if the head is above the maximum extinction depth specific to formulation used here at the point scale. Otherwise ET is zero. A critical assumption made in this thesis is that the form of the evapotranspiration (ET), recharge (R), and discharge (D) functions in equation 2.2 changes with scale. The upscaling of the left hand side of equation 2.2 has been addressed elsewhere in the literature (Wen and Gómez-Hernaández, 1996; Vermeulen et al., 2006) and is not considered here.

2.2.2 Recharge, Drains and Conductance

Recharge and discharge via seepage and direct SW connection are key processes that add and remove water from the subsurface. The amount of water added or removed is typically dependent upon the water table elevation. When the water table is sufficiently deep below the land surface, recharge is able to enter the system. When the water table elevation is near or connected with the land surface, then the system can discharge water across the GW-SW interface into the surface water system, mediated by vadose zone processes. Often, the water table will be connected to the land surface in one location (e.g., in a river valley or wetland) and disconnected from it in another, resulting in both recharge and discharge occurring simultaneously within a basin (see figures 2.2 and 2.3).

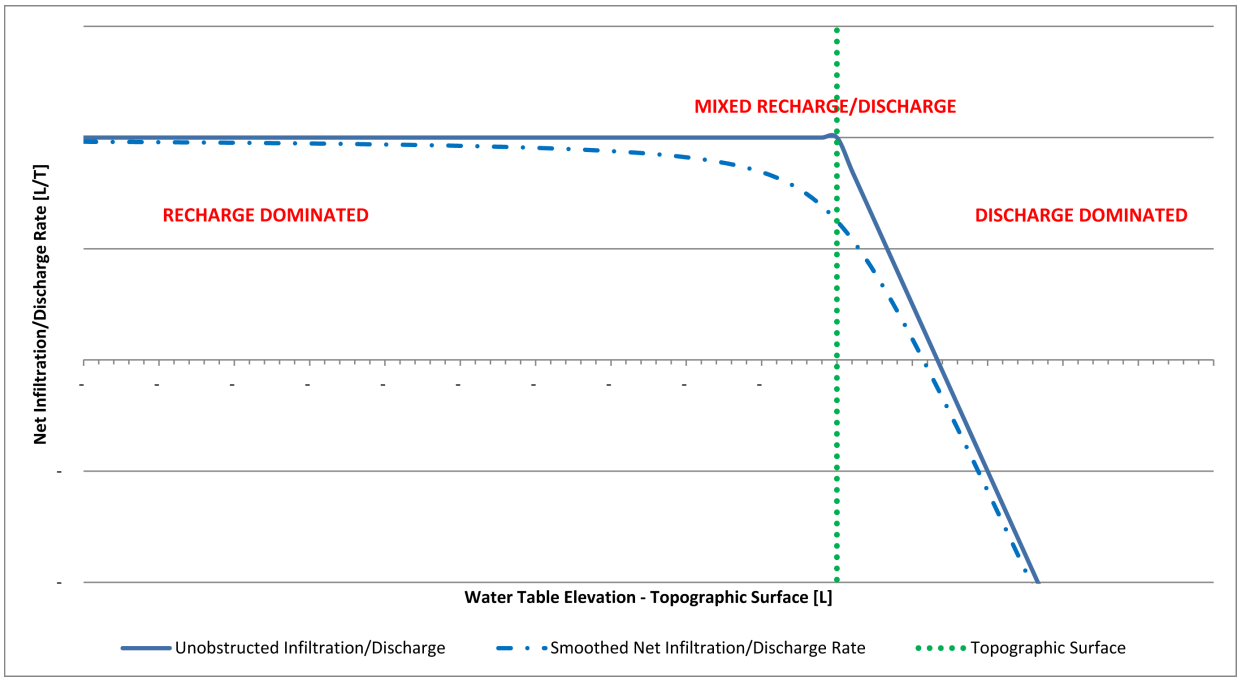

Figure 2.3: Graph showing that when the water table is below the topographic surface, the system is recharge dominated. As the water table nears the topographic surface, mixed recharge/discharge occurs. If the water table reaches the topographic surface, the system becomes discharge dominant.

Several papers (Haitjema and Mitchell-Bruker (2005); Marklund and Wörman (2011); Gleeson et al. (2011)) have investigated groundwater-surface water systems by classifying the systems as recharge-controlled or topography-controlled. Recharge-controlled systems may have low water tables (e.g., mountainous regions, arid areas) where there can be large amounts of recharge to the groundwater system that dictates the shape of the water table. Topography-controlled systems often have shallow water tables (e.g., humid regions) where the shape of the water table can be a subdued replication of the topographic surface. Part of these studies investigated how to determine if a system is recharge- or topography-controlled, often through the calculation of a classification value such as the water table ratio (Haitjema and Mitchell-Bruker (2005); Gleeson et al. (2011)). They also looked at how to best determine the shape of the water table given a topography-controlled system and a known topography. Spectral analysis and Fourier analyses have been used to attempt an explanation of how water tables relate to topography at multiple scales (Marklund and Wörman, 2011). These studies help to predict when a system is topography-controlled and how exchange flux rate magnitudes may change when shallow water tables connect with the topographic surface. This is important to understand when upscaling exchange fluxes such as discharge.

Discharge across the GW-SW interface is often controlled in GW models via the conductance approach, which was described in detail by Rushton (2007). This method uses an (often hypothetical) 'clogging layer' at the topographic surface or along river bottoms to control the flow into and out of the subsurface when applied to exchange between silt-bottomed streams and rivers. A 'clogging layer' is a thin layer with a conductance value sufficiently high as to restrict the flow rate between the surface and subsurface. Conductance values can be calculated based on the properties of the river using the following equation:

$$C = \frac{K_r L W}{M} \tag{2.3}$$

where C is the conductance value $[LT^{-1}]$, K_r is the riverbed hydraulic conductivity $[LT^{-1}]$, L is the reach length $[L]$, W is the river channel width $[L]$, and M is the low permeability riverbed thickness $[L]$ (Rushton, 2007). However, in practice, the conductance term is often determined through calibration. Also, an arbitrarily large conductance can be used to treat GW-SW exchange across the land surface when a real clogging layer is not present. While in theory, such a conductance should be infinity leading to an equivalent SW and GW pressure, in practice it is lowered for numerical stability.

The conductance approach, which implicitly accounts for scaling effects, can be imple-

mented to determine drainage rates using:

$$q = C(h - h_t) \tag{2.4}$$

where q is the drainage rate across the interface $[L^3T^{-1}]$.

This method is used both in ParFlow (Kollet and Maxwell, 2006) and HydroGeoSphere (Jones et al., 2006) to mediate GW-SW fluxes, except the topographic head is replaced with the overland flow surface elevation which is often well approximated by h_t. In ParFlow, the conductance term is referred to as the proportionality constant. It is often assumed to be a ratio between the interface permeability and the interface thickness (Kollet and Maxwell, 2006). HydroGeoSphere assigns a conductance term value and a drain elevation to surface nodes and then implements the conductance approach as specified in equation 2.3. Both models solve Richards equation coupled with diffuse wave overland flow and are capable of conducting simulations in unsaturated conditions, but still rely upon the conductance approach.

2.2.3 Evapotranspiration

Evapotranspiration (ET) is the hydrological process where liquid water - in the ground, on the surface or contained in plants - is transformed to a gaseous form and lost to the atmosphere. Evapotranspiration can be broken into two distinct processes; (1) evaporation (the conversion of liquid water into water vapour via radiative energy transfer) and (2) transpiration (the conversion of water from plants into water vapour). This process occurs continuously, often at a very low rate, but the rate will increase with increased temperature and exposure to elements (e.g., wind).

In GW models, ET is conventionally treated as a function of water table depth, which can vary significantly within a large grid cell. It is recognized in the literature that the actual relationship between water table depth and water/energy transfer across the soil surface is much more complex than is characterized by this simple description, especially when the vadose zone is considered (Kollet and Maxwell, 2008). However, at the scales considered here, where it is recognized that this relationship is likely heterogeneous and difficult to characterize, it can revert to the linear function used successfully in a number of regional modelling studies where ET plays a significant role (e.g., Bradley (2002); Bradford and Acreman (2003); Wang et al. (2008); del Pilar Alvarez et al. (2012)). This relationship is more appropriate for the common situation where there is insufficient data to support a more complex treatment of the ET-WT depth relationship.

Unsurprisingly, the ET from shallow groundwater, which is dependent upon WT depth, has been found to be prone to errors when naïvely upscaled (i.e., simply applying point-scale ET relationships directly on coarse grids) (Kambhammettu et al., 2011, 2013). These studies found that the ability to simulate ET at large scales was dependent on the correct interpretation of digital elevation model (DEM) data. Similar results are expected for baseflow and saturated area, which are similarly dependent upon the relation between the water table and topographic surface. Scale mismatches between DEM and simulation cell sizes as well as fluxes (e.g., evapotranspiration, stream leakage, net recharge) that are dependent upon surface elevations can be negatively impacted when subgrid elevation data is ignored and/or incorrectly integrated into models. The errors generated are then carried throughout the model, culminating in errors in water table elevations and mass budgets (Li et al., 2008). Since this study is concerned with the upscaling of GW-SW exchange fluxes, it should be noted that the aforementioned errors in ET (Kambhammettu et al., 2011, 2013) were found to occur under specific conditions: (1) when the terrain is undulating, with steep terrain elevations occurring between cells and (2) when the simulation cell size is large compared to the DEM resolution. Both are symptoms of inappropriate upscaling.

For this research, evapotranspiration at the point scale was treated using a linear relationship (see figure 2.4) based upon an extinction depth method, as done in MODFLOW (Harbaugh, 2005):

$$ET = \begin{cases} 0 & \text{if } ((h_t - e_{ET}) - h) > 0 \\ PET & \text{if } (h - h_t) > 0 \\ \frac{(|((h_t - e_{ET}) - h)|)}{e_{ET}} PET & \text{otherwise} \end{cases} \tag{2.5}$$

Modflow's ET algorithm calculates ET as a fraction of the maximum potential evapotranspiration (PET). It uses a linear approximation that assumes that ET when the water table is at the ground surface is equal to 100% of the maximum PET and that a user-defined extinction depth specifies the depth where ET becomes zero. Shah et al. (2007) suggested that the extinction depth for an area (with trees) should be 2 metres deep. Luo et al. (2009) showed that extinction depths for linear approximations of ET can extend beyond 3 metres in depth. PET may be estimated using a variety of methods (e.g., the Priestley-Taylor (Gunston and Batchelor, 1983) or Penman (Gunston and Batchelor, 1983) algorithms, amongst others)

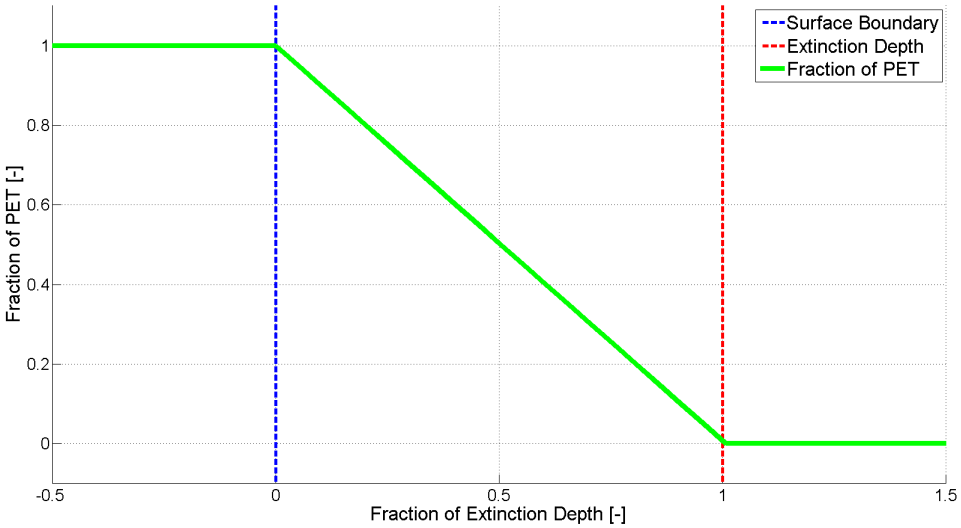

Figure 2.4: Fraction of ET based on extinction depth

2.2.4 Control Volume Finite Difference

Here a control volume finite difference method (CVFD) is used to discretize and solve equation 2.2. CVFD approaches are popular in computational fluid dynamics due to their ability to conserve local mass balance (Botte et al., 2000). They are a modification of a standard finite difference approach in that the differential equation is integrated over a control volume. This is useful when trying to calculate the flux between areas with different physical properties (Hoffman, 2001).

By integrating equation 2.2 over a control volume:

$$\int_V (K \nabla h)\, dV = \frac{\partial}{\partial t} \int_V (S_S h)\, dV + \int_V W dV \tag{2.6}$$

(where W includes all of the exchange flux terms). The volume integral can be converted to a surface integral:

$$\int_S (K \nabla h)\, \mathbf{n} dS = S_S V \frac{\partial h}{\partial t} + WV \tag{2.7}$$

where $\mathbf{n}$ is an outward point unit normal vector on the volume surface and S is the surface of the control volume (Anderson et al., 2015). When applying the CVFD method, each

integral is applied on a cell-by-cell basis with interfacial matching of flux calculations. This leads, for each time step, to a system of N equations for the unknown heads in N control volumes.

To improve the solution of CVFD problems, it is beneficial to use a two-step process that can deal with the nonlinearity commonly found in hydrogeological problems. This can be accomplished by using an outer solver that handles the nonlinearity and an inner solver that solves the linear system of equations. An outer solver, such as the Newton-Raphson method, takes the system of nonlinear equations and linearizes them; the inner solver (e.g., a BiConjugate Gradient method) solves the resulting system of linear equations. Both inner and outer solvers have convergence criteria that can be set to control a desired level of accuracy. Details on the inner and outer solvers can be found in section 3.4.5.

Chapter 3

Methods

Some material covered in this chapter is from Snowdon and Craig (2015)

3.1 Proof of Concept

Objective 1 of this thesis was to examine and characterize relationships between terrain physiography and fluxes across the land surface in order to identify useful relationships between subgrid topographic characteristics, spatially averaged groundwater head, and spatially averaged exchange fluxes. This is here done by evaluating how exchange flux rates are affected by changes in hydraulic head for a given terrain type under steady state conditions using a control volume finite difference model.

The initial work in support of this goal was conducted using a 2-dimensional control volume finite difference (CVFD) groundwater model (developed in Matlab) to assess the validity of the assumption that fine-scale models could be used to examine the effects of terrain type on hydrological process fluxes and groundwater head. The CVFD model was implemented using a Dupuit-Forchheimer approximation for saturated groundwater flow with recharge and evapotranspiration as exchange fluxes. The 3-dimensional groundwater equation (equation 2.1) was vertically integrated and discretized using a control volume finite difference approach (equation 2.6 and 2.7), leading to the following non-linear system of equations:

$$\sum \left(\left(\frac{A_{nm} K_{nm}}{L_{nm}} \right) \left(h_m^t - h_n^t \right) \right) + \left(\frac{-S_{Sn} V_n}{\Delta t} h_n^t \right) - W^* = \frac{-S_{Sn} V_n h_n^{t-1}}{\Delta t} \quad n = 1..NC \quad (3.1)$$

where n is the current cell [-], m is the neighbouring cell [-], A_{nm} is the saturated area between cells n and m $[L^2]$, K_{nm} is the hydraulic conductivity between cell n and cell m $[LT^{-1}]$, L_nm is the distance between the centroids of cell n and cell m (measured perpendicular to the interface between cells n and m) $[L]$, h_m and h_n are the hydraulic heads in cell m and n respectively $[L]$, S_{Sn} is the specific storage of cell n $[L^{-1}]$, V_n is the volume of cell n $[L^3]$, δt is the timestep $[T]$, h_n^t is the hydraulic head for cell n for the current timestep $[L]$, h_m^t is the hydraulic head for cell m for the current timestep $[L]$, h_n^{t-1} is the hydraulic head for cell n from the previous timestep and W^* is the sinks/sources for the system (ET, recharge, and discharge) $[LT^{-1}]$.

For the proof of concept simulations, a test topographic surface (see figure 3.1) was used, with drainage fluxes represented using the river conductance method, as described by Rushton (2007). Unlike common approaches of the river conductance method, where a hypothetical clogging layer is placed between the river bed and groundwater system, here a hypothetical clogging layer was applied over the entire topographic surface to moderate the rate of drainage across the topographic surface similar to the recharge spreading layer described by Beckers and Frind (2000). This was a mathematical convenience to control convergence properties; conductance of the clogging layer was maximized to emulate a perfect drain condition. The topographic surface was defined through the use of a simple digital elevation model (DEM).

Data (e.g., hydraulic head, ET rates) extracted from these tests were then analysed using Matlab to find spatial-averaged heads and average flux rates. These heads and flux rates were then used as relationship curves which the model could use to interpolate flux rates for the same simulations using the same DEM with coarsely resolved cells. The upscaled simulation results were compared with the fine-scale simulation results to assess the accuracy of the simplified upscaling approach. These results are reported in section 4.1.

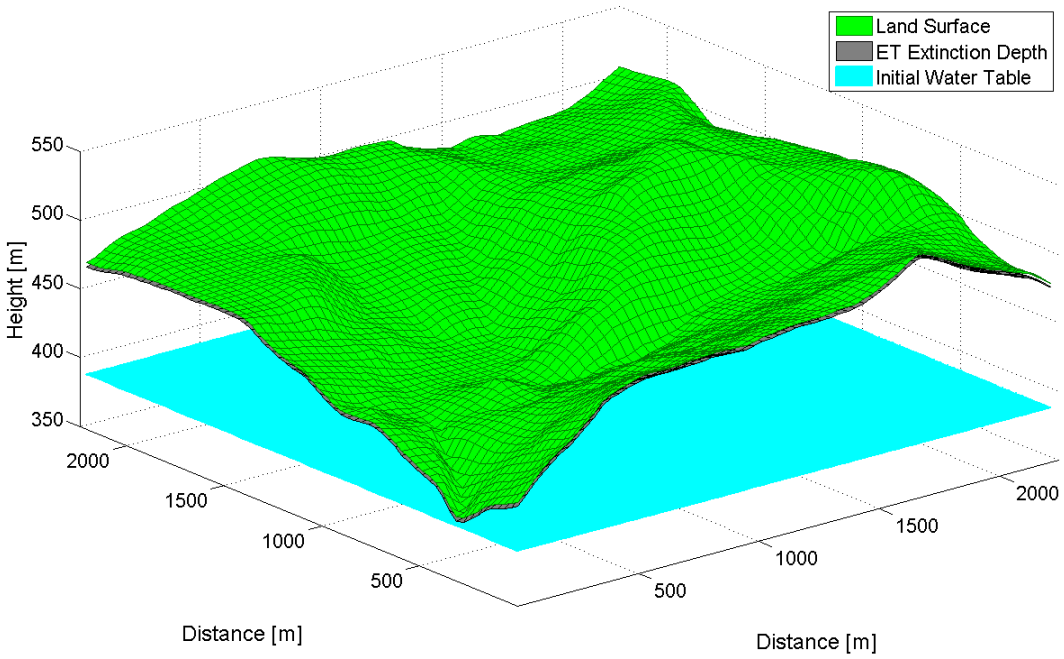

Figure 3.1: Simple DEM used during proof of concept testing

3.2 Fine Scale Modelling

Moving beyond the proof of concept into development of a fully realized upscaling approach required the use of known and established models for benchmarking and validation. Through the use of Modflow (Harbaugh, 2005) and HydroGeosphere (Brunner and Simmons, 2012), more sophisticated simulations were designed that could be used to extract relevant fine-resolution data and, later, to be used in the validation of the UFR upscaling approach.

All fine-resolution models were developed using topographic details from real world locations.

3.2.1 Terrains

Multiple topographic surface configurations were tested during the development of the upscaled method. These terrains were chosen because they were all the same terrain type, but exhibited different geometry, elevation ranges and topographic statistics. For the bulk of the work during this dissertation, hummocky terrains (A-E) (as defined by Howes and Kenk (1997) were chosen as the terrain type to test the upscaling approach. Additional tests on vertical scaling used randomly selected Canadian terrains (F-H). The physical characteristics of the selected topographies can be found in table 3.1. DEMs of terrains A-E are in figure 3.2 and terrains F-H are in figure 3.3.

Terrain	**Terrain Location**	**Resolution**	**Number of Cells**	**Elevation Range**	**Elevation Mean**	**Standard Deviation**
A	Parrsboro, NS, Canada	30 metres	100 x 100	57 - 187 m	174.6 m	20.4 m
B	Southern AB, Canada	30 metres	100 x 100	789 - 847 m	823.2 m	7.2 m
C	Talla Water, UK	30 metres	100 x 100	141 - 219 m	170.8 m	4.6 m
D	Branxton, UK	30 metres	100 x 100	239 - 387 m	344.6 m	8.3 m
E	Postling, UK	30 metres	100 x 100	104 - 178 m	146.5 m	5.3 m
F	Western AB, Canada	30 metres	100 x 100	1192 - 1292 m	1243.4 m	16.3 m
G	Guelph, ON, Canada	30 metres	100 x 100	277 - 373 m	324.7 m	11.8 m
H	Western NS, Canada	30 metres	100 x 100	43 - 119 m	76.3 m	10.8 m

Table 3.1: Digital Elevation Model information

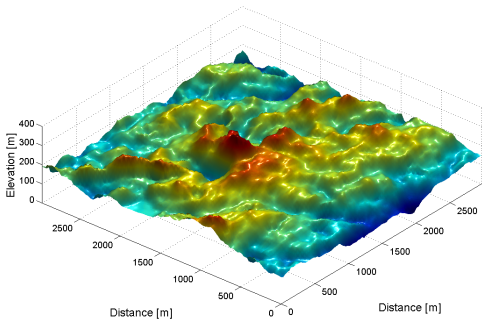

(a)

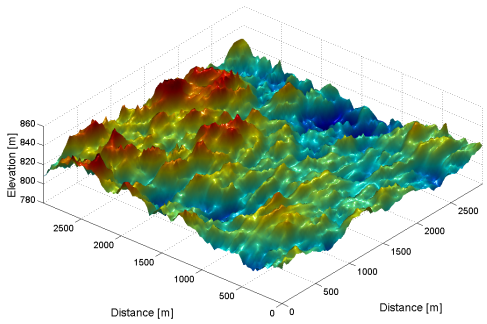

(b)

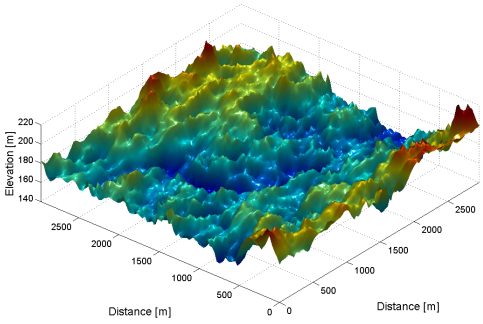

(c)

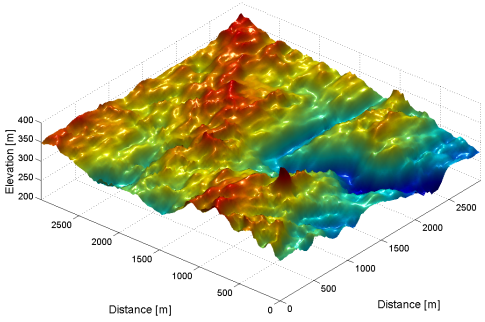

(d)

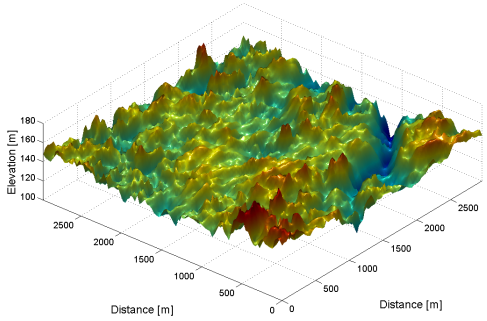

(e)

Figure 3.2: DEMs of hummocky terrains; (a) Terrain A, (b) Terrain B, (c) Terrain C, (d) Terrain D, (e) Terrain E, (f) Terrain F, (g) Terrain G, (h) Terrain H (obtained from LP DAAC (2012)

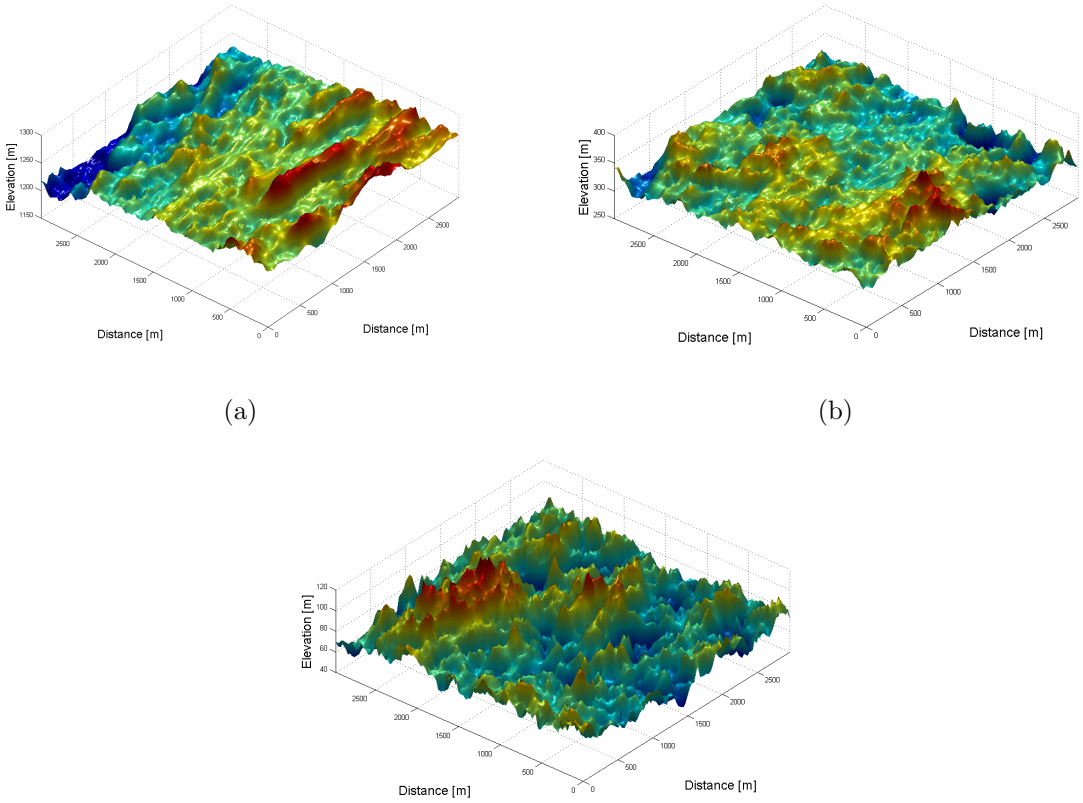

Figure 3.3: DEMs of select Canadian terrains; (a) Terrain F, (b) Terrain G, (c) Terrain H (obtained from LP DAAC (2012)

3.2.2 Overview of Simulations

Saturated steady state, saturated transient and unsaturated transient simulations were conducted using fine-scale 2-dimensional Dupuit-Forchheimer models to determine how GW-SW exchange fluxes and hydraulic head relate to each other and the terrain due to different conditions; saturated/unsaturated, steady state/transient, variation in certain model parameters. Select parameters such as hydraulic conductivity and maximum ET rate were varied between simulations on the same terrains. Specified recharge was directly applied to the water table in all cases and modified to simulate a range of average hydraulic heads in the modelled domain. Specific details on the three types of simulations undertaken are discussed in the following sections. The results of these simulations were then compared to a potentially simpler ("naïve") means of generating UFRs - by simply calculating PET, discharge, and saturated area for each fine resolution DEM cell based upon the uncorrected mean hydraulic head, thus ignoring the important impact of water table and terrain shape (see equations 3.2, 3.3 , and 3.4). Assessment of the accuracy of UFRs at multiple scales was tested using the E30 test case while varying the coarse cell size and vertical scale. Further simulations were conducted to examine the potential sensitivity to mild heterogeneity of hydraulic conductivity.

$$ET_{nv} = \frac{1}{N_C} \sum \left(PET \cdot max \left(1 - \frac{|\bar{h} - h_t^i|}{e_{ET}}, 0 \right) \right) \tag{3.2}$$

$$\text{where } ET_{nv} = 1 \text{ if } \left(\bar{h} - h_t^i\right) > 0$$

$$D_{nv} = \frac{1}{N_C} \sum c \left(\bar{h} - h_t^i\right) \tag{3.3}$$

$$\text{where } D_{nv} = 0 \text{ if } \left(\bar{h} - h_t^i\right) < 0$$

$$SA_{nv} = \frac{1}{N_C} \sum \left(\bar{h} - h_t^i\right) \tag{3.4}$$

$$\text{where } SA_{nv} = 1 \text{ if } \left(\bar{h} - h_t^i\right) > 0$$

where ET_{nv} is the naïve upscaled ET $[LT^{-1}]$, h_t^i is the topographic surface elevation at cell i $[L]$, D_{nv} is the naïve upscaled discharge $[LT^{-}1]$, c is the topographic conductance $[LT^{-}1]$, and SA_{nv} is the naïve upscaled saturated area [-].

3.2.3 Steady State Simulations

Five digital elevation maps for multiple hummocky terrains from Canada and the United Kingdom were used to generate the top boundary of the GW models. Table 3.1 shows the

terrain information for these sites. For each terrain, seven fine-scale test cases were run, varying maximum PET rates and hydraulic conductivities by orders of magnitude (see table 3.2), and simulating a range of average hydraulic heads by modifying recharge rates. In the test simulations, actual subsurface geology of the sites was not incorporated. Instead, the sites were presumed to be homogeneous with a uniform base elevation, to reduce the complexity of the problem. It is here assumed that systems which are nearly homogeneous (in the horizontal direction) will exhibit comparable relationships, though controlled by an effective bulk hydraulic conductivity. No-flow boundary conditions were applied to the outside edges of each simulation. These test cases were 2-dimensional steady state simulations with an unconfined water table and simulated with Modflow. Each case was tested over a range of 18 different constant recharge rates applied at the surface. To assign physically realistic recharge rates, the rule-of-thumb suggested by Haitjema and Mitchell-Bruker (2005) where r/k = 0.2 (where r is specified recharge $[LT^{-1}]$ and k is hydraulic conductivity $[LT^{-1}]$) was used as a starting point. For steady state simulations, a range of r/k between 0 and 0.4 was deemed physically realistic, with r/k = 0.4 representing an extreme physical condition that is unlikely to occur in practice. It should be noted that the recharge rate is moderated in low lying areas by ET and discharge to the surface, and the net recharge (defined as the amount of water discharging minus that recharging) in each steady-state simulation is zero.

Run ***(X = Terrain Letter)***	**Hydraulic Conductivity (m/d)**	**Maximum PET Rate (m/d)**
$X00$ (Base case)	8.64	0.001
$X10$	0.864	0.001
$X20$	0.0864	0.001
$X30$	0.00864	0.001
$X01$	8.64	0.1
$X02$	8.64	0.01
$X03$	8.64	0.0001

Table 3.2: Model variables for 7 variations of simulations using same terrain type

Surface water features were not treated explicitly using Dirichlet or General Head Boundary conditions; rather, the entire ground surface was treated using a drain condition whereby discharge occurs only when the hydraulic head exceeds the ground surface elevation. All water at or above the ground surface elevation is considered discharge through the surface and becomes overland runoff or baseflow. Surface water is not explicitly simulated. It is assumed that all discharged water runs off to a surface water network without

increasing infiltration elsewhere (i.e., no run-off infiltration) and that the depth of surface water (which would moderate discharge estimates) minimally impacts grid-scale fluxes. In all simulations, drain conductance was chosen to be large enough such that the water table did not exceed the topographic surface by a significant amount (i.e., the ground surface provided minimal resistance).

With 5 terrains, 7 parameter combinations per terrain, and 18 recharge rates applied, 630 steady state simulations were conducted in total. All averaged flux diagnostics that were used to produce UFRs for ET versus $\bar{h}$, discharge versus $\bar{h}$, and saturated area versus $\bar{h}$, were then normalized to account for variations in the maximum and minimum terrain elevations, extinction depth, the maximum PET rates and the hydraulic conductivity, using equations 3.5 through 3.9. Normalization of the UFR data makes comparing the various simulations easier and aids in identifying patterns and correlations. The normalized quantities are as follows:

$$t_N = \frac{t - t_{min}}{t_{max} - t_{min}} \tag{3.5}$$

$$h_N = \frac{\bar{h} - t_{min}}{\bar{t} - t_{min}} \tag{3.6}$$

$$ET_N = \frac{\overline{ET}}{PET} \tag{3.7}$$

$$D_N = \frac{\bar{D}}{K} \tag{3.8}$$

$$SA = \frac{\sum_1^{N_c} S_i}{N_c} \qquad \text{where } S_i = \begin{cases} 1 & \text{if } h_i \geq t_i \\ 0 & \text{otherwise} \end{cases} \tag{3.9}$$

where t_N is the normalized topographic elevation [-], t is the topographic elevation $[L]$, h_N is the normalized head, $\bar{h}$ is the average head $[L]$, $\bar{t}$ is the average topography elevation $[L]$, t_{min} is the topographic surface minimum $[L]$, ET_N is the normalized ET, $\overline{ET}$ is the average ET $[LT^{-1}]$, PET is the specified maximum allowable ET $[LT^{-1}]$, D_N is the normalized discharge, $\bar{D}$ is the average discharge $[LT^{-1}]$, K is the hydraulic conductivity $[LT^{-1}]$, SA is the averaged saturated area [-], S_i is the saturated area of a single cell [-],N_c is the number of cells being averaged, h_i is the head in a single cell $[L]$, and t_i is the terrain elevation is a single cell $[L]$.

This method of normalization was selected because it reduced all heads and topographies to a fractional value between 0 and 1 allowing an easy comparison between all terrains, accounting for the maximum potential evapotranspiration rate, and the impact of

hydraulic conductivity with respect to drains. This in the end reduces the exchange fluxes to smaller values and in most cases to a fractional value between 0 and 1. Results for the steady state tests and associated generated UFRs are summarized in section 4.2.1. It is the goal of these tests to verify the hypothesis that UFRs can be used to upscale GW-SW exchange fluxes based on the normalized value of spatially averaged hydraulic head.

3.2.4 Transient Simulations

Multiple fine resolution transient scenarios were also simulated and are summarized in table 3.3. Recognizing that there will be some deviation of the transient relations from the steady-state UFRs, the objective of these transient simulations is to ascertain the degree of this deviation. The constant-term transient cases are denoted as 'quarter', 'half' and 'double' recharge cases with the qualifier referring to the change in steady recharge rate with respect to the recharge rate used to generate the initial conditions. The variable-term transient cases use initial heads from steady state simulations (defined in section 3.2.3) that used the same recharge rate as the first recharge rate in the transient simulation. The constant-term cases are 840 days in duration, use 14 stress periods with 4 timesteps per stress period and were run on each of the 5 terrains. The variable-term cases also use 14 stress periods, each 60 days in length (for a total of 840 days) with 4 timesteps per stress period and were run on each of the 5 terrains. The constant-term cases examined the transition from one steady-state condition to another in response to a single abrupt change in recharge rate (as might be considered in climate change investigations). The variable-term cases use linearly increasing and decreasing recharge rates or fluctuating recharge rates, as defined in table 3.3. For all simulations, a specific yield of 0.22 was used. Results for the transient tests and associated generated UFRs are summarized in section 4.2.2.

Cases	Recharge	# of Stress Periods	Stress Period Length	# of Timesteps	Hydraulic Conductivity	PET rate	Specific Yield
Variable conditions							
Increasing	0.0002 – 0.0012 m/d	14	60 days	4	0.00864 m/d	0.001 m/d	0.22
Decreasing	0.0012 – 0.0002 m/d	14	60 days	4	0.00864 m/d	0.001 m/d	0.22
Fluctuating	0.0002 – 0.0012 m/d (in random order)	14	60 days	4	0.00864 m/d	0.001 m/d	0.22
Constant conditions							
Quarter	0.0005 m/d	14	60 days	4	0.00864 m/d	0.001 m/d	0.22
Half	0.001 m/d	14	60 days	4	0.00864 m/d	0.001 m/d	0.22
Double	0.00346 m/d	14	60 days	4	0.00864 m/d	0.001 m/d	0.22

Table 3.3: Parameters used in transient simulations; steady state model E30 was used for generating initial conditions

3.2.5 Unsaturated Simulations

To explore the potential impact of ignoring vadose zone effects on the generation of UFRs, a 2-dimensional cross-sectional model that includes the vadose zone was developed using the integrated model HydroGeoSphere. The 2-dimensional cross-section consisted of 100 uniformly spaced rectangular cells each 30 metres in length horizontally with 10 layers vertically. The uppermost four layers were one metre in height with the remaining six being uniformly spaced from four metres in depth to the base of the model domain. HydroGeoSphere was set to use a finite difference approach to solve for transient flow and unsaturated conditions with dual nodes at the surface to allow for the capture of exchange fluxes. The soil properties were set to be the same as the parameters (e.g., maximum PET rate, hydraulic conductivity) that were used to implement the E30 test case (see table 3.2). Unsaturated conditions were defined through the use of saturation-relative k and pressure-saturation tables created using the Van Genuchten equation (Van Genuchten (1980); Yang and You (2013)). The Van Genuchten equation is defined as:

$$\theta = \theta_r + \frac{\theta_s - \theta_r}{[1 + |\alpha h|^n]^m} \tag{3.10}$$

where θ is the soil water content $[L^3L^{-3}]$, θ_r is the soil residual water content $[L^3L^{-3}]$, θ_s is the soil saturated water content $[L^3L^{-3}]$, h is the soil water potential $[P]$, α is the scale parameter inversely proportional to mean pore diameter $[L^{-1}]$, n and m are the shape parameters of soil water characteristic. Using equation 3.10, the pressure-saturation table was generated for a range of pressures using the following values; $\theta_r = 0.0025$, $\theta_s = 1$,

$\alpha = 1$, $n = 1.8$, and $m = 0.44$. The relative K values were determined for the range of saturation values in the previous step using:

$$K_{rel} = \theta^2 \tag{3.11}$$

The HydroGeoSphere simulations were conducted using 15 steady recharge rates until quasi-steady state solutions were obtained. Results for the unsaturated tests and associated generated UFRs are summarized in section 4.2.3.

3.2.6 Heterogeneous Hydraulic Conductivity

To examine the potential sensitivity of the UFRs to mild heterogeneity, UFRs were also generated for a mean conductivity equivalent to the E30 case amended with a spatially uncorrelated lognormally distributed random hydraulic conductivity field with a standard deviation of 0.5. Five hundred realizations were run and the range of UFR outputs was assessed. Results of these simulations are shown in section 4.2.4.

3.2.7 Spatial Scale

3.2.7.1 Horizontal Scale

UFRs are intended to be representative of exchange fluxes at coarser scales, however it is unknown if a single UFR may represent the fluxes for an entire watershed or if each subbasin should be represented with its own, or if there is a clear relationship between the UFRs at the watershed scale and at the subbasin scale. To explore this topic, the results of fine-scale simulation E30 were used to generate UFRs for multiple scales. Each subset of the original 100x100 cell fine scale simulation was processed by averaging the hydraulic head, exchange fluxes and saturated area. These values were then normalized as outlined in equations 3.5 through 3.9. Each of the exchange fluxes and saturated area was then plotted against the average head for the subset for the entirety of the simulations run to generate a UFR for each subset. UFRs for a single cell, a 2x2 grid (4 cells), and a 4x4 grid (16 cells) were produced to see if the relationships would be the same, similar or completely different from each other. The results of this are shown in section 4.2.5.

3.2.7.2 Vertical Scale

To assess the impact of vertical scaling on UFR generation, terrains F-H were used to generate fine resolution model results. Each terrain was used in three Modflow simulations;

using its original values, 50% vertically scaled values, and 25% vertically scaled values. The DEM scaling was based upon the range of the elevations using the minimum elevation as a constant data point. The original DEMs along with CDFs of the terrain elevations can been seen in figure 4.12.

Using the same model design as used in the X30 simulations, the three sets of three simulations were conducted so that the exchange fluxes and saturated area could be post-processed and normalized (using equations 3.5 through 3.9). The resulting UFRs were then plotted with the UFRs from the scaled DEMs to investigate changes in UFR shape due to vertical scaling of topographic elevations for the same terrain.

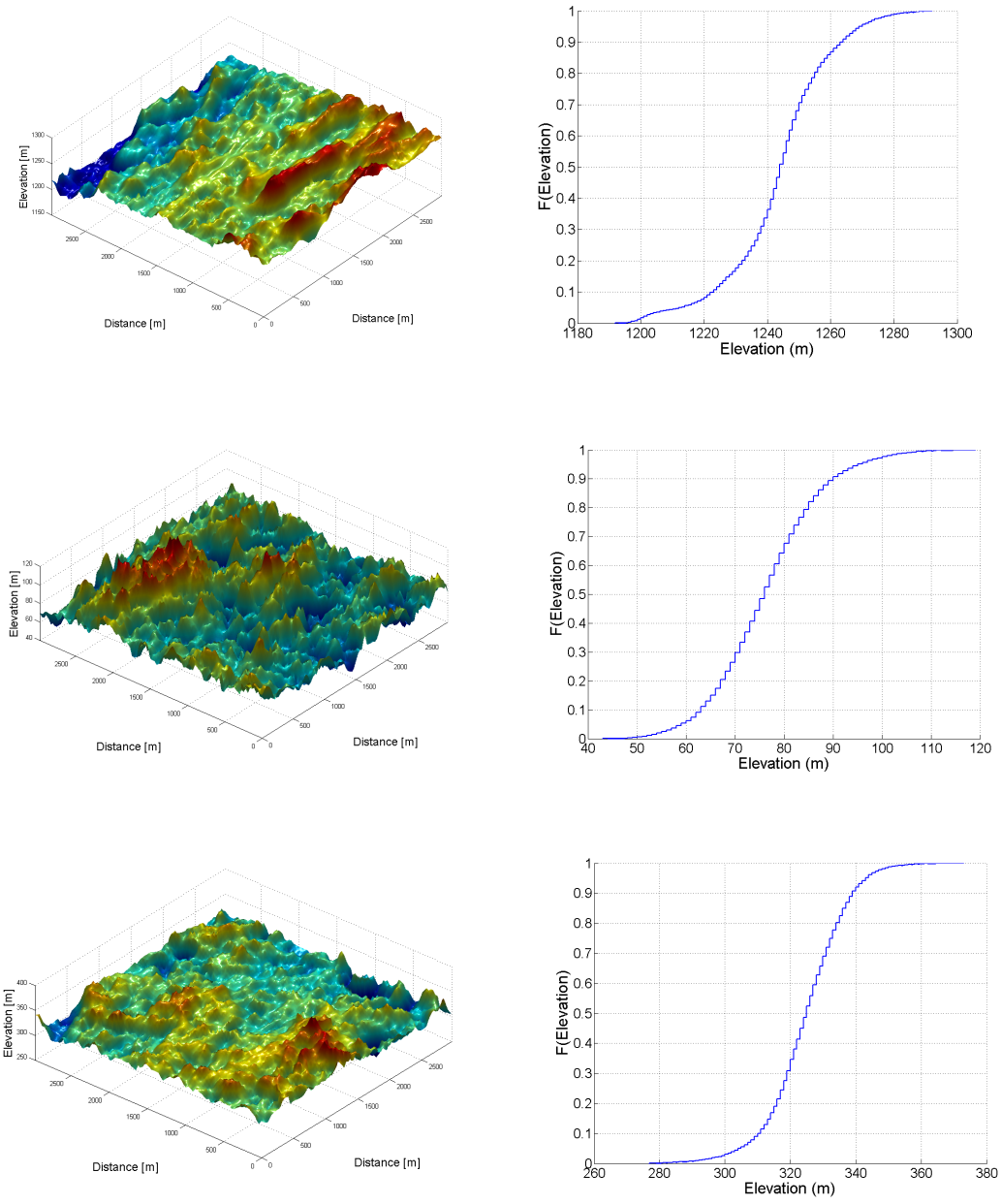

(a) DEM (b) CDF

Figure 3.4: DEMs of terrains F, G, and H along with cumulative distribution functions of topography elevations

3.3 Novel Upscaling Approach

The goal of objective 2 was to evaluate the relationship between bulk exchange fluxes and bulk aquifer storage from the fine-resolution simulations on a specific terrain type in order to determine if generalizable relationships can be discerned for use in coarse-resolution GW-SW models. These relationships are discerned from high-resolution Dupuit-Forchheimer models (as done in Saleh et al. (2011)) under steady-state and transient conditions and used to assess commonalities in upscaled behaviour. To accomplish this, following the development of the fine-scale models, UFRs were generated from simulation results. Using the UFRs, testing could ensue to establish generalizable equations that may be capable of determining the exchange fluxes between groundwater and surface water systems at multiple scales, without the need for first deploying fine resolution simulations.

By using the UFRs, it may be possible to estimate upscaled exchange fluxes for a specific terrain type given a mean hydraulic head. The UFRs could be included in a groundwater component of a model replacing standard pointwise relations between fluxes and head for more appropriate treatment in coarse resolution simulations. Before the UFRs could be used in simulations, it is necessary to test them under various conditions to establish under what conditions they are a valid alternative to fine resolution simulations.

3.3.1 Developing Upscaled Flux Relationships

Figure 3.5 shows how normalized fluxes at the point scale relate to normalized hydraulic head and topography. It can be seen that ET starts at 0 for some depth below the topographic surface and linearly increases until the hydraulic head reaches the topographic surface. At the topographic surface, ET is at a maximum value where it stays constant for further increases in hydraulic head. Discharge is 0 until the hydraulic head reaches the topographic surface where it begins to increase. It will continue to increase as hydraulic head increases. Saturated area is 0 until hydraulic head reaches the topographic surface where it becomes 1 representing full saturation of the ground surface. Saturated area cannot exceed 1 (or fully saturated) so this will remain 1 if hydraulic head does not decrease below the topographic surface. The use of point-scale processes is effective when used for fine-scale operations but breaks down when applied during upscaling to coarser resolutions.

In order to characterize the relationships between coarse-resolution state variables (e.g., average hydraulic head) and coarse-resolution exchange fluxes, an empirical approach was taken based upon generalizing the results from fine-resolution simulations. Post-processing to average data at multiple coarse cell sizes was used to develop UFRs between spatially

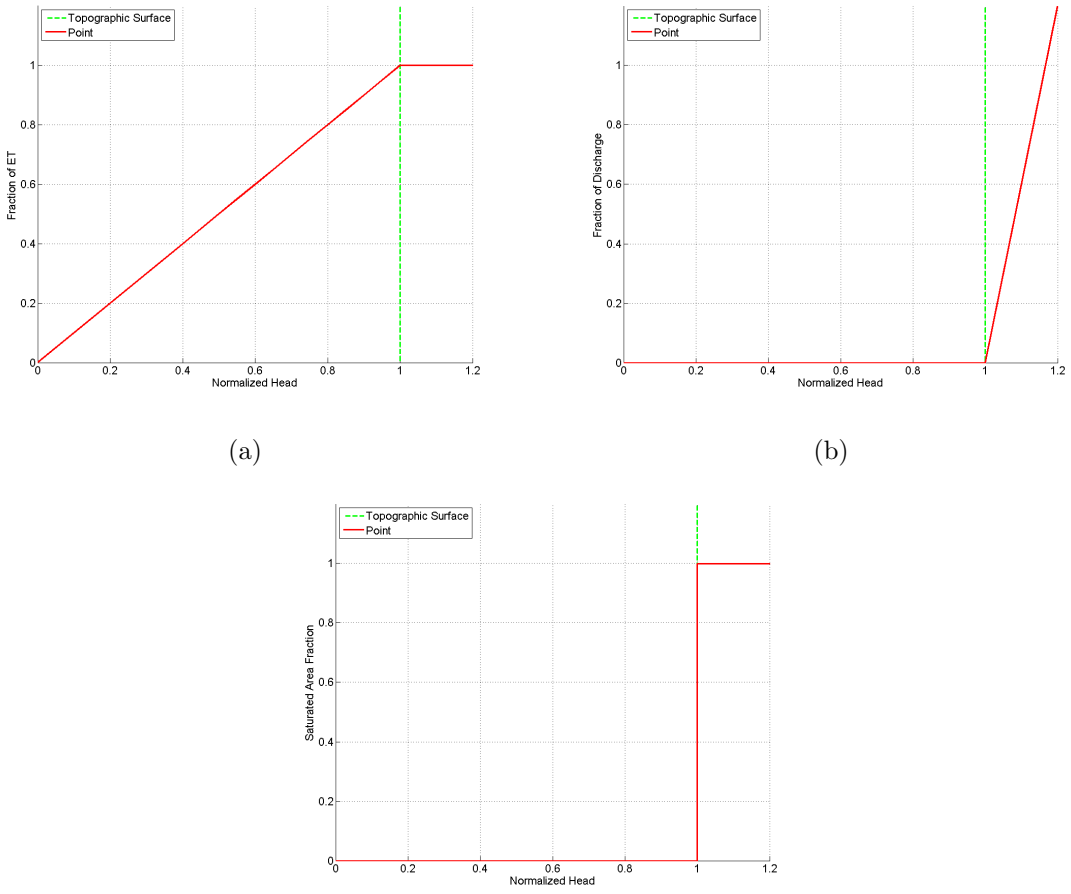

Figure 3.5: Point scale exchange flux rates for (a) ET, (b) discharge and (c) saturated area

averaged hydraulic head and spatially averaged exchange fluxes (see figure 3.6), with a focus on the relationships between hydraulic head, ET, discharge, and saturated area. It is expected that UFRs will follow a power law trend which controls the general shape of the UFR. In theory, a UFR should pass through point (1,1) which would signify that the normalized process rate and normalized head have both reached their maximum value, however this may not always be the case when additional fluxes are added such as in cases where pumping wells exist. It is expected that pumping wells will not change the shape of UFRs significantly since UFRs are intended to be applied at regional scales. Additionally, discharge curves may not pass through (1,1) for processes like discharge as discharge rates do not have a maximum value.

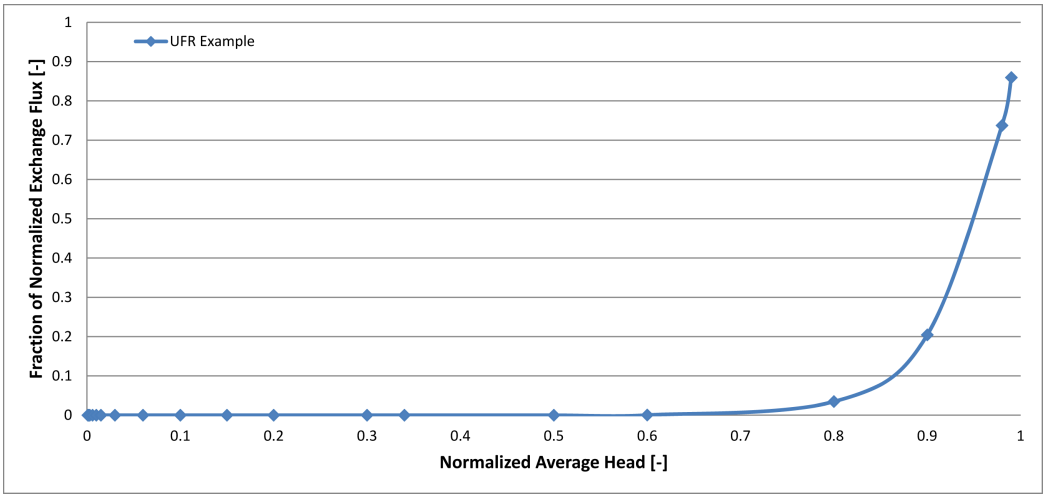

Figure 3.6: Example UFR showing relationship between normalized process and normalized hydraulic head

Here, focus is upon the assessment of horizontal scale effects when moving to coarser resolutions in fully-saturated and unsaturated models with the aim of understanding these scaling issues under controlled conditions; this work can later be repeated with fully-coupled models allowing a more complicated treatment of the groundwater-surface water interface, as advocated by Camporese et al. (2010).

At steady state, the relationships between spatially averaged head and spatially averaged fluxes with respect to terrain is assumed to be described by equation 3.12, the upscaled version of equation 2.2:

$$\frac{\partial}{\partial x}\left(K_n b_n \frac{\partial \bar{h}_n}{\partial x}\right) = D\left(\bar{h}_n\right) + ET\left(\bar{h}_n\right) - R\left(1 - \frac{A_S\left(\bar{h}_n\right)}{A}\right) \tag{3.12}$$

where b_n is the saturated thickness of cell n $[L]$, $\bar{h}_n$ is the average hydraulic head for cell n $[L]$, D is the upscaled drain rate $[LT^{-1}]$, ET is the upscaled evapotranspiration rate $[LT^{-1}]$, R is a specified recharge rate $[LT^{-1}]$, A_S is the saturated surface area $[L^2]$, and A is the total surface area $[L^2]$. The assumption here is that lateral flow is still controlled by Darcy's law, but surface flux relations are different at the point scale versus regional scales (i.e., the expression on the right hand side of equation 3.12 can be replaced with empirically determined UFRs). Since UFRs represent a coarser scale incorporating a range of topographic elevations, it may be assumed that there is a smoothing effect which results in the gentle curve versus the abrupt changes of the point scale approach. The shape and degree of smoothing is analyzed and discussed in section 4.2.2.

As was just mentioned, the method for discerning UFRs in this research was primarily through the use of fine-scale simulations, but two other approaches will be used. The second method requires extracting terrain indices (see table 3.4) using GIS software such as ArcMap and then conducting a linear regression analysis to generate an equation based upon those indices that is capable of replicating the UFR. This approach is explained in section 3.3.2. The third method to find UFRs is via calibration after assuming a specific functional form of the UFRs with adjustable parameters. By calibrating for power law coefficients during simulations, it is possible to determine the UFR for a particular terrain. This method is applied during test cases 1 and 2 and the results are summarized in sections 4.5 and 4.6, respectively.

3.3.2 Regression-Based UFR Parameterization

Following the generation of the UFRs, multiple approaches were attempted to establish a method of determining generalizable equations that could be used for a specific terrain type at a coarse scale. The goal was to develop general equations to describe exchange fluxes at a regional level, with the assumption that terrain characteristics dominate the estimation of power law coefficients determined using the methods of section 3.2.

First, terrain indices that could be used to classify each terrain were determined using ArcMap. The parameters that were considered key terrain indices (as suggested by Günter et al. (2004) and Jencso and McGlynn (2011)) are listed in table 3.4.

Using the 16 parameters in table 3.4 for each terrain along with both power law and exponential functions as templates, multiple stepwise linear regression analyses (Montgomery

Hydraulic Conductivity	Max. PET Rate	ET Extinction Depth	Max. Topography Height
Min. Topography Height	Mean Topography Height	Standard Deviation of Topography	Skewness of Topography
Kurtosis of Topography	Aspect	Curvature	Flow Accumulation
Flow Length	Slope	Upslope Area	Wetness Index

Table 3.4: Terrain indices used for relationship analyses

et al., 2012) were performed using Matlab. The regression analyses were used to determine generalizable relationship equations determined from the UFRs for all fine-scale simulation results with the intention of developing standalone equations using the terrain indices to characterize exchange flux rates given an average hydraulic head. The basic functions for evapotranspiration, drainage and saturated area are as follows:

$$\overline{ET} = F\left(\overrightarrow{P}, \overrightarrow{h}\right) = \bar{h}^{\beta} \tag{3.13}$$

$$\overline{D} = F\left(\overrightarrow{P}, \overrightarrow{h}\right) = \alpha\bar{h}^{\beta} \tag{3.14}$$

$$\overline{SA} = F\left(\overrightarrow{P}, \overrightarrow{h}\right) = \bar{h}^{\beta} \tag{3.15}$$

where the parameters α and β for each power law are functions of the terrain index vector $\overrightarrow{P}$. The results of the regression analysis were tested using 1134 additional fine-scale simulations that were conducted using 9 previously unused hummocky terrains. Results for the regression analyses, the test cases and the equations determined are in section 4.2.6.

3.4 Implementation of a Coupled Model

A new groundwater model, for use at the basin to regional scale, was developed using a control volume finite difference method which was then coupled with Raven (Craig and the Raven Developement Team, 2013). This is in line with objective 4 of this dissertation.

3.4.1 Raven

Raven is an object-oriented open source hydrological model. It is a mixed lumped/semi-distributed model that was designed to be flexible and adaptable. It allows users to understand the hydrological operations of watersheds for streamflow analysis, climate prediction, flood potential, as well as long-term mass and energy balances. Users can select specific

process algorithms to build a custom simulation and therefore easily tailor Raven to solve a specific hydrological problem.

Raven calculates the redistribution of mass and energy between state variables (i.e., storage units such as soil) via hydrologic processes (e.g., infiltration). To do this, Raven's input files specify the model type (i.e., surface water, single soil layer, multi-layer soil), the physical characteristics (i.e., land use, soil properties, HRUs properties) and the hydrologic processes that will be simulated. The model type dictates whether Raven is to be operated as a standalone model or if it should act as the GW and SW systems are coupled. The number of soil layers determines, in part which hydrological processes can be used, and the complexity of the shallow GW system. The physical characteristics are the set of parameters that are necessary to describe and/or calculate real world conditions (e.g., radiation, wind, precipitation) ensuring that the model can replicate accurate approximations of a physical environment. During a simulation, Raven calculates the movement of water/energy in a stream network by moving from upstream to downstream through subbasins via their HRUs where it determines the flux rates between the state variables controlled by the hydrologic processes chosen by the operator (see figure 3.7). The hydrological processes that determine the flux rates are represented using recognized empirical and analytical methods

Raven was initially developed with a focus on surface water processes with a simplified groundwater system. It lacked the ability to calculate lateral groundwater flow. The addition of a unique groundwater component to Raven was completed for this research.

3.4.2 New Groundwater Component

Raven's new groundwater component is a CVFD model that works with unstructured grids. The addition of this CVFD GW component required incorporating new input files that specify an unstructured grid for aquifers, the inclusion of new process algorithms for calculating exchange fluxes in both the traditional and UFR approaches, additional solvers for the solution of lateral flow that could handle the non-linear and linear system of equations, and implementation of the algorithm for coupling the GW and SW systems. Figure 3.7 shows a flow chart of Raven's SW operations with the new GW component included.

The coupling of Raven and the new groundwater component is unique in that the mass/energy balance for all the HRUs, including the associated aquifers, is calculated simultaneously with the lateral GW flow within the aquifer handled via operator splitting (Farago, 2008). Operator splitting is a process of decomposing complex sets of equations

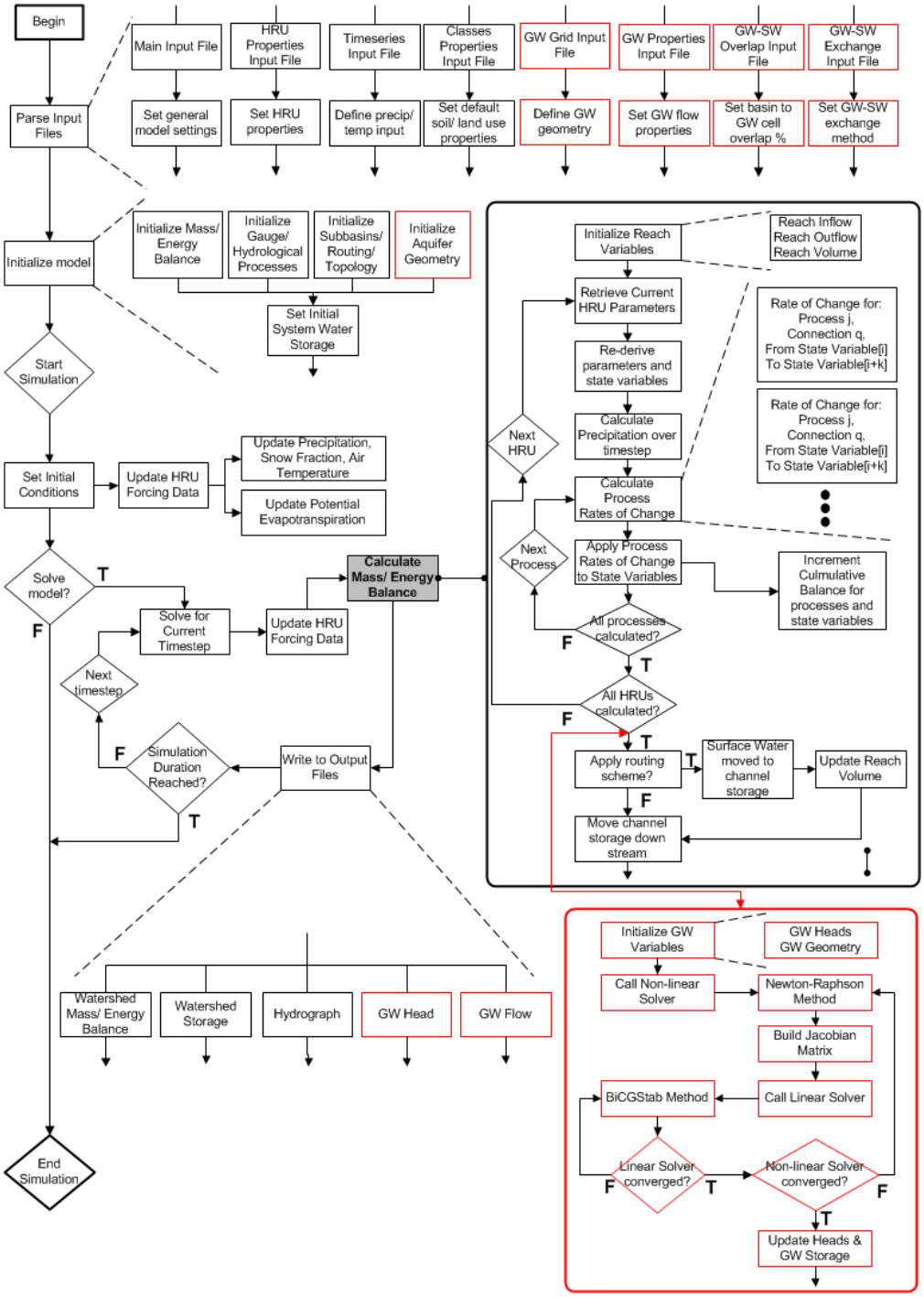

Figure 3.7: Flowchart of Raven simulation with new groundwater component (highlighted in red) (modified from Snowdon (2009) and Craig and the Raven Developement Team (2013))

in order to solve each one with its own specialized algorithm or numerical method. This makes solving the individual aspects simpler. The output from each individual operation is then able to be reported back to the global system to be used as feedback for the next operation. This makes almost all feedback between the two systems occur simultaneously without the need to run the two models independently.

While designing the groundwater component of the model, many design choices had to be taken into consideration. Coupling a transient groundwater to an existing surface model requires understanding where the optimal location in the code is to add the communication or feedback between the systems. The bulk of the groundwater component is defined in new object classes that define the geometry and properties of the aquifers. Likwise, new classes for the groundwater geometry, the groundwater stress periods, the surface water-groundwater cell overlap, and the UFR exchange flux parameters were created. An additional class created by James Craig and Richard Simms for conducting sparse matrix operations was modified for this research (Simms, 2013) and incorporated into Raven. New input files were created to be parsed by Raven which characterize these new classes for simulations. The heart of the groundwater component is the groundwater solver. As will be discussed in section 3.4.5, the groundwater solver is approached in two parts; an outer and an inner solver.

Since Raven was already designed with HRUs as the primary computational unit, it was decided to link each HRU to an aquifer stack (i.e., a vertical representation of the aquifer below the HRU). This allows the groundwater mesh to be unstructured, like the surface water mesh, and at the same scale as the surface water cells while simplifying the number of connections between the GW and SW systems. Each HRU communicates directly to a single aquifer cell (but only if the SW and GW cells are 1:1). Each aquifer stack can be vertically divided into layers in the same manner as the soil profiles defined for the surface water model (which allows for vadose zone simulation).

Hydraulic head in the aquifers is not explicitly represented. Instead, water in the aquifers is represented using a water storage value, in millimeters, to be consistent with the SW mass balance in Raven. These storage values are converted to hydraulic head prior to solving for lateral flow. The hydraulic head values (post lateral solution) are then converted back to storage values to keep consistent with Raven's formatting. This allows Raven to calculate the global mass balance using existing methods without revision.

Several new hydrologic process algorithms were added to Raven's libraries to calculate exchange fluxes. Specified recharge, evapotranspiration (both a linear function based on Modflow's and the UFR approach), and surface drains (both a conductance approach similar to Modflow's and the UFR approach) were included.

The operation of Raven with the added groundwater component is summarized in the flowchart of figure 3.7. When the model starts, it parses the input files for the surface water system, groundwater system, time series data, and initial conditions. The model is initialized and proceeds marching forward in time. Each process is solved, for each HRU, and the associated state variables are updated to reflect the removal and addition of moved mass. After this, the updated storage for the aquifers is converted to hydraulic head and the lateral flow groundwater solver is called. It solves for lateral flow before providing feedback to the surface water system with new head values which can then be converted to storage.

3.4.3 Sparse Matrix Storage

Groundwater models require the storage of a large amount of information that characterizes the coefficients and parameters needed to solve the GW flow system of equations. This information is typically stored in matrices which have the potential to become very large and can increase the computational burden of the model. To minimize the memory required to store large matrices, it is beneficial to use a sparse matrix storage method. In hydrological models, a majority of the values stored in matrices are zeroes and these zeroes use valuable memory. By only storing the non-zero values, the amount of memory needed to store a matrix is greatly reduced.

For this research, a modified Compressed Sparse Row (MSR) storage method (Press et al., 1992) was implemented (see equation 3.16). This storage scheme greatly reduces the amount of data being stored by eliminating all the zero values (that are not diagonal values).

$$\begin{pmatrix} 2 & 1 & 0 & 0 \\ 0 & 4 & 3 & 5 \\ 7 & 0 & 6 & 0 \\ 0 & 0 & 0 & 8 \end{pmatrix} = \begin{matrix} \begin{bmatrix} 2 & 4 & 6 & 8 & * & 1 & 3 & 5 & 7 \end{bmatrix} & \text{(value array)} \\ \begin{bmatrix} 5 & 6 & 8 & 9 & 9 & 1 & 2 & 3 & 0 \end{bmatrix} & \text{(index array)} \end{matrix} \tag{3.16}$$

3.4.4 Unstructured Grid Control Volume Finite Difference

In designing the low-resolution coupled model, the discretization of the surface water and groundwater components is done as suggested in the overview of objective 4 (see section 1.2.4). Recall that two of the discretization options were a 1:1 GW-SW basin discretization and a M:N GW-SW exchange. The surface water and new groundwater components of

Raven were built to allow for both of these options. An example discretization using similar unstructured spatial grids or meshes for both the SW and GW systems can be seen in figure 3.8.

The coupled model contains surface water cells which are defined by the basins, subbasins and/or HRUs of a watershed as well as groundwater cells which are defined using Voronoi polygons. Surface water cells were defined by the basin/subbasin boundaries using ArcMap. The groundwater cells were then created from the surface water cells in order to provide a mesh that has equal distances between cell centroids. The SW and GW cells share the same centroid.

Since the surface water basins and groundwater cells are not required to share the same boundaries (in an M:N GW-SW discretization), it is necessary to determine the amount of overlap between the GW and SW cells in order to ensure that the exchange fluxes are occurring between the correct GW and SW cells. A python script was used that analyzes Arcmap shape files for the SW cells and GW cells and then generates a table with the percentage of overlap. This table is then able to be used as an Raven input file to determines exchange fluxes using an area-weighted flux distribution approach:

$$F_i = \sum \frac{A_j F_j}{A_i} \tag{3.17}$$

where F_i is the flux to the surface water cell $[LT^{-1}]$, A_j is the area of the groundwater cell $[L^2]$, A_i is the area of the surface water cell $[L^2]$,and F_j is the flux to the groundwater cell $[LT^{-1}]$.

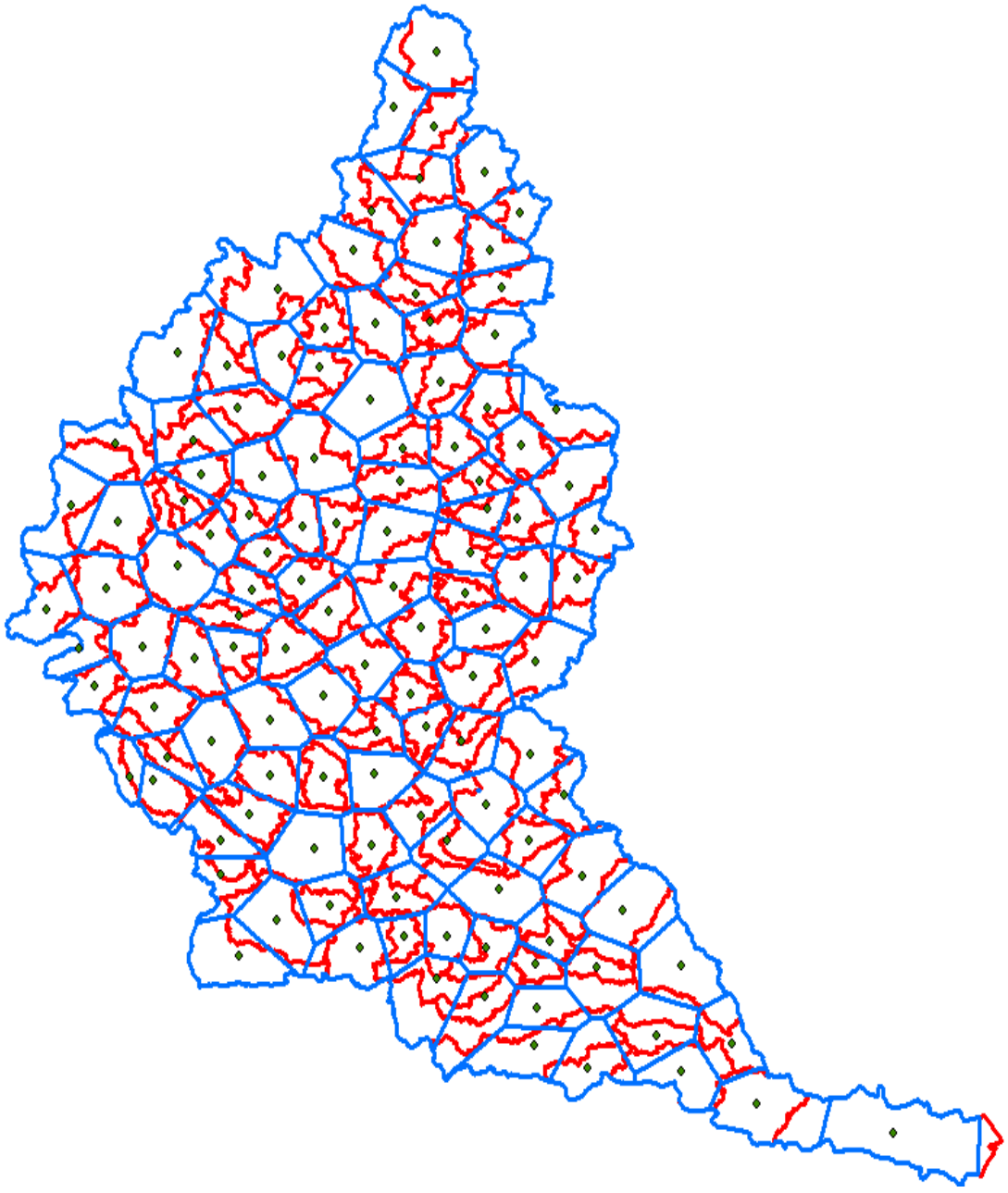

Figure 3.8: Unstructured meshes for GW and SW cells using similar discretization. Surface water cells are outlined in red, groundwater cells in blue. Cell centroids are marked with points

3.4.5 Solver

To solve for groundwater flow when using an unstructured grid (equation 3.1), a nonlinear solver is required. As mentioned in chapter 2, an outer solver such as the Newton-Raphson method is first used to linearize the non-linear system of equations which can then be solved by the inner solver.

Before understanding the Newton-Raphson method, it is necessary to discuss the Jacobian matrix. The Jacobian matrix is an integral part of linearizing a non-linear system of equations. A Jacobian matrix consists of all the first order partial derivatives of a vector of functions with respect to a vector of influential parameters. The Jacobian matrix, required with the Newton-Raphson method, allows a system of non-linear equations to be solved with a linear approach. The Jacobian of a function is an MxN matrix usually in the form of:

$$\begin{pmatrix} \frac{\partial R_1}{\partial h_1} & \cdots & \frac{\partial R_1}{\partial h_n} \\ \vdots & \ddots & \vdots \\ \frac{\partial R_m}{\partial h_1} & \cdots & \frac{\partial R_m}{\partial h_n} \end{pmatrix} \tag{3.18}$$

where R is a vector-valued function (with N-input parameters and M-dimensional outputs) and h_j is an input to the function R.

The Newton-Raphson method is used to solve non-linear algebraic equations and is well suited for use in CVFD models. The Newton-Raphson method saves time and reduces the solution complexity by solving the system of equations without requiring direct inversion of the Jacobian matrix. The Newton-Raphson method can be described using:

$$\mathbf{J}_R\left(\vec{h}^k\right)\left(\vec{h}^{k+1} - \vec{h}^k\right) = -R\left(\vec{h}^k\right) \tag{3.19}$$

where $\mathbf{J}_R$ is the Jacobian matrix, $\vec{h}$ is the iterate value of interest (in the proposed algorithm, h = hydraulic head) and R is the residual vector. The residual vector, for this application, contains the flow residual or mass balance error for each cell. Linearization of equation 3.19 is accomplished by recognizing that, for a single estimate of h_n, its form is equivalent to the linear expression:

$$\mathbf{A}\vec{h} = \vec{b} \tag{3.20}$$

By expanding equation 3.19 using equation 3.20, the matrix form of the Newton-Raphson method is seen:

$$\begin{pmatrix} \frac{\partial R_1}{\partial h_1} & \cdots & \frac{\partial R_1}{\partial h_n} \\ \vdots & \ddots & \vdots \\ \frac{\partial R_m}{\partial h_1} & \cdots & \frac{\partial R_m}{\partial h_n} \end{pmatrix} \begin{pmatrix} \vec{h}_1^{k+1} - \vec{h}_1^{k} \\ \vdots \\ \vec{h}_n^{k+1} - \vec{h}_n^{k} \end{pmatrix} = - \begin{pmatrix} R_1 \\ \vdots \\ R_n \end{pmatrix} \tag{3.21}$$

where k signifies the iteration number.

The Newton-Raphson method consists of a series of iterations that are performed until a convergence criteria has been satisfied. The set of linear equations (equation 3.21) can then be solved using a linear solver such as the Picard Method or a BiCongugate Gradient method for each iteration. The linear solver of interest in this research is the BiConjugate Gradient (Stabilized) method (BiCGStab). BiCGStab (a variant of the BiConjugate Gradient method that converges faster and more smoothly) is an iterative method for the solution of nonsymmetric linear systems (Van der Vorst, 1992).

To modify the Newton-Raphson method so that it solves for groundwater head and not an update in head, equation 3.19 was recast in the following form:

$$\mathbf{J}_R\left(\vec{h}^k\right)\left(\vec{h}^{k+1}\right) = -R\left(\vec{h}^k\right) + \mathbf{J}_R\left(\vec{h}^k\right)\left(\vec{h}^k\right) \tag{3.22}$$

Then, equation 3.1 can be simplified using the following definitions:

$$C_{nm} = \frac{A_{nm}K_{nm}}{L_{nm}} \tag{3.23}$$

$$Q_C = \frac{-S_{Sn}V_n}{\Delta t} \tag{3.24}$$

$$RHS_n = \frac{-S_{Sn}V_n h_n^{t-1}}{\Delta t} \tag{3.25}$$

Leading to a set of non-linear equations:

$$\sum \left(C_{nm}\left(h_m^t - h_n^t\right)\right) + Q_C - W^* - RHS_n = R_n \quad n = 1..NC \tag{3.26}$$

where R_n is the residual to be minimized. W^* is ignored in the groundwater implementation beyond this step as all flux terms are handled in Ravens global surface water solver via operator splitting. (If the exchange fluxes were to be solved by the groundwater solver, all sinks/sources that are head dependent would be including in the RHS_n term and all sinks/sources that are not head dependent would be included in the Q_C term.) Partial

derivatives of the residual with respect to the unknown hydraulic heads are determined to construct the Jacobian matrix for use in the Newton-Raphson method (equation 3.21) as follows:

$$\frac{\partial R_n}{\partial h_n} = Q_C - \frac{\partial RHS_n}{\partial h_n} + \sum \frac{\partial Q_{nm}}{\partial h_n} \tag{3.27}$$

$$\frac{\partial R_n}{\partial h_m} = \frac{\partial Q_{nm}}{\partial h_m} \tag{3.28}$$

$$R_n = Q_C \left(h_n^{k-1}\right) - RHS_n + \sum Q_{nm} \tag{3.29}$$

$$Q_{nm} = C_{nm} \left(h_m - h_n\right) \tag{3.30}$$

$$\frac{\partial Q_{nm}}{\partial h_n} = -C_{nm} f\left(h_{us}\right) + C_{nm} \frac{\partial f\left(h_{us}\right)}{\partial h_n} \left(h_m - h_n\right) \tag{3.31}$$

$$\frac{\partial Q_{nm}}{\partial h_n} = C_{nm} f\left(h_{us}\right) + C_{nm} \frac{\partial f\left(h_{us}\right)}{\partial h_m} \left(h_m - h_n\right) \tag{3.32}$$

where C_{nm} is conductance term $[L^2T^{-1}]$, Q_C is the coefficient of flow $[L^2T^{-1}]$, Q_{nm} is the flow between cells n and m $[L^3T^{-1}]$, R_n is the residual of the function for cell n, and $f(h_{US})$ is a smoothing function that eases the discontinuities between cells [-] (Panday et al., 2013). Subbing equations 3.23 through 3.25 and 3.27 through 3.32 into equation 3.22 linearizes the groundwater flow equations so that they are in the form of equation 3.20 and are capable of being solved through the use of a linear solver. This approach is very similar to that used in the new unstructured version of Modflow (Panday et al., 2013).

3.4.6 Implementation of Exchange Fluxes

Traditionally, exchange fluxes in an individual grid cell are calculated using the same equations used at the point scale. This method works well when the cells for the GW and SW systems are small enough that point scale representation is appropriate (e.g., 1 m^2). However, at larger scales, point scale physics are not appropriate and this can lead to inaccurate exchange flux rates. Raven's point scale process equations are here used for comparison purposes with the new upscaling approach.

Upscaled flux relationships are implemented in Raven as a lookup table describing the UFR curve. The relationships are applied through the interpolation of curve data and, eventually, through the expression of generalized relationship equations. Raven uses a cell's upscaled head value to calculate the appropriate exchange flux rate to be used in equation 3.12.

3.5 Testing

Several tests have been developed to investigate the accuracy and validity of the new upscaling GW-SW exchange method within Raven. Benchmarking, model comparison and real world application have been tested as outlined in the following sections.

3.5.1 Benchmarking - Modflow versus Raven

To benchmark Raven's new groundwater component, it was compared to Modflow simulation results using terrain E (figure 3.9). Both Raven and Modflow simulations were set up using a regular grid with traditional exchange flux methods (see equations 2.4 and 2.5). A 100 by 100 cell grid was used with grid spacings of 30 metres (figure 3.9). These simulations were transient with 365 timesteps, each 1 day in duration, with a fixed recharge flux, linearly varying ET flux and uniform drainage conductance in every cell.

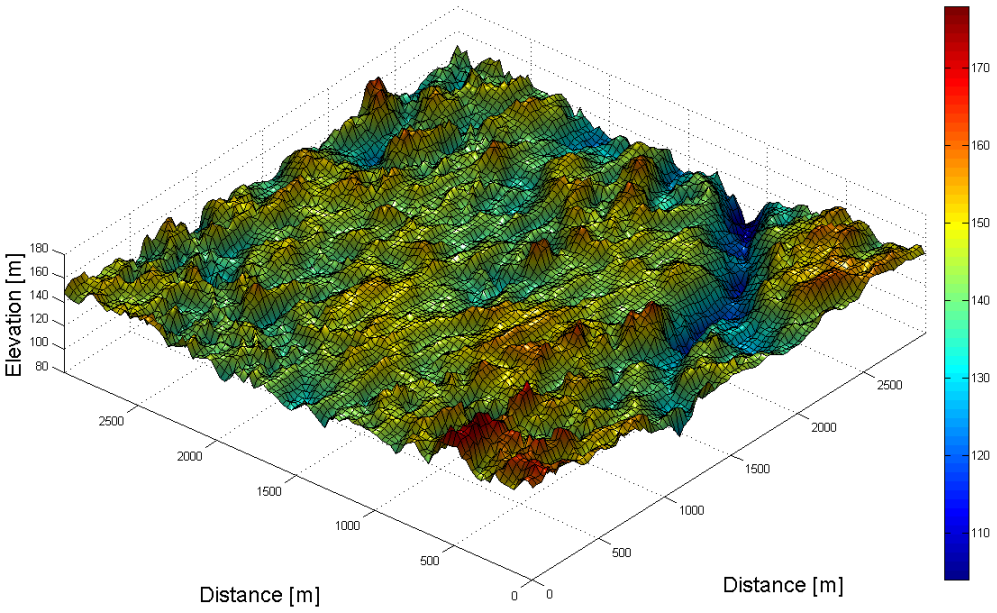

Figure 3.9: Surface plot of terrain E with mesh overlay used in benchmarking of Raven with Modflow

Recharge was fixed at 10 mm/d, maximum ET was 5 mm/d and drains exist at every surface node as described in section 3.2.3. A comparison between Modflow and Raven was performed to assess the accuracy of Raven's groundwater component for simulating saturated lateral groundwater flow and GW/SW exchange fluxes. All parameters and grid were identical for Modflow's and Raven's simulations.

3.5.2 Test Case 1 - Unstructured versus Structured Grid

This test case was the first test of Raven's groundwater component using the novel upscaling approach. An upscaled unstructured grid was implemented in Raven and a regular grid was used in Modflow. The Raven grid consists of 16 unstructured cells of varying sizes (see table 3.5, figure 3.10) while Modflow's grid is a 16 by 16 rectangular mesh (30m by 30m cells) for a total of 256 cells. UFRs were used to calculate GW-SW exchanges in the coarse unstructured Raven model while traditional exchange flux methods were used in Modflow. Calibration of the hydraulic head in Raven was accomplished by adjusting the power law coefficients that govern the UFRs for drainage and ET. Each cell has a potentially unique UFR for describing ET and discharge. Each UFR has an α and a β coefficient that are able to be calibrated to adjust the exchanges. 16 groundwater cells with two coefficients for each UFR results in 64 calibration parameters. Figure 3.11 shows the terrain that was used during this test case and figure 3.10 shows the unstructured grid used by Raven to defined the groundwater system. Results for test case 1 are summarized in section 4.5.

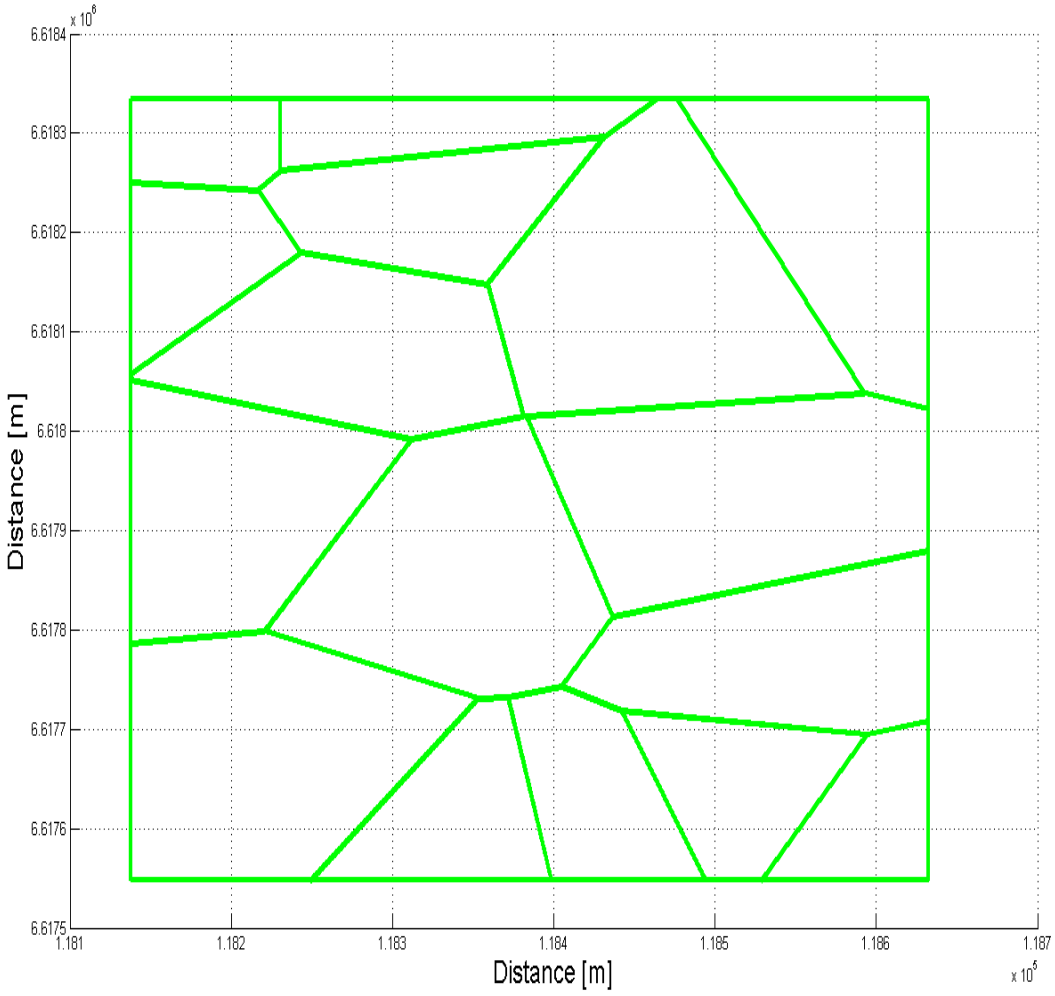

Figure 3.10: Unstructured groundwater cell grid used in test case 1

Aquifer Cell	Soil Type	Top Layer Elevation [m]	Thickness [m]	Area [m2]	Hydraulic Conductivity [m/d]	Specific Yield [1/m]
AQ1	Sand	149.25	149.25	8082.147	0.864	0.181
AQ2	Sand	152.4	152.4	11714.44	0.864	0.181
AQ3	Sand	147.91	147.91	19009.96	0.864	0.181
AQ4	Sand	142.88	142.88	12535.14	0.864	0.181
AQ5	Sand	147	147	29243.98	0.864	0.181
AQ6	Sand	141.47	141.47	29378.31	0.864	0.181
AQ7	Sand	141.28	141.28	44792.03	0.864	0.181
AQ8	Sand	145.08	145.08	41341.29	0.864	0.181
AQ9	Sand	145.53	145.53	30583.5	0.864	0.181
AQ10	Sand	146.82	146.82	38007.542	0.864	0.181
AQ11	Sand	143.76	143.76	28994.405	0.864	0.181
AQ12	Sand	151.21	151.21	39532.005	0.864	0.181
AQ13	Sand	154.11	154.11	15422.448	0.864	0.181
AQ14	Sand	152.4	151.4	15071.391	0.864	0.181
AQ15	Sand	143.56	143.56	14933.111	0.864	0.181
AQ16	Sand	139.83	139.83	10711.128	0.864	0.181

Table 3.5: Unstructured cell properties for test case 1

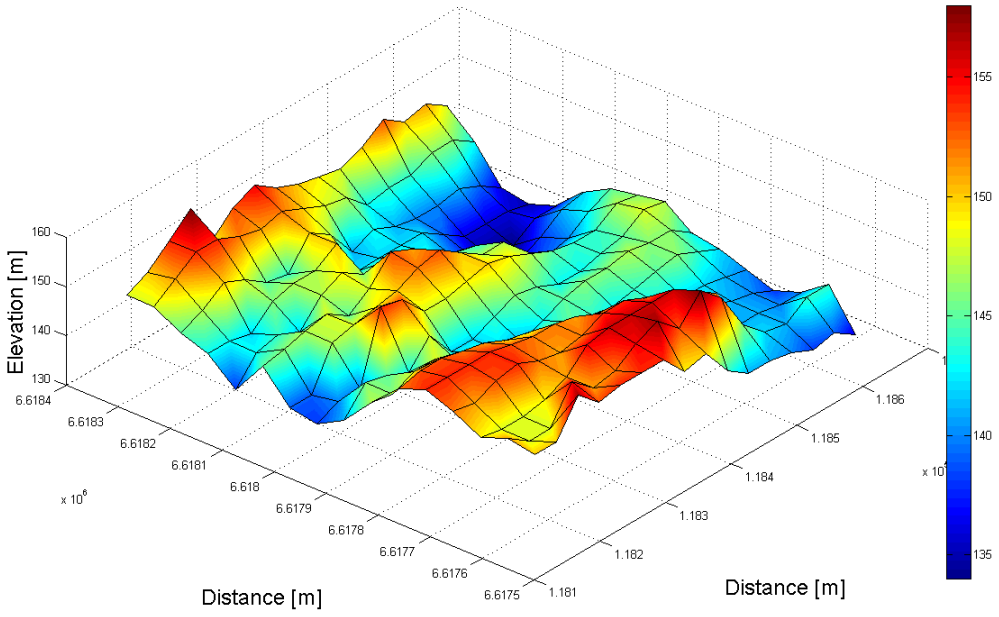

Figure 3.11: Surface plot of terrain with mesh overlay used in test case 1

3.5.3 Test Case 2 - Real World Test Case

A comprehensive test of Raven's coupled surface water /groundwater model is needed to verify its accuracy. The Grand River watershed in southern Ontario, Canada will be used for this test. The surface water model was modified from a surface water model of the Grand created by Mahyar Shafii (Shafii, 2015). The Grand River watershed is located at 44° north and 80.32° west. Its elevation ranges from 170 masl to 540 masl (see figure 3.12). Land use in the basin is forested, agriculture and urban areas. Aquifer soils are a clayey silt overlain by a metre of sandy silt. There are 122 subbasins (see figure 3.13) identified and a comprehensive set of flow gauges (see table 3.6) and groundwater monitoring wells (see table 3.7).

STATION	**Description**	**Latitude**	**Longitude**
2GA039	CONESTOGO RIVER ABOVE DRAYTON	43°47′0.3”	80°38′14”
2GA003	GRAND RIVER AT GALT	43°21′11”	80°18′57”
2GA015	SPEED RIVER BELOW GUELPH	43°31′35”	80°15′38”
2GA014	GRAND RIVER NEAR MARSVILLE	43°51′41”	80°16′20”
02GA006	CONESTOGO RIVER AT ST. JACOBS	43°32′28”	80°33′12”
02GAC06	GRAND RIVER AT YORK	43°1′18”	79°53′31”
02GA010	NITH RIVER NEAR CANNING	43°11′23”	80°27′18”

Table 3.6: Stream flow gauges in the Grand River Watershed used for calibration

The unstructured groundwater cells were determined by finding the centroids of the subbasins and building a thessien (Voronoi) polygon grid (figure 3.14). The simulation was designed with a hydraulic conductivity of 0.001 m/d (auto calculated by Raven based on soil properties) and a specific yield of 0.05. The model was calibrated over a 3 year simulation using data from 7 flow gauges and 16 groundwater monitoring wells (see figure 3.15). While an abundance of groundwater monitoring wells exist, it was deemed sufficient to use the selected wells as they provided a range of spatial coverage and contained a reasonable data range to allow for calibration of the model. 488 variables (i.e., the ET and discharge UFR α and β terms for each GW cell) were calibrated. Results for this test case are shown in section 4.6.

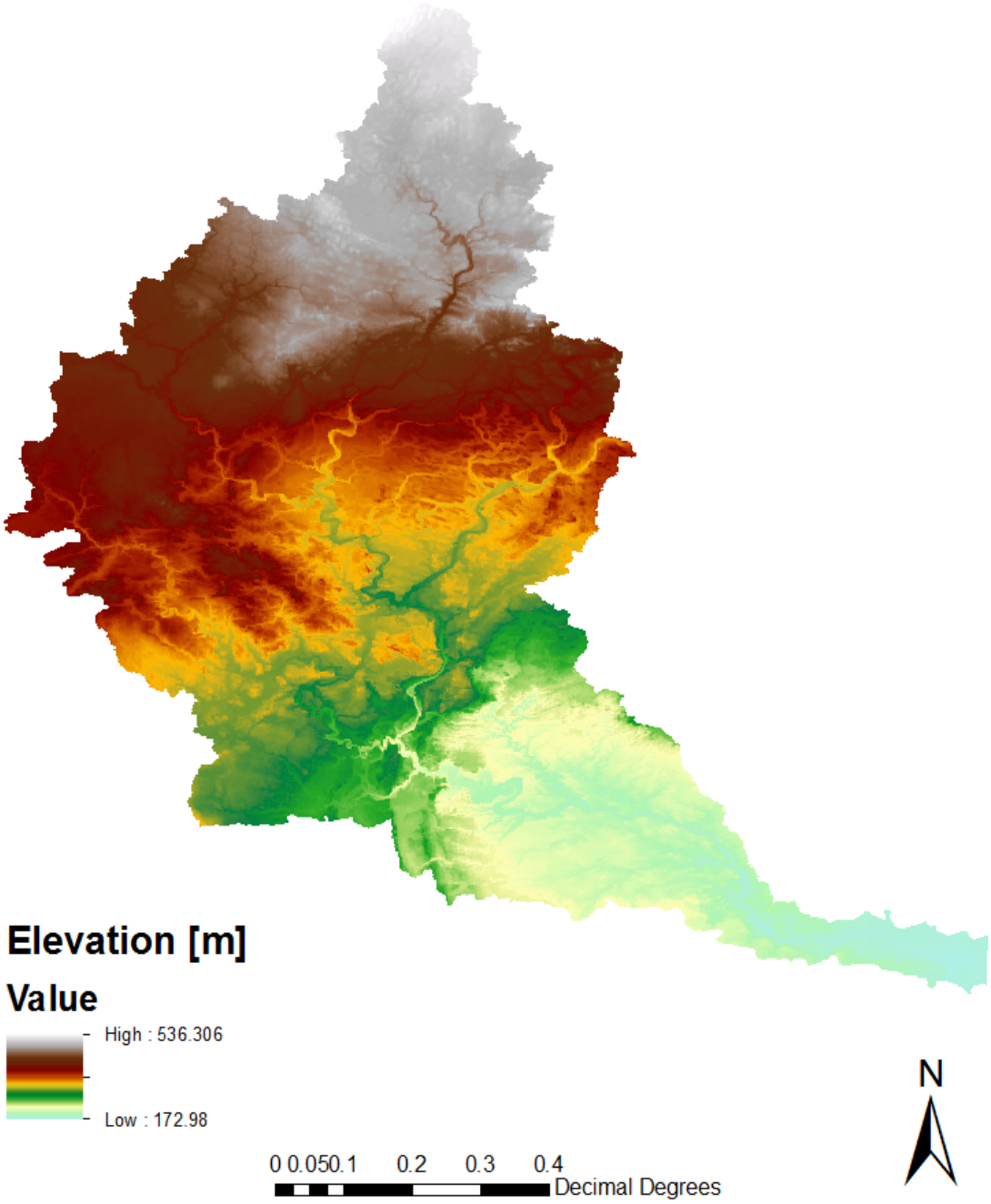

Figure 3.12: Elevation map for the Grand River Watershed

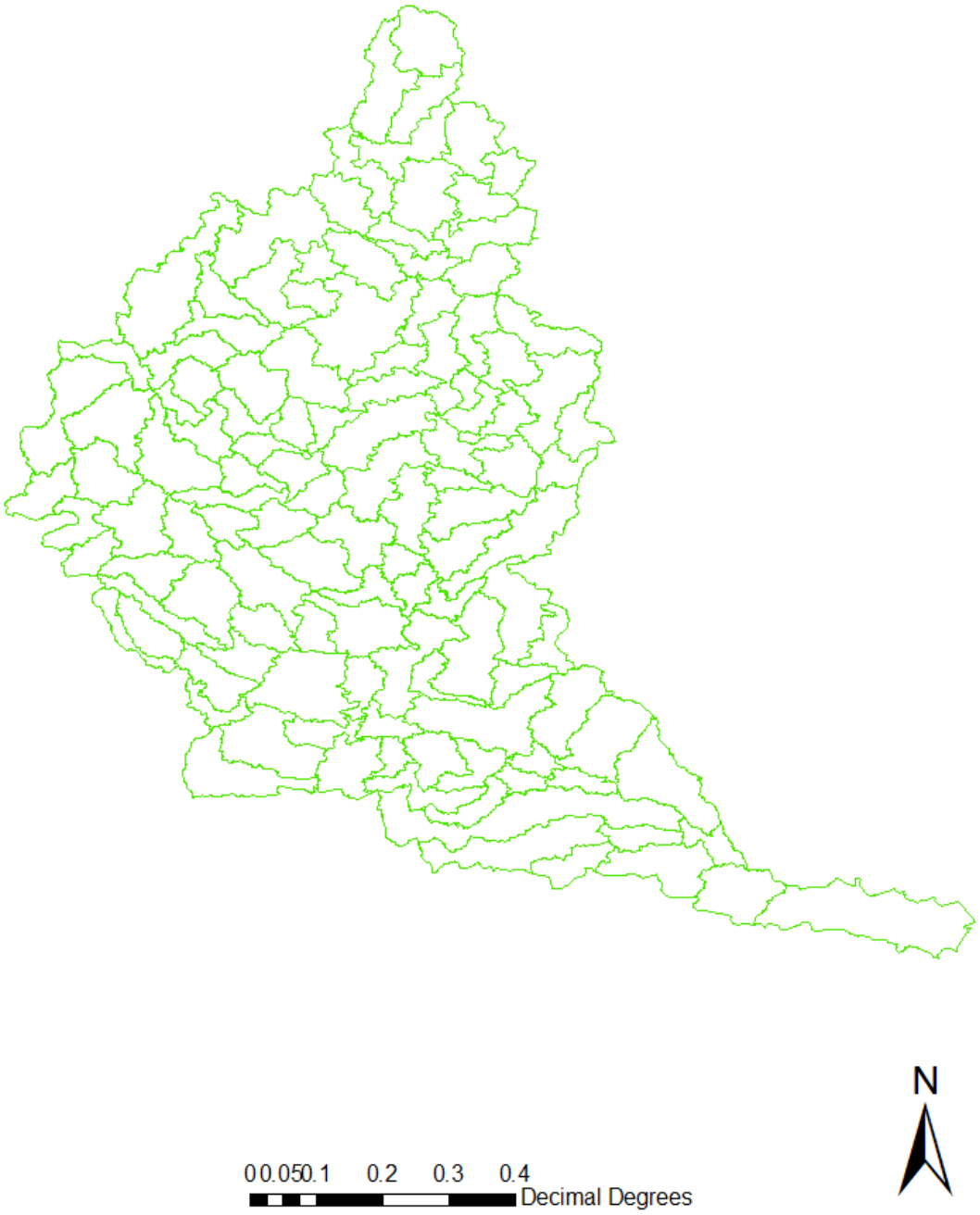

Figure 3.13: Grand River Watershed Subbasins

Well Name	Latitude	Longitude
W0000347-2	44°9′10”N	80°18′41”W
W0000421-1	44°2′50”N	80°20′10”W
W0000023-1	43°54′15”N	80°18′7”W
W0000424-1	43°34′55”N	80°41′18”W
W0000423-1	43°34′23”N	80°31′32”W
W0000003-1	43°32′12”N	80°6′25”W
W0000046-1	43°32′47”N	80°10′45”W
W0000035-5	43°21′56”N	80°23′19”W
W0000024-2	43°27′5”N	80°12′58”W
W0000306-1	43°17′31”N	80°23′7”W
W0000427-1	43°22′33”N	80°40′14”W
W0000428-1	43°21′26”N	80°33′55”W
W0000309-2	43°20′13”N	80°22′W
W0000065-4	43°5′33”N	80°25′W
W0000307-1	43°19′18”N	80°9′21”W
W0000178-1	42°56′40”N	79°56′46”W

Table 3.7: Groundwater monitoring wells in the Grand River Watershed used for calibration (PGMN, 2015)

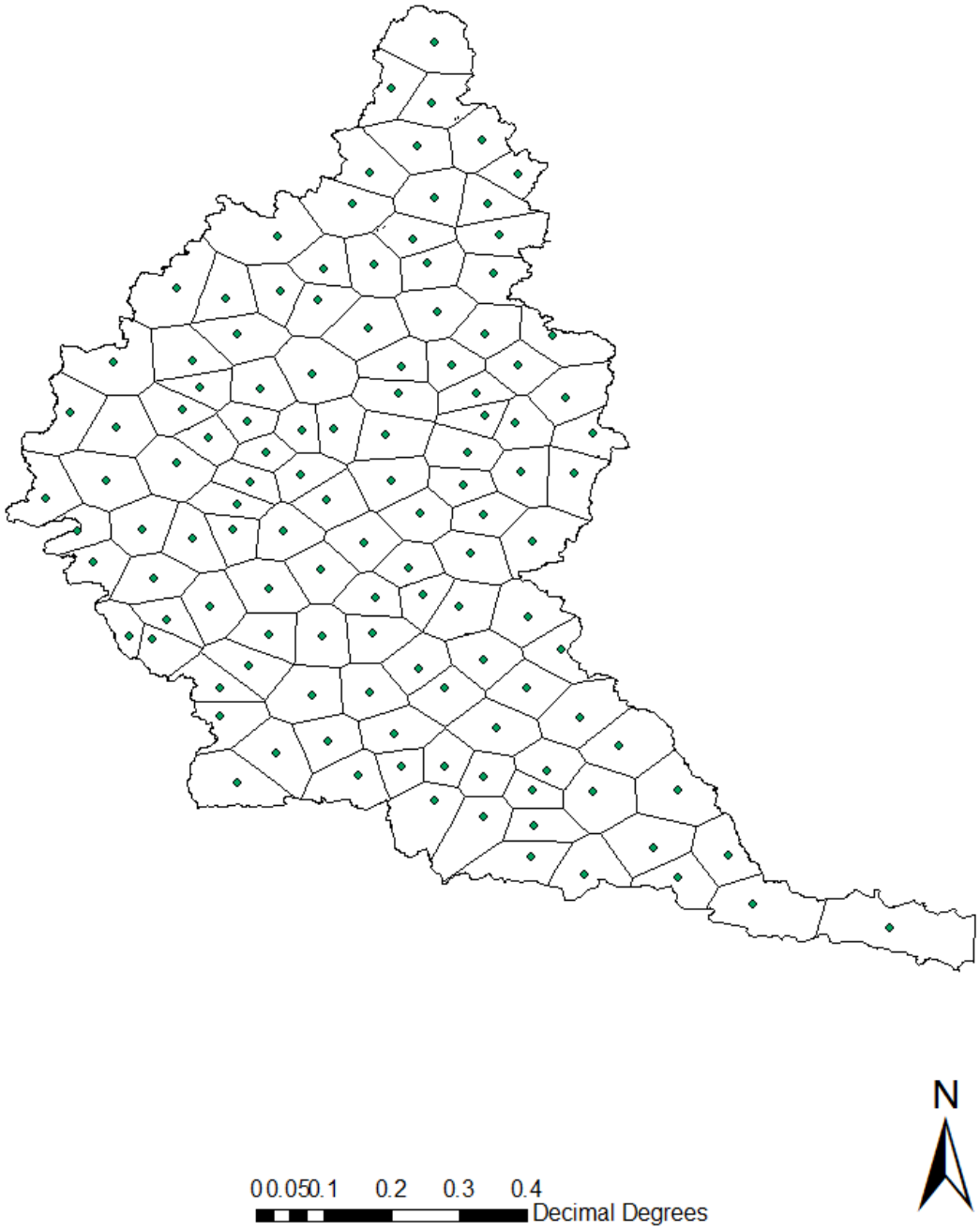

Figure 3.14: Unstructured groundwater cells for the Grand River Watershed with marked cell centroids

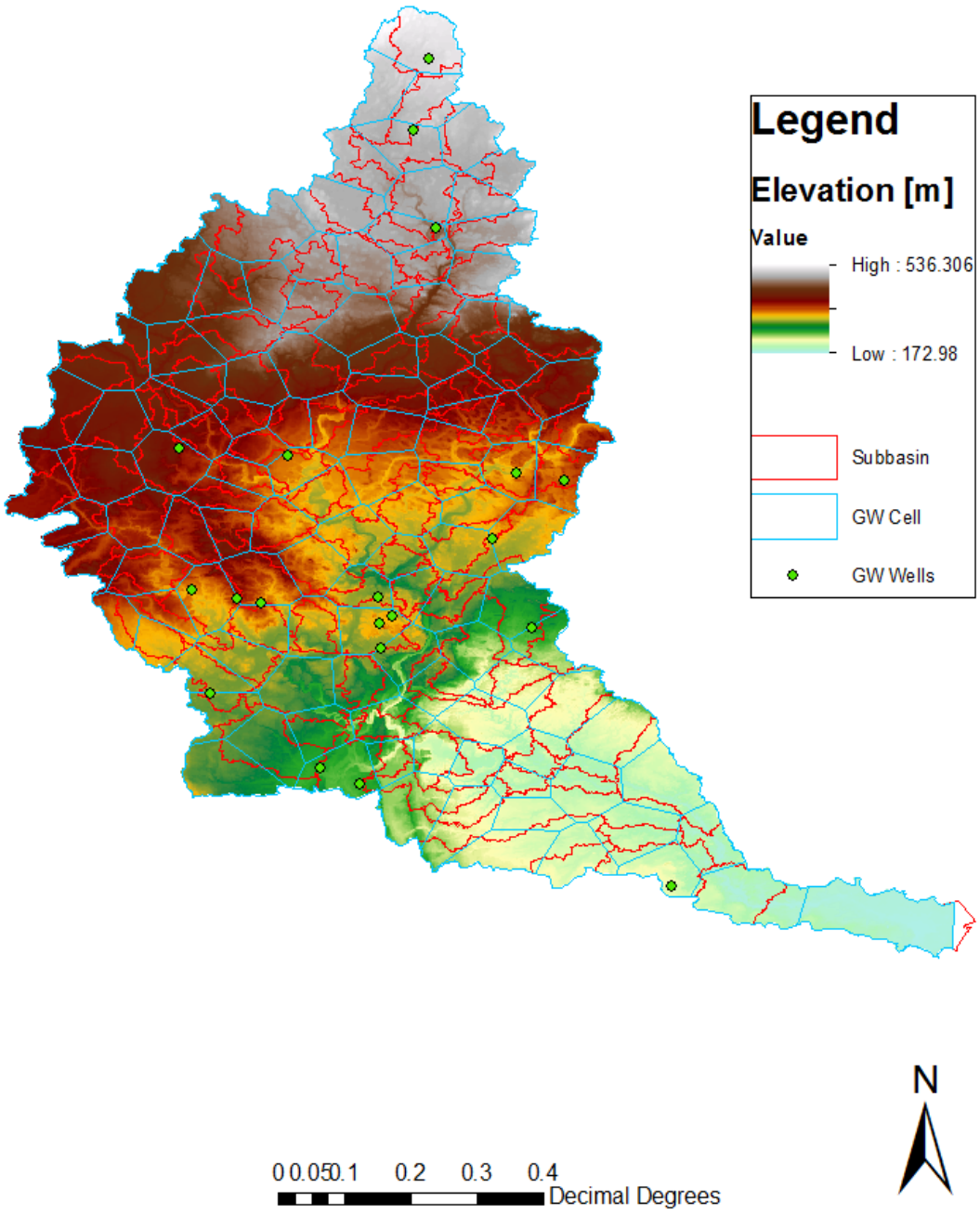

Figure 3.15: Overview of the Grand River Watershed with surface water subbasins, groundwater cells, and groundwater monitoring well locations

Chapter 4

Results and Discussion

Some material covered in this chapter is from Snowdon and Craig (2015)

4.1 Proof of Concept

The proof of concept for this research has two mandates; (1) to show that UFRs outperform point-scale physics approaches at the coarse-scale and (2) to show that UFRs could calculate the spatially-averaged hydraulic head in a basin and that head may be considered to be an accurate representation of a fine-scale simulation.

The results of the initial tests during the proof of concept phase of research are shown in this section. Figure 4.1 shows a terrain simulated using a steady state CVFD model with multiple recharge rates. The figures show the results of multiple simulations with the fine-scale solution shown in blue and the upscaled solution shown in red. Terrain is shown as a green mesh.

The terrain used during the proof of concept work was 64 by 64 cell grids. Specified recharge rates were increased between simulations (see table 4.1). Recharge rates were changed between simulations to see how exchange fluxes are affected in relation to the hydraulic head in multiple steady state conditions. The water table for both the fine-scale simulations and the coarse-scale simulations rises with increasing recharge rate as expected. The water table is a subdued representation of the topography as it rises (figure 4.1).

Similar results are visible here where the water table rises with increased recharge rate and is a subdued representation of the topography. The fine-scale and coarse-scale solutions closely match each other in height and shape.

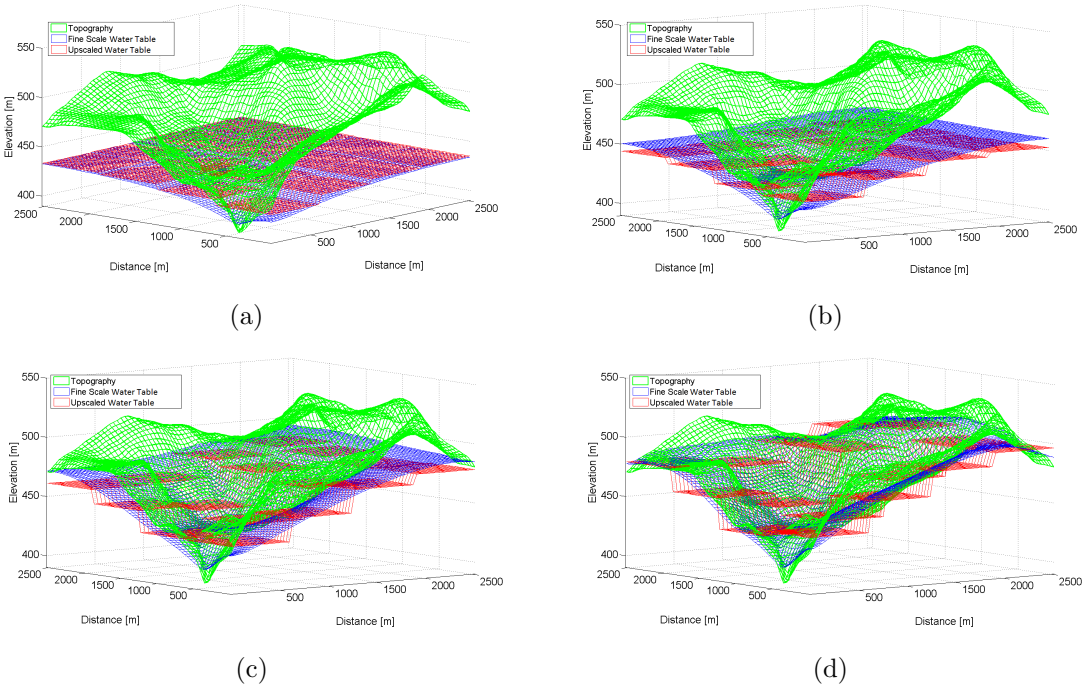

Figure 4.1: Fine-scale solution (blue) compared with cell-averaged (coarse-scale) solution (red) for steady state simulations with varying recharge rates

Simulation run #	**Recharge Rate [mm/d]**
1	0.001
2	0.01
3	0.02
4	0.03
5	0.04
6	0.05
7	0.08
8	0.1
9	0.3
10	0.5
11	0.75
12	0.9
13	1
14	1.5
15	2
16	3
17	4
18	5

Table 4.1: Recharge rates for proof of concept tests for each simulation

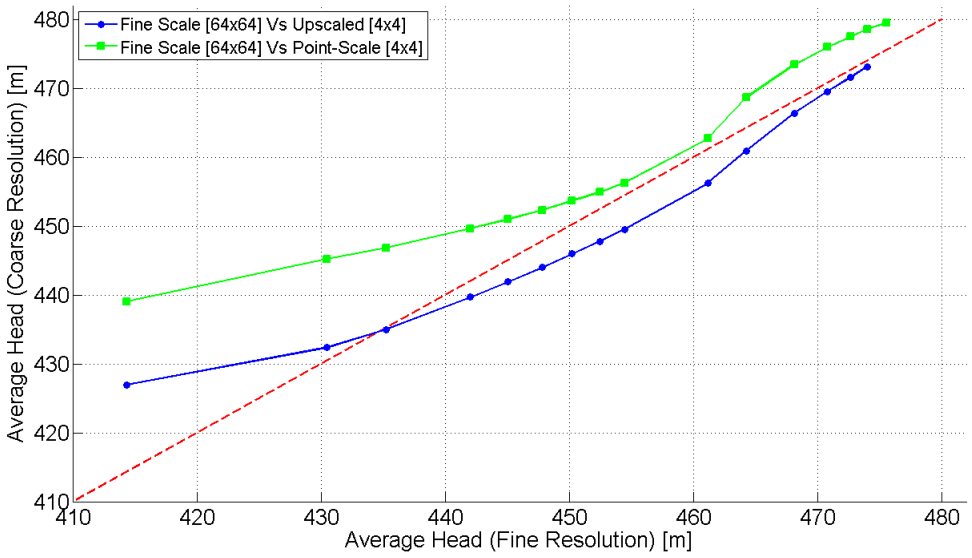

Figure 4.2: Coarse-scale head solution versus fine-scale head solution for 2D proof of concept testing

Since the use of point-scale methods to model exchange processes at coarse resolutions is a common approach, tests were conducted on terrains to understand how UFR upscaling compared to a point-scale method. The UFRs were determined through the analysis of ET fluxes, drain fluxes and saturated area as simulated by fine-scale simulations. The fluxes and saturated area were averaged and plotted against spatially averaged head to generate curves. These curves could then be used to interpolate a rate for ET or discharge given an average hydraulic head. Figure 4.2 shows the ratio between average modeled head from the direct fine-scale solution, the averaged model head using the UFR-generated coarse-scale head, and as well as the average modeled head generated by simply applying the point scale method for simulating exchange fluxes, but on the coarse grid. The plot was created from simulations using a range of recharge rates with static ET. The comparison of the fine-scale results to the upscaled approach and the coarse-scale point-scale method show that for the majority of the simulated recharge rates, the upscaled method produces hydraulic head values that are closer to the fine-scale results than the coarse-grid point-scale method. This is promising as it suggests that upscaling using the new approach is more effective that a naive method of applying point-scale exchange fluxes on coarser grids.

From figures 4.1 and 4.2, it can be seen that the interpolation of fluxes from the UFR

curves can be used in a simulation and seems to outperform the point-scale approach, especially for systems with deeper water table configurations. When comparing the fine-scale solution to the point-scale or upscaled approach, it can be seen that the upscaled approach is generally closer in solution to the fine-scale solution than the use of a point-scale approach at a coarse scale. This means that UFRs potentially can better represent exchange fluxes at coarse-scales than point-scale approaches. It should be noted that the upscaling of the lateral fluxes between cells is not considered here, so even if the UFR approach worked perfectly, there would still be artifacts due to neglect of scale impacts on lateral flux calculations.

Tests to determine if UFR upscaling performs better than the use of point-scale physics were promising. While these basic tests cannot explicitly state that UFRs would perform better than point-scale methods, they did show that UFRs may be more consistently closely to the fine scale simulation results. Additionally, the results from using the UFR method suggests that they may be able to be used to predicted basin-scale hydraulic heads without the use of fine-scale models. This leads to two potential advantages when modelling; a more accurate way to approach coarse-scale simulations and the ability to model without using a fine-scale approach. Higher accuracy is always sought and being able to bypass the fine-scale approach will allow large cumbersome, data intensive models to be calibrated as well as have uncertainty analyses performed on them.

4.2 Terrain and Exchange Flux Relationships (UFRs)

The results of the tests in this section are used to examine how exchange fluxes and saturated area generally relate to average hydraulic head without concern for whether these relationships may be directly used in a modelling context. Multiple scenarios were simulated to understand how UFRs are affected by parameters such as maximum ET and also by conditions (i.e., whether the model is steady state or transient, fully saturated or saturated/unsaturated. Additional tests were also conducted to investigate the impact of scale and sensitivity to mild hydraulic conductivity heterogeneity.

4.2.1 Saturated Steady State UFRs

The results from the simulations (see table 3.2) performed with terrain E are here described to aid in interpreting all of the simulation results. Terrain E is shown in figure 4.3, both as a contour plot and a 3D surface map. The normalized elevation is shown in the contour

plot; actual elevations range from 104 metres to 178 metres; the terrain is quite hummocky with a low valley in the southeast corner of the DEM. Hummocky, for this study, refers to terrains with steep sided hillocks and hollows with many multidirectional slopes that exceed 15° (Howes and Kenk, 1997). The results of the E30 simulations for a range of steady recharge conditions are depicted in figure 4.4. These show that, as the recharge rates increase, the water table elevation and exchange fluxes of ET and discharge increase as would be expected. The net water balance is preserved. As the mean water table elevation increases, so too does the saturated surface area.

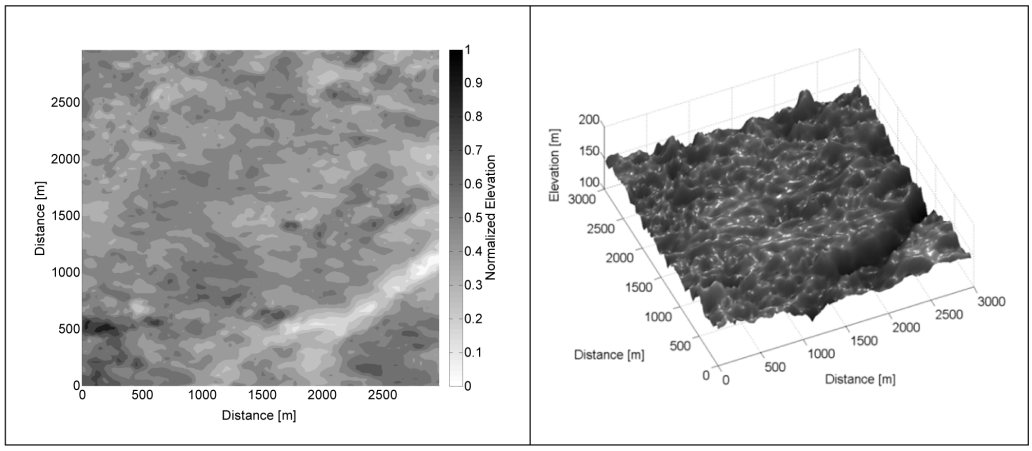

Figure 4.3: Contour plot and 3-dimensional surface plot of terrain E

As can be seen in figure 4.4, when the water table is at the minimum elevation, there are almost no GW-SW exchange fluxes occurring and when the water table reaches a theoretical maximum elevation (at what is well in excess of a physically realistic steady recharge rate), ET and discharge occur across the entire domain of the simulation with only the highest topographic elevations acting as recharge sources. Increasing average hydraulic head increases GW-SW exchange flux rates quickly at low lying points of the terrain first in a predictable pattern. It can be seen that the range of recharge conditions leads to a range of average water table heights, which is a direct surrogate for saturated GW storage. It is clear that this relationship will in all cases be monotonic. What is less clear is what impact the terrain properties will have on the shape of the UFR curves describing average head-flux relations.

Results from terrains A through D (figure 4.5) X30 simulation output shows comparable behaviour; only the output from moderate recharge rates is shown. Moderate recharge rates generate moderate ET rates and a saturated area that covers a portion of the domain

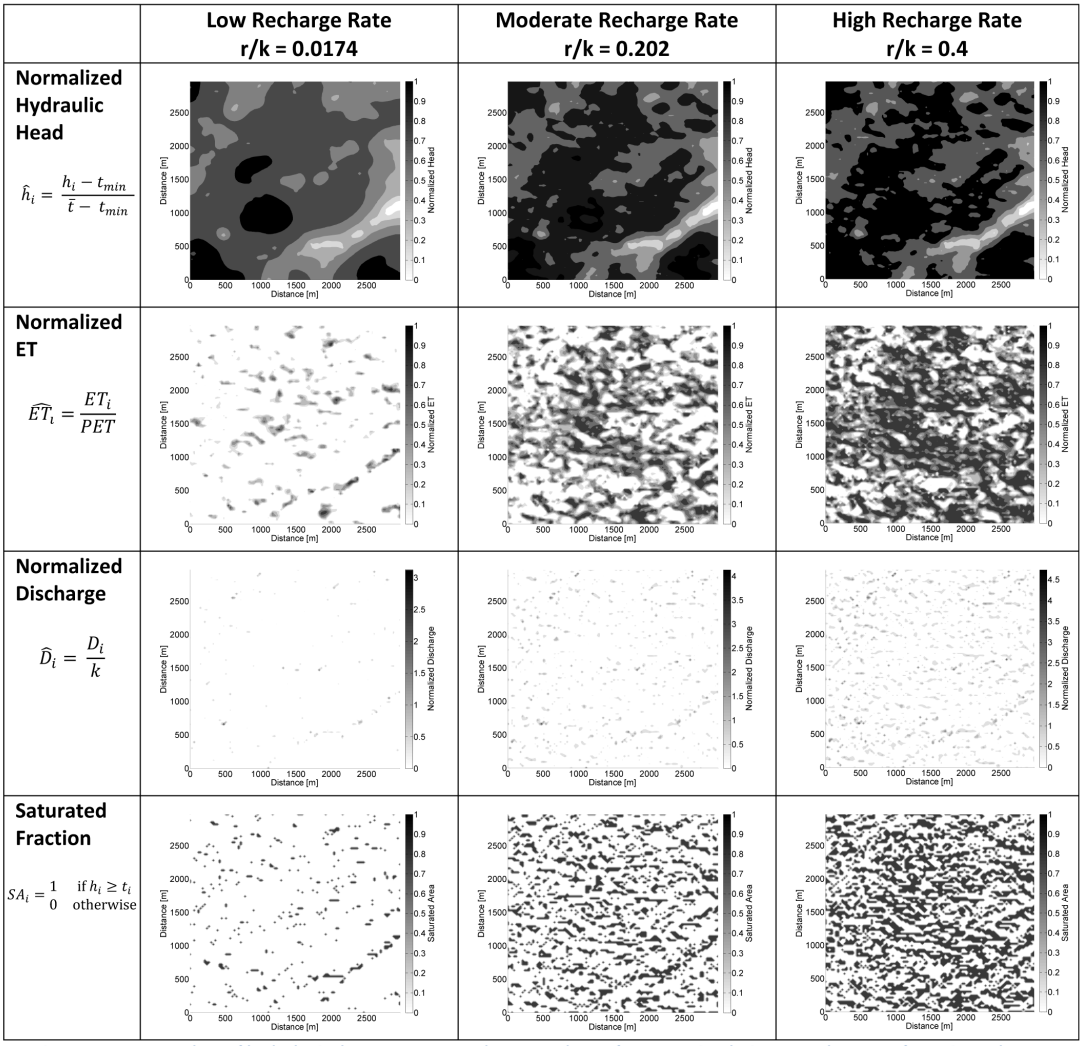

Figure 4.4: Normalized hydraulic head and exchange flux rates for low, moderate and high recharge rates in simulation E30

(9-24%). As with terrain E results, the discharge rate is lower than the ET.

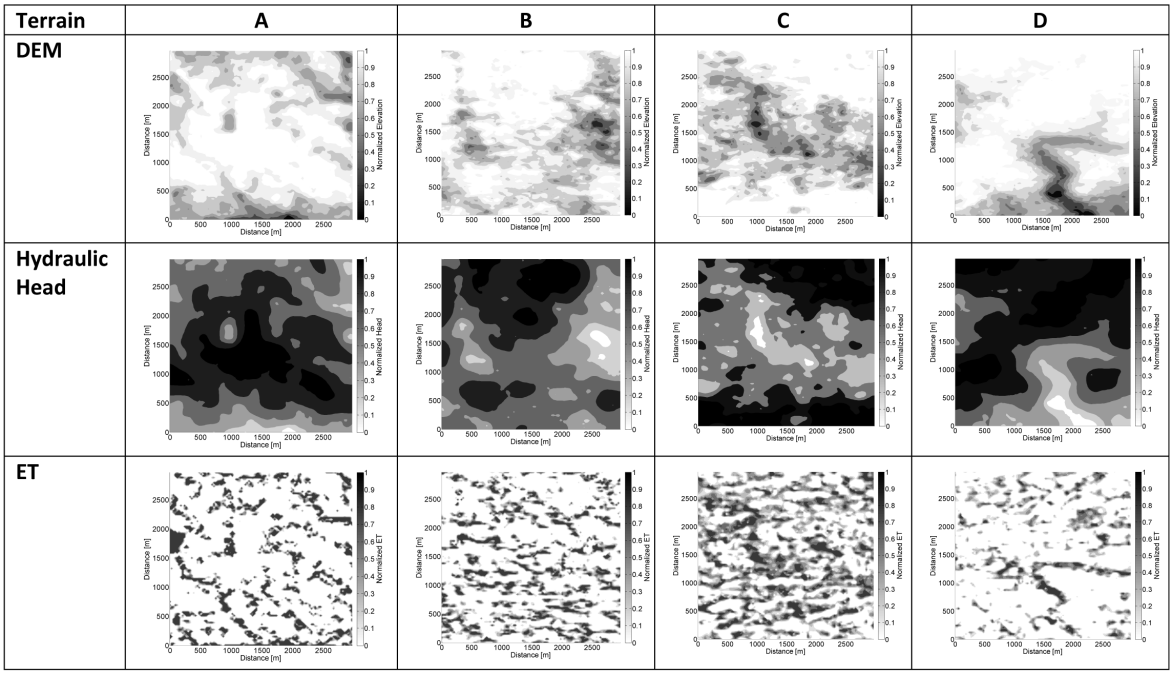

Figure 4.5: Terrains A-D from X30 simulations using moderate recharge rate

The output from the fine-scale model was post-processed through a custom script to calculate the average hydraulic head, exchange fluxes and saturated area values over the entirety of the modelled domain. It can be seen in figure 4.6 that the UFRs appear to follow a power law trend. The UFRs clearly show that as the mean hydraulic head approaches the mean surface elevation of the terrain, the discharge and ET fluxes will approach an asymptote. They also show that as this maximum normalized mean head is approached, the ET rate and the saturated area approach their maximums of PET and 1, respectively. Discharge rates continue to rise as the mean normalized head is approached. The UFRs that are generated for terrains A-D are similar to the UFRs from terrain E. Each is well-described by a power law relation which is supported by the range of R^2 values for each curve (R^2_{ET} = 0.989-0.99, R^2_D = 0.96-0.98, R^2_{SA} = 0.95-0.98). The DEMs used to generate the fine-scale simulations have a 30 metre resolution and it is expected that a finer resolution DEM would not affect the shape of the UFRs. Higher resolution DEMs may increase the accuracy of UFRs (although this is unknown) but it is thought that this will be minor as UFRs are the result of fine-scale simultion results averaged over a large area.

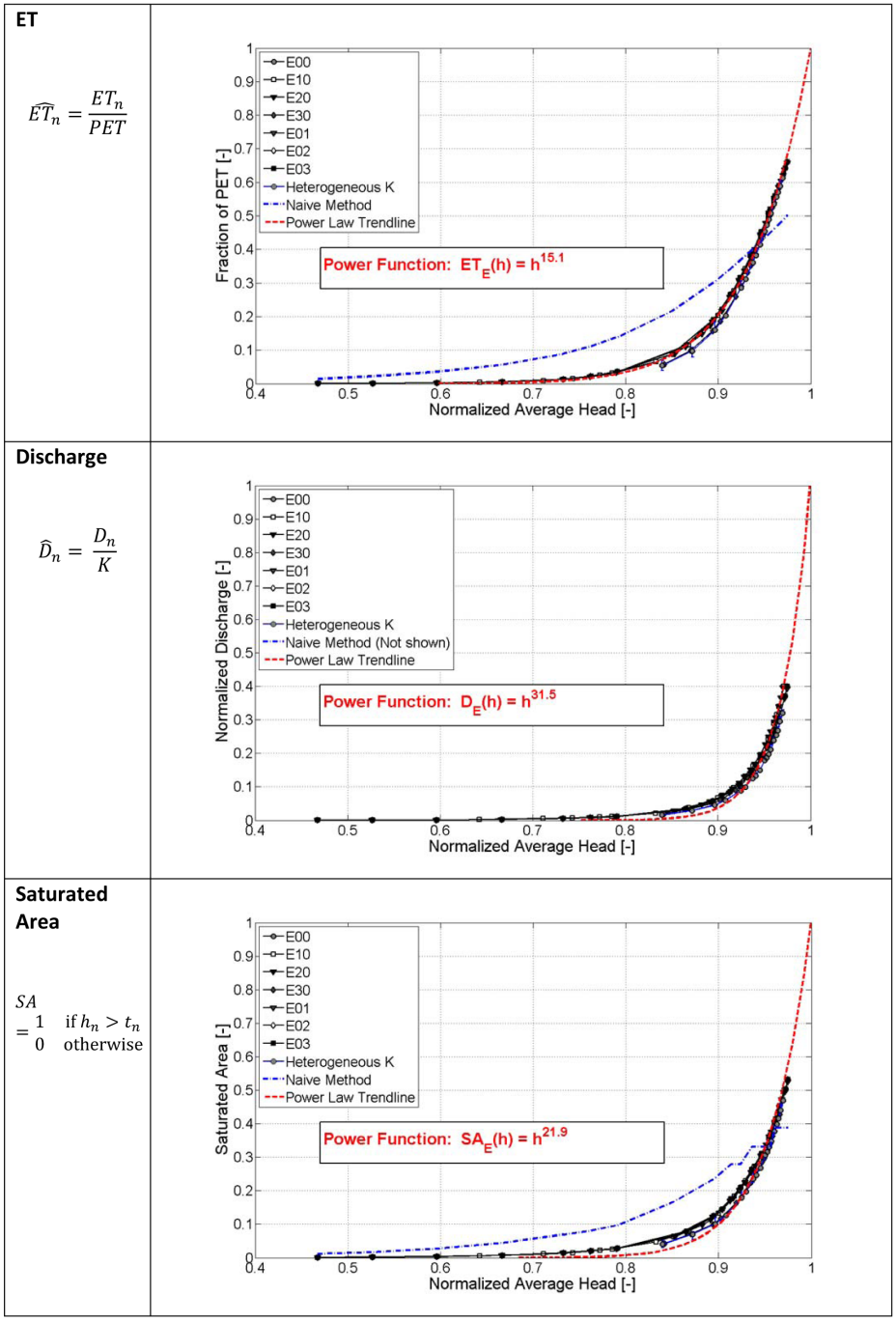

Figure 4.6: Terrain E UFRs for ET, discharge, and saturated area from fine-scale, heterogeneous K and naïve simulations

The best-fit power law equations that describe ET, discharge and saturated area for terrain E are:

$$ET_E(h) = h^{15.1} \qquad R^2_{ET} = 0.989 - 0.99 \tag{4.1}$$

$$D_E(h) = h^{31.5} \qquad R^2_{D} = 0.96 - 0.98 \tag{4.2}$$

$$SA_E(h) = h^{21.9} \qquad R^2_{SA} = 0.95 - 0.98 \tag{4.3}$$

To check that upscaling with UFRs could not be accomplished simply by using topographic statistics (without considering the water table and terrain), a naïve approach was investigated. As can be seen in figure 4.6, the naïve upscaling method over estimates the exchange fluxes and saturated area when the normalized average head in the system is low and underestimates as the average head approaches its maximum. The discharge flux rate is so grossly overestimated that it is too high to be plotted along with the other UFRs on the normalized discharge plot.

The results here clearly show that the UFRs follow a power law trend. Increases in normalized head cause exchange fluxes and saturated area to approach asymptotes. As mentioned previously, the ET rate and saturated area will eventually reach a maximum of 1 since they are normalized values, but the discharge rate will continue to climb. This is in agreement with the suggestion by Frei et al. (2010), who examined surface-groundwater interactions at finer scales of 0.1-1 m^2, that a nonlinear relationship may exist between water table depth and discharge. Since simulation results do not indicate a maximum value for discharge in these simulations, discharge normalization on a useful scale is more challenging. However, it is clear that the discharge rate to average head relationship follows the same trend as the other two features.

It is important to note that, after normalization, all simulations conducted using the same terrain produce the same general UFR independent of PET maximums and hydraulic conductivity. This is significant because it could mean that steady simulations for individual terrains may be characterized with a relatively simple relationship between vertical fluxes and average hydraulic head, generated via a single fine-resolution simulation. The exception to this is where the naïve upscaling method was used (see figure 4.6). The introduction of the naïve approach was to clarify that upscaling cannot simply be achieved by using topographic statistics. Figure 4.6 shows that the naïve approach is unable to properly estimate accurate flux rates when hydraulic head values are low or when approaching a maximum. This clearly shows that using only the topography statistics (without consideration of the water table and terrain geometry) to estimate upscaled fluxes is insufficient for characterizing the behaviour of the system.

4.2.2 Saturated Transient UFRs

After generating the steady-state UFRs, additional simulations were performed using a suite of different transient recharge conditions. Figure 4.7 shows the output from the multiple transient cases as outlined in table 3.3. Output from simulation E30 is shown as characteristic results for these tests, which were performed on all terrains. The constant-term transient cases are denoted as 'quarter', 'half' and 'double' recharge cases with the qualifier referring to the change in steady recharge rate with respect to the recharge rate used to generate the initial conditions. The variable-term transient cases use initial heads from steady state simulations that used the same recharge rate as the first recharge rate in the transient simulation. The constant-term cases are 840 days in duration, use 14 stress periods with 4 timesteps per stress period and were run on each of the 5 terrains. The variable-term cases also use 14 stress periods, each 60 days in length (for a total of 840 days) with 4 timesteps per stress period and were run on each of the 5 terrains. The constant-term cases examined the transition from one steady-state condition to another in response to a single abrupt change in recharge rate (as might be considered in climate change investigations). The variable-term cases use linearly increasing and decreasing recharge rates or fluctuating recharge rates, as defined in table 3.3. For all simulations, a specific yield of 0.22 was used.

As figure 4.7 shows, the constant-term transient cases using a steady recharge rate start with heads at a steady state position and slowly migrate over time towards another steady state position. The migration is almost linear, indicating that for transitions from one steady recharge condition to another, it may be possible to use steady state UFRs to represent simulation fluxes. The variable-term cases, however, show that when using realistic recharge values, the simulation output tends to overlap the steady UFR, deviating by as much as 4.7% in the worst case for ET and 3.4% in the worst case for saturated area. It appears that hysteresis effects are small in these cases although it could become more pronounced for aquifers with high diffusivity. Surprisingly, the simulation results for all cases show that the ET, discharge and saturated areas are generally consistent with the power law trend determined from the steady-state case. These results imply that this method of upscaling could be applied to both steady state and transient simulations using a single set of UFRs, though care must be taken. It is also encouraging that power laws are indeed justifiable for characterizing storage-flux relations at the watershed or basin scale since many existing models (e.g., VIC/ARNO (Zhao, 1977), FUSE (Clark et al., 2008) and the Sacramento (Burnash et al., 1973)) already use power law based methods for this purpose. It is likely that the primary controls on these power law exponents are the elevation distributions and topographic connections, which may be characterized using

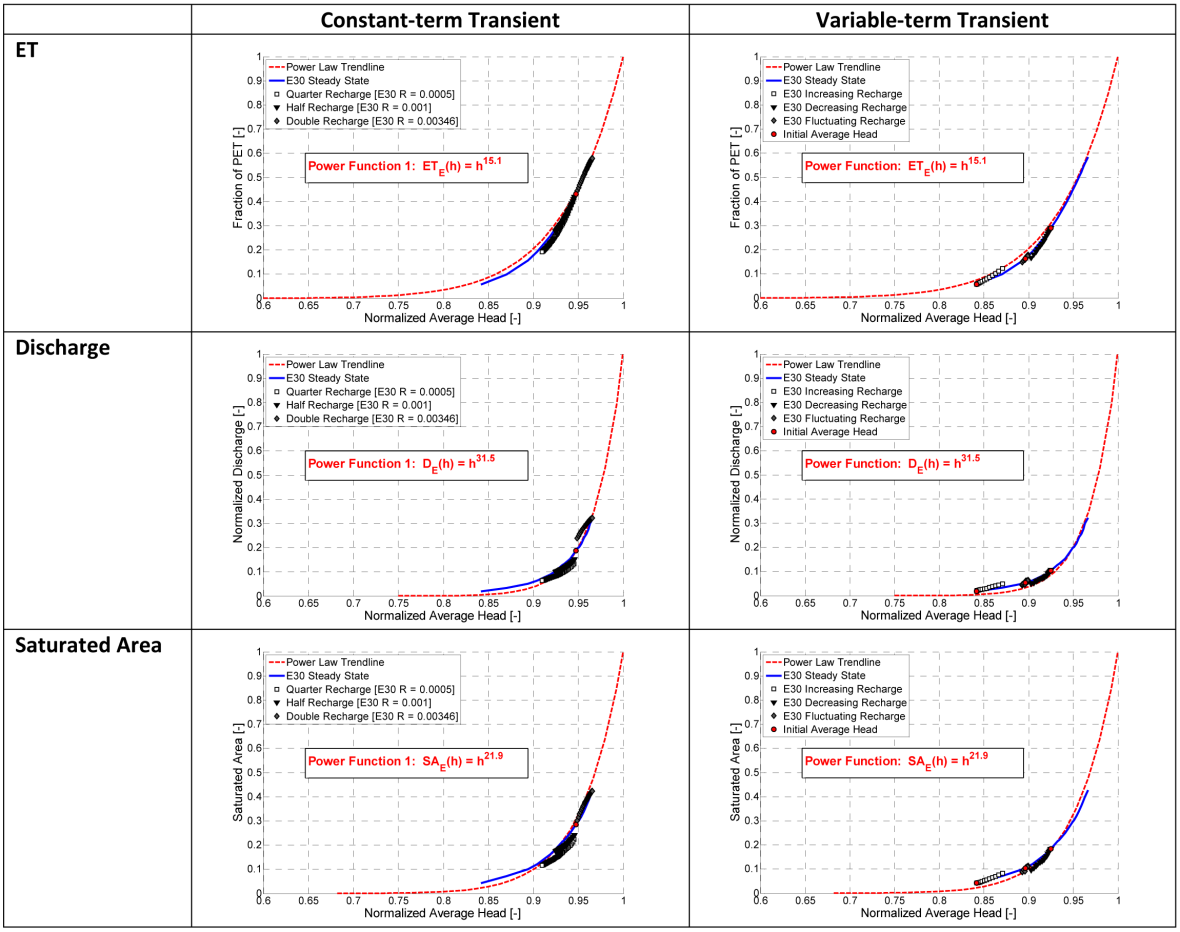

Figure 4.7: Terrain E UFRs for multiple transient simulations as outlined in table 3.3 in comparison with the steady state UFR

various terrain indices such as flow accumulation, wetness index, terrain slope, or terrain elevation. Preliminary testing (see figure 4.14), discussed in section 4.2.6, indicates that the relationships between standard topographic metrics and the power law coefficients are difficult to characterize, and warrant further study. However, some rough guidelines may be considered by contemplating extreme cases. For a completely flat topography, the up-scaled relations will revert to the point scale, i.e., with a power law exponent of β=1. For non-planar topography, the curvature of the UFR curve is likely partially controlled by the characteristics of the elevation distribution. For instance, sharply incised landscapes, where the surface water feature is well below the rest of the landscape, will have roughly linear discharge-head relations, controlled by the integrated head gradient along the incised feature. However, because the water table will be generally deep except along the incised feature, such landscapes will have ET-head and saturated area-head relations which only increase in value for relatively large values of average head, i.e., they will have large β exponents. Undulating topographies with more uniform elevation distributions, as examined here, will fall somewhere between these two extremes of spatially uniform hydraulic connection and spatially concentrated hydraulic connection.

4.2.3 Unsaturated Transient UFRs

The inclusion of the vadose zone, simulated here with HydroGeoSphere, leads to UFRs exhibiting similar power law trends as are apparent in the saturated Modflow simulations. Figure 4.8 shows the ET, discharge and saturated area results as UFRs, with the top left figure depicting the cross-sectional model used. These tests show that using (or not using) a highly parameterized formulation of the vadose zone and that the choice of complexity in ET method do not significantly alter the assumption that the relationships defined by the UFRs can be described using a power law relationship.

So far, all the UFR tests were conducted using saturated systems, which is a less complex problem. But unsaturated systems are ubiquitous, so it is important to characterize and represent the movement of water across the vadose zone. Modflow is not the ideal model for representing vadose zone calculations since some of the artefacts of the Dupuit-Forcheimer assumption and neglect of the vadose zone are apparent. Unsaturated testing was conducted using HydroGeosphere which can calculate unsaturated water flow with high accuracy. For instance, the unsaturated zone in the HGS model enables discharge of groundwater through the unsaturated ground surface, therefore there is, for a similar average domain head, a larger simulated saturated area from the Modflow model. For similar reasons, the Modflow model tends to over-predict ET for similar mean heads; the water table is closer to the surface in valleys and further from the surface beneath hills than in

the HGS simulations. Regardless, the power law trends are apparent in both models (see figure 4.8). This is an important discovery since it could mean that UFRs are appropriate for upscaling use in both saturated and unsaturated systems.

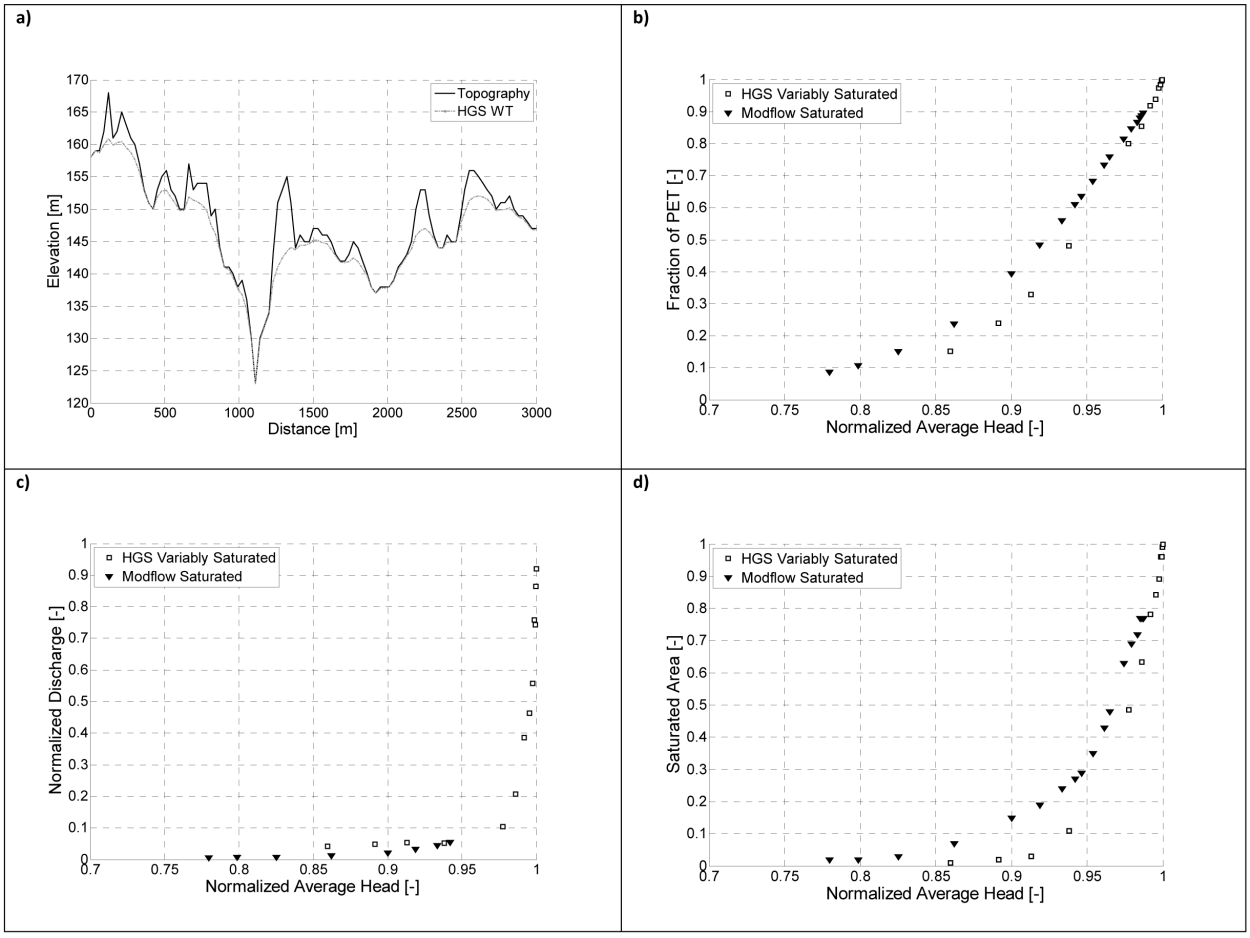

Figure 4.8: a) Topography and water table from HGS simulation; b-d) UFRs from unsaturated HGS simulations with varying recharge rates for ET, drainage, and saturated area

4.2.4 UFRs and Heterogeneity

The use of mild hydraulic conductivity heterogeneity for five hundred realizations of test case E30 shows that the presence of mild heterogeneity did not impact the shape of the

UFR curves. The curves showing these results are included in figure 4.6 with whisker bars depicting the maximum and minimum ranges of the normalized data for ET rate, discharge rate and saturated area.

4.2.5 UFRs and Scale

4.2.5.1 Horizontal Scale

To determine how UFRs may change as horizontal scale changes, several UFRs were generated from simulation E30. The UFRs were generated, using the 100x100 cell domain fine-scale simulation results, for 16 cells, 4 cells, and 1 cell. The extents of the UFRs for ET, discharge and saturated area are shown in figure 4.9. To see the individual UFRs for each cell, see figure B.1 in Appendix B.

As figure 4.9 shows, the UFRs for 4 cells and 16 cells do not collapse into a single uniform relationship, indicating that horizontal scale does affect UFRs. It can be seen that regardless of horizontal scale, all the UFRs follow the same general power law trend. For ET and saturated area, the UFRs should pass through point (1,1) when the head and fluxes are normalized. This would make the α coefficient of the power law equal to one, which would leave only the β term (the exponent) to dictate the shape and magnitude of the UFR. Plotting β terms against the mean normalized topographic elevation (equation 3.5, figure 4.10) shows that as horizontal scale coarsens, β terms tend to increase. The change is more noticeable when comparing the single upscaled cell to the other tests and less obvious when comparing between 16 subsets and 4 subsets. This would further confirm, as suggested in section 4.2.2, that the more non-planar a topography is or the greater the range in topographic elevations, the higher the β term will be. It can be inferred that as cell size coarsens, the uniform distributions of topographic elevation decreases which necessitates higher β terms. Some outliers exist showing that higher β values tend to occur at finer-resolutions when the mean normalized topographic elevation is higher. This may be a result of a quick shift from low to high process response as the cell becomes saturated when the mean normalized topographic elevation is higher.

To further analyze the effects of horizontal scale on UFRs, the β terms were plotted again topographic elevation standard deviation for the upscaled cells (see figure 4.11). It can be seen that as the standard deviation increases, β values increase which may indicate that a greater overall spread of topographic elevations may result in exchange flux rates that abruptly change from "off" to "on". This phenomenon is discuss further in section 4.3.

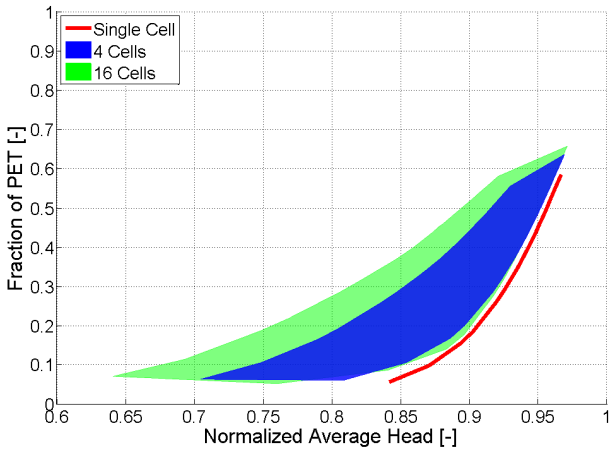

(a)

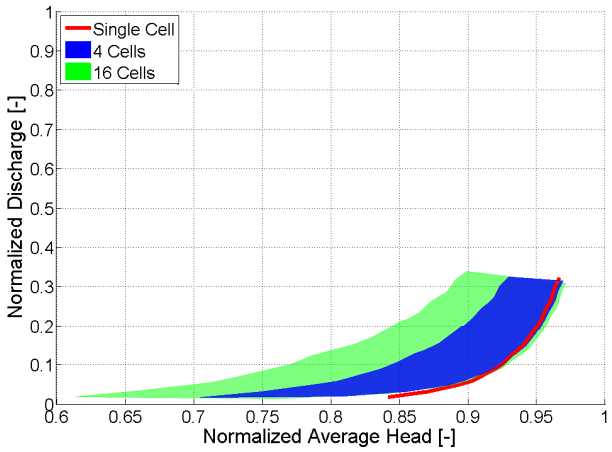

(b)

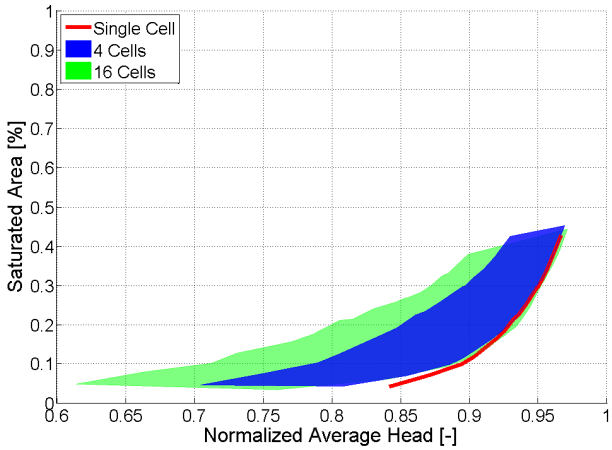

(c)

Figure 4.9: UFR ranges for (a) ET, (b) discharge and (c) saturated area for 16 cells, 4 cells and 1 cell

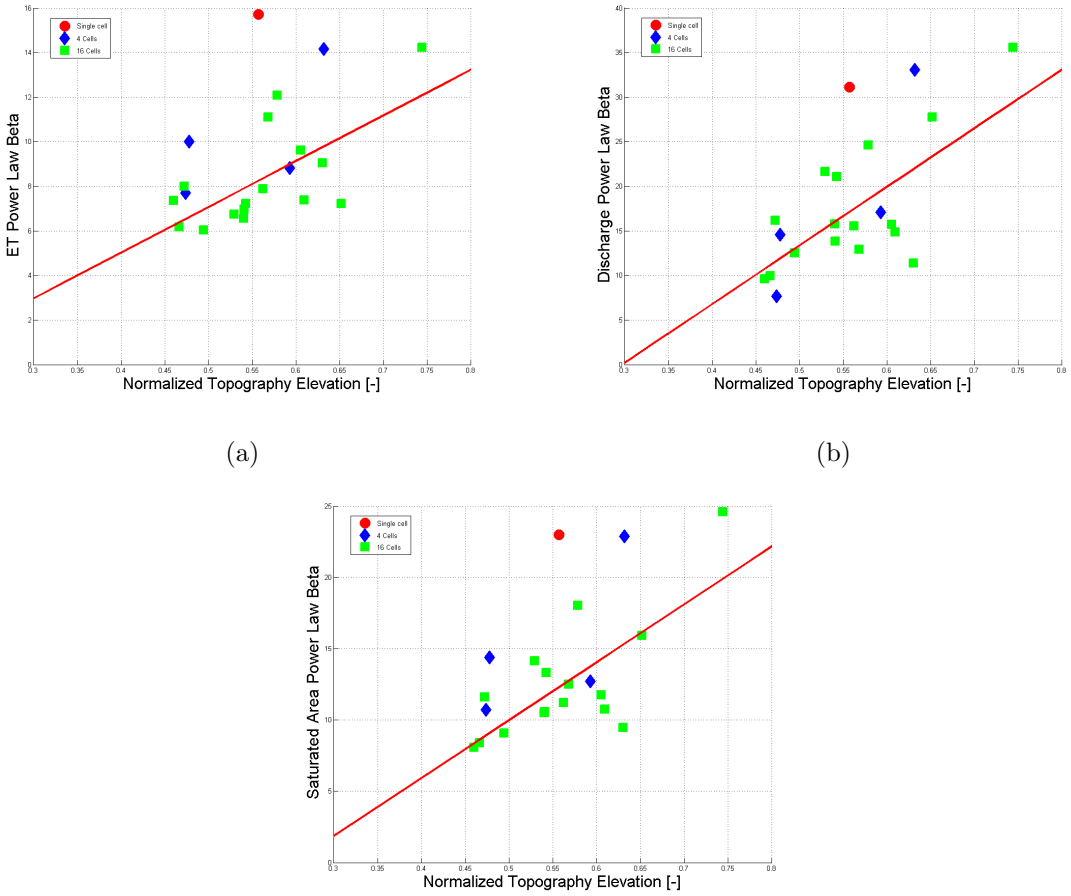

Figure 4.10: Power law β term versus normalized topography elevation for (a) ET, (b) discharge and (c) saturated area for 16 cells, 4 cells and 1 cell. Trendline shows the linear trend in the 16 cell data.

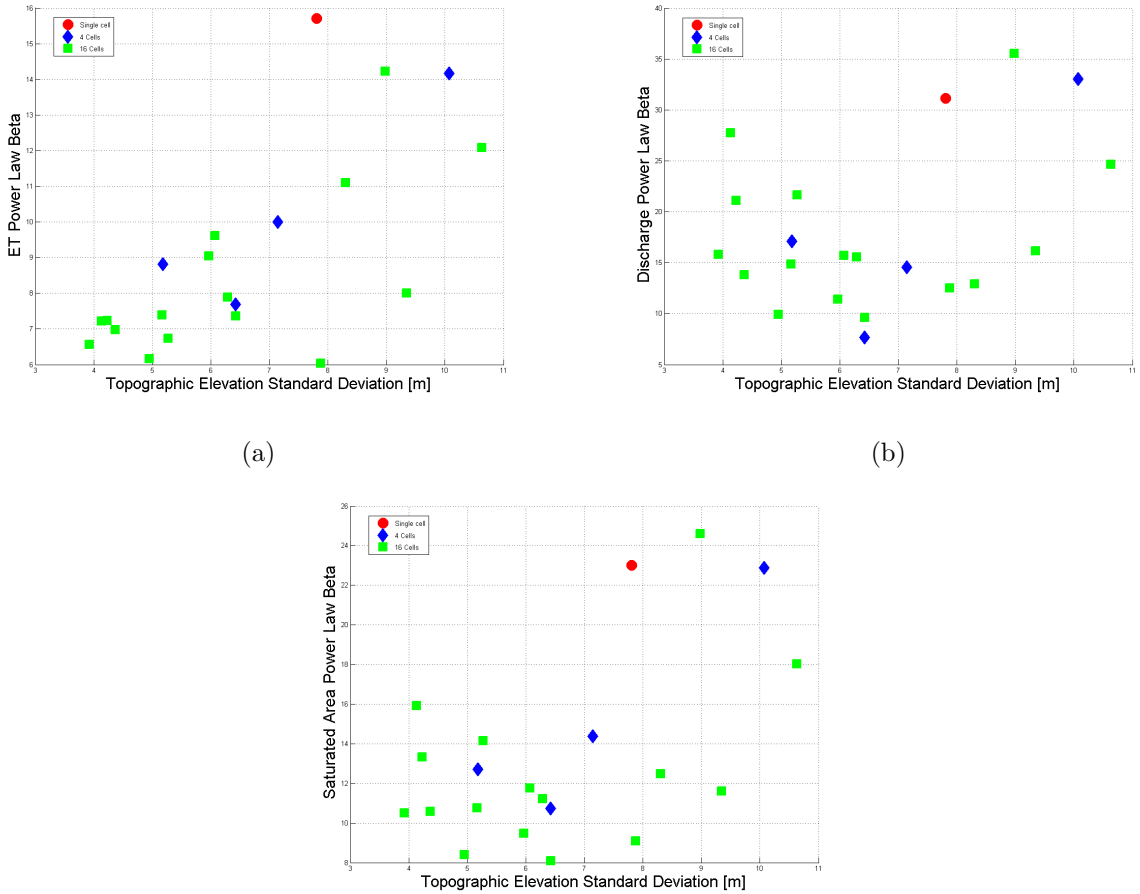

(a) (b)

(c)

Figure 4.11: Power law β term versus topographic elevation standard deviation for (a) ET, (b) discharge and (c) saturated area for 16 cells, 4 cells and 1 cell

4.2.5.2 Vertical Scale

Simulations using terrains F, G, and H were used to investigate how vertical scale impacts the shape and form of the UFR. The X30 test case was run using these terrains to generate new UFRs. The topographic elevations for each terrain were then modified to 50% and 25% of their original values based on the minimum topographic elevation and the X30 models were run again. All simulation results were post-processed and UFRs were produced for comparison. Figure 4.12 shows the UFRs for terrain G given the scaling options (i.e., 100%, 50%, 25%) as described in section 3.2.7.2.

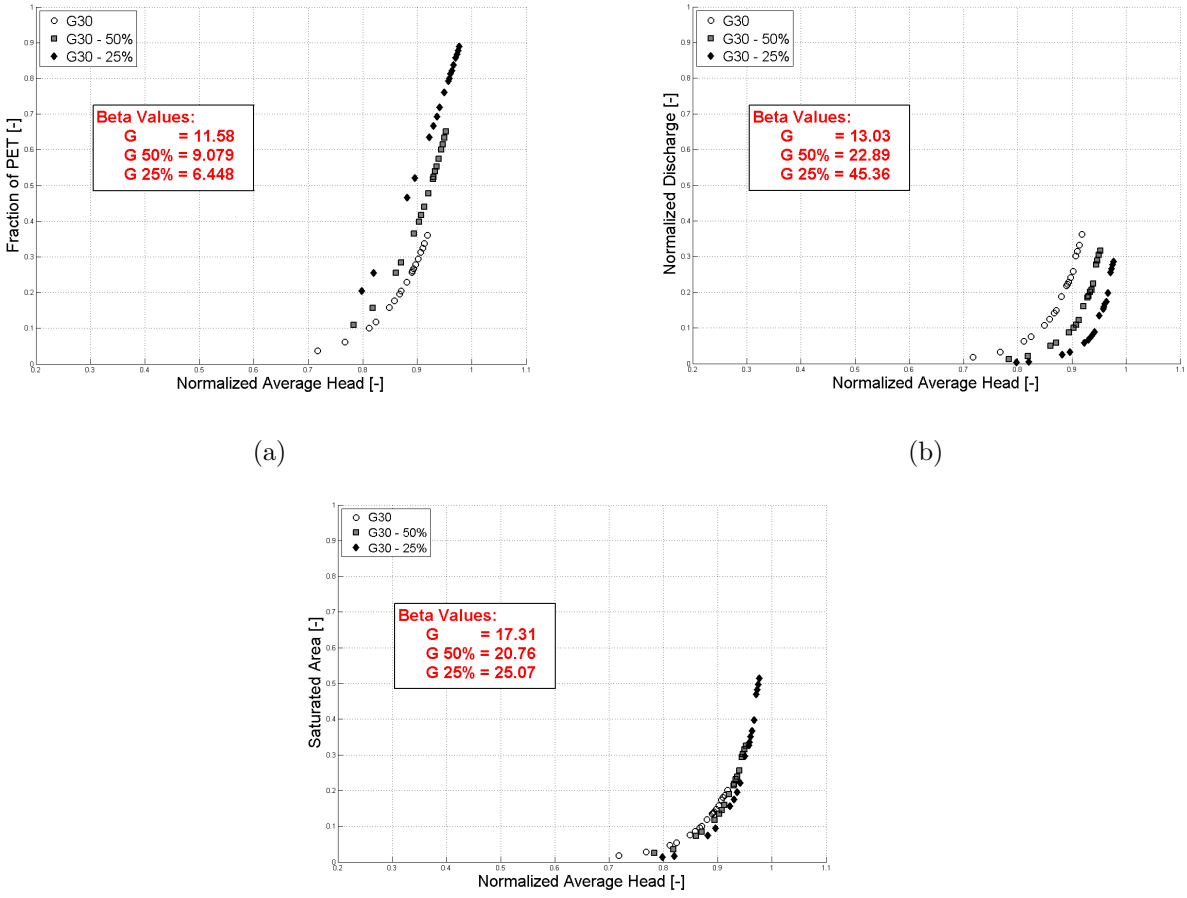

Figure 4.12: UFRs generated from fine resolution vertical scaling simulations using terrains F, G, and H at 100% scale, 50% scale, and 25% scale with simulation E30 UFR (red dash); (a) ET, (b) discharge and (c) saturated area

Looking at figure 4.12a, it can be seen that the UFRs for evapotranspiration at the same scale overlap which is consistent with the results of previous tests using steady state and transient saturated conditions (see sections 4.2.1-4.2.2). This overlap occurs at each level of vertical scale reduction. β values, that define UFR shape, for each exchange flux are included on figure 4.12a showing that for ET, the β term decreases as scale is reduced, and for the β term increases with scale reduction for discharge and saturated area. The effect of the β terms can be seen in the shape of the UFRs. UFRs generated with the original (100%) terrains show the expected power law curve with a β larger than 1. As the vertical scale is reduced from 50% and then to 25%, the UFR shape changes. For ET, β is decreasing toward a value of 1. For discharge and saturated area, β is increasing. This implies that as terrain becomes flatter and less variable, UFRs will approach point scale representations. This holds true for all the topographies tested.

The discharge UFRs (figure 4.12b) for the vertical scaling simulations show the highest variability amongst the UFRs produced with none of the curves at the same scale overlapping. However, this is expected given how much discharge can vary and that the normalization of discharge does not constrain the flux rate to an upper limit of 1. The UFRs show that as vertical scale is reduced, the β term will increase. This is the opposite response to what was found in the ET curves with a reduction in topographic variability, but it shows that as variability is reduced, the UFR approaches the point scale discharge representation which is consistent with the ET test results. Figure 4.13b shows the comparison of the β terms against the topographic variance revealing that as the variance is reduced, β terms are increased confirming the assumption made from the UFR shape.

Unlike the UFRs for ET and discharge, the UFRs for saturated area (figure 4.12c) have little variability between curves for individual terrains. By examining the UFRs closely, it can be seen that the response to vertical scaling is similar to the discharge UFRs. As the vertical scale is reduced and with it the topographic variability, the UFRs approach the point scale saturated area curve. This implies that for a reduction in topographic variability, there would be an increase in β for the power law governing the UFR as was found in the discharge UFR tests. The comparison of the β terms and normalized topographic elevation variance (figure 4.13c) shows the same response in the β terms to a reduction in variance as was found in the discharge tests.

The effect of changes in vertical topographic scale on UFRs can be seen to be variable depending on the exchange flux of interest. The lower the topographic variance is, the more a UFR will appear like its point scale representation. This results in lower β terms for ET and higher β terms for discharge/saturated area.

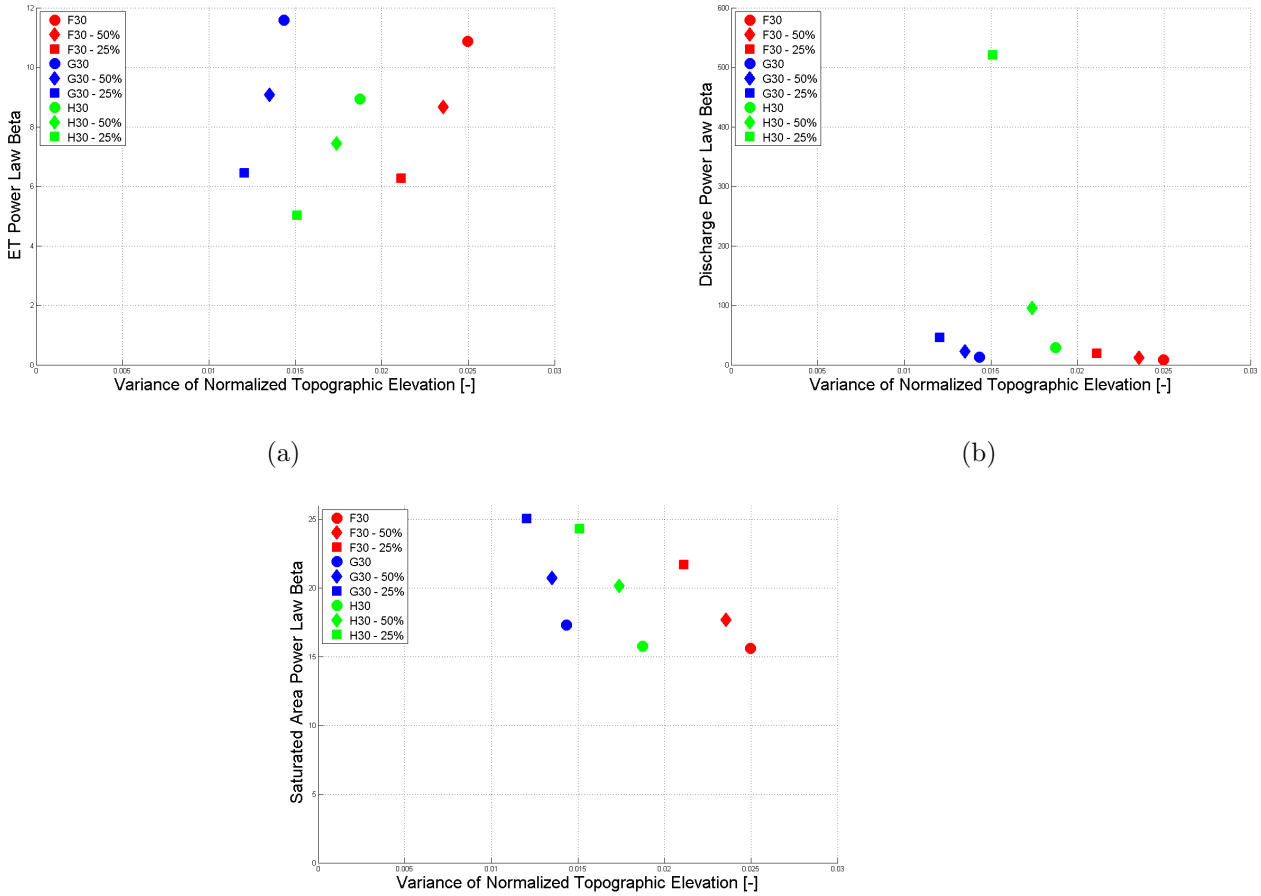

Figure 4.13: Power law β term versus normalized topographic elevation variance for (a) ET, (b) discharge and (c) saturated area for terrains F, G, and H at 100% scale, 50% scale, and 25% scale

4.2.6 Regression Analysis and General Relationships

Regression analysis of the UFR data to find generalizable equations that would describe the relationship between spatially-averaged head and exchange fluxes was conducted with power law functions and exponential functions as the equation template. Multiple terrain indices (see table 3.4) were included in the regression analyses in attempts to determine the generalizable equations.

Data from UFRs for terrains A-D were used for regression with terrains E and I-N being used for validation. Only the largest scale was used, i.e, the subgrid UFRs were not scrutinized. Though it appears from the results of section 4.2.5 that this may be problematic, a generalizable equation to describe exchange fluxes for hummocky terrains has not been determined. A sample of the test results showing the approximated head to exchange flux provided by the general equations is shown in validation plots for ET, drainage and saturated area (see figure 4.14).

While it is expected that this avenue of research may eventually yield general equations that can be used to create UFRs based on terrain indices, at the present time, those equations have not been determined with enough confidence to report them in detail. Promising preliminary steps, as can be seen in figure 4.14, indicate that the concept may be useful but at the moment a critical piece may be missing. It is suspected that additional parameters, not included in table 3.4, may need to be considered in the regression analyses to find accurate generalizable relationships.

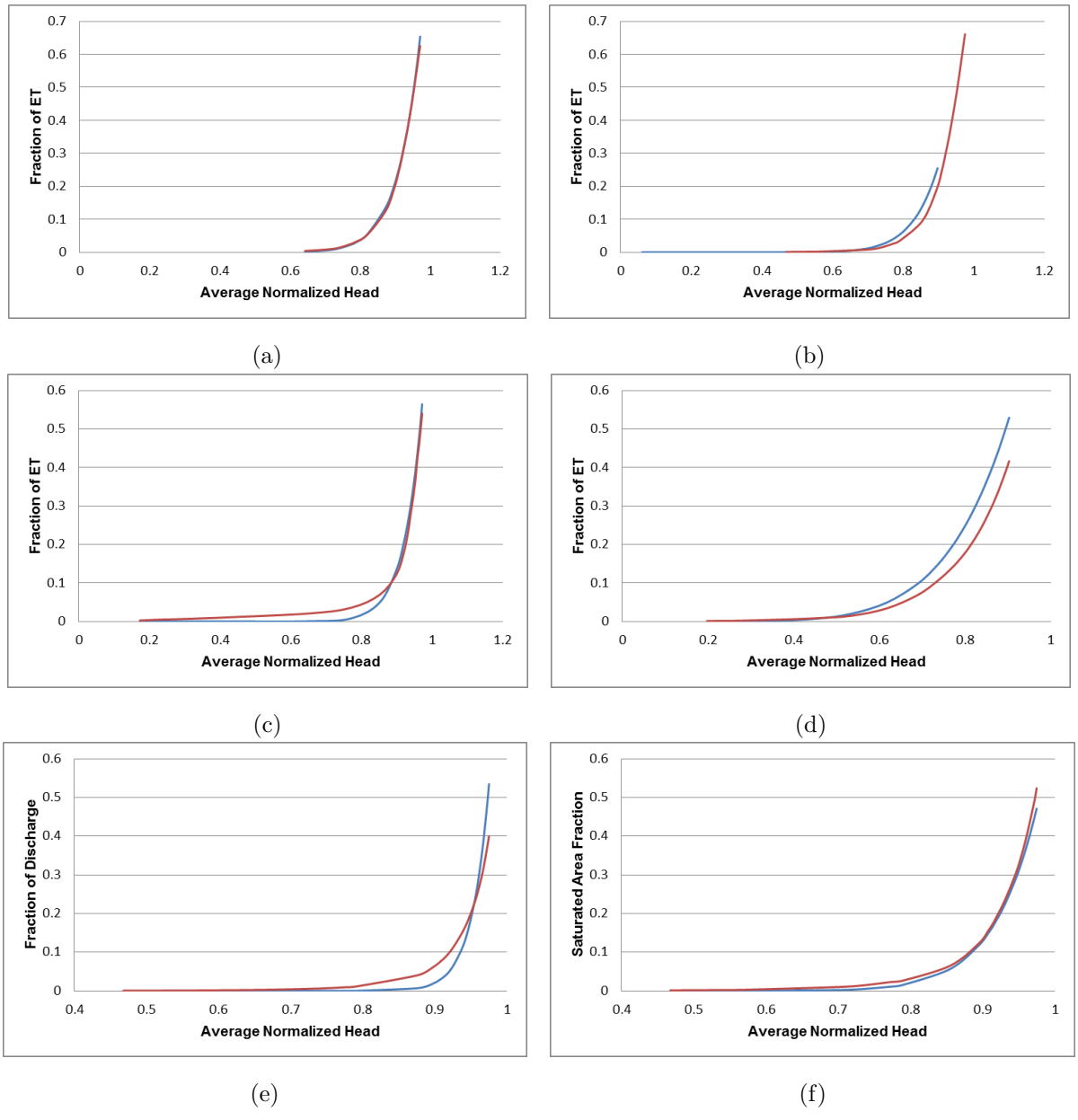

Figure 4.14: Validation plots for general equation (red line is curve extrapolated from fine-scale results, blue is equation predicted); a) E10 PET; b) I02 PET; c) M20 PET; d) N00 PET; e) E00 Discharge; f) E03 saturated area

4.3 UFRs, Physical Parameters, and Power Laws

So far it has been shown that UFRs can be generated from fine-resolution models and through regression analyses. These UFRs may be used to represent upscaled exchange fluxes between groundwater and surface water systems. To date, the UFRs generated all following a power law trend and (with the exception of the discharge UFR) pass through point (1,1) when normalized, it possible to ignore the power law α term in order to focus on the significance of the β term.

In section 3.3.1, point scale representations of ET, discharge and saturated area were discussed. By taking the point scale representations shown in figure 3.5 and adding hypothetical UFRs (power law curves) to the plot, it is possible to see how upscaled flux relationships may change with changing β terms and how they compare to their point scale representations. Figure 4.15 shows example UFRs for ET, discharge, and saturated area using a range of β values. It can be seen that for evapotranspiration, when β is close to 1, the UFR approaches the ET point scale representation and for discharge and saturated area, when β is much greater than 1, the UFR is similar to the discharge and saturated area point scale representations.

Based on the results from the previous sections on scaling (sections 4.2.5.1 and 4.2.5.2), it is possible to make certain hypotheses about when a β term may be a certain value. For example, an incised topography as shown in figure 4.16a will likely produce a UFR with a β value greater than 1 which will yield a UFR similar to the one shown in figure 4.16b. In this case, there is a gradual increase in exchange flux rate as the low topography becomes saturated followed by a sharp increase in flux rate as the higher topographic elevation saturates. In figure 4.16c, a valley topography exists where the majority of the terrain is lower than the remainder. In a situation like this, a β term between 0 and 1 is likely which will produce a UFR similar to figure 4.16d. Here, a sharp increase in flux response occurs at a low hydraulic head with a gradual flux change occurring as the remaining topography becomes saturated. This information helps narrow the possible range of the β term for a given topographic surface. Since a UFR begins when an exchange flux is greater than 0, which typically occurs when the water table has risen above the ET extinction depth or has made contact with the topographic surface, knowledge about the aquifer bottom boundary depth is not needed. It is predicted that UFRs do not need to explicitly include deeper groundwater for them to predict exchange fluxes.

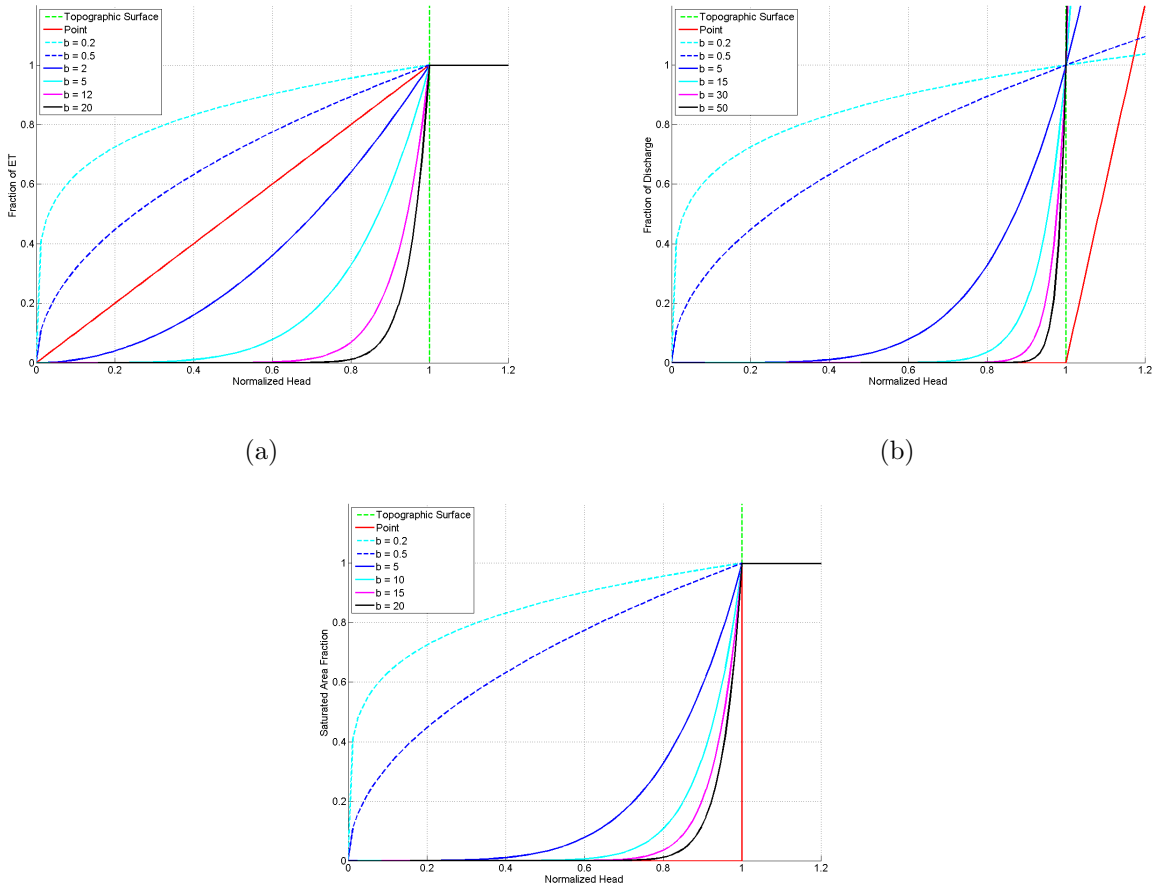

Figure 4.15: Point scale and UFR curves (with varying beta parameter) for (a) ET, (b) discharge and (c) saturated area

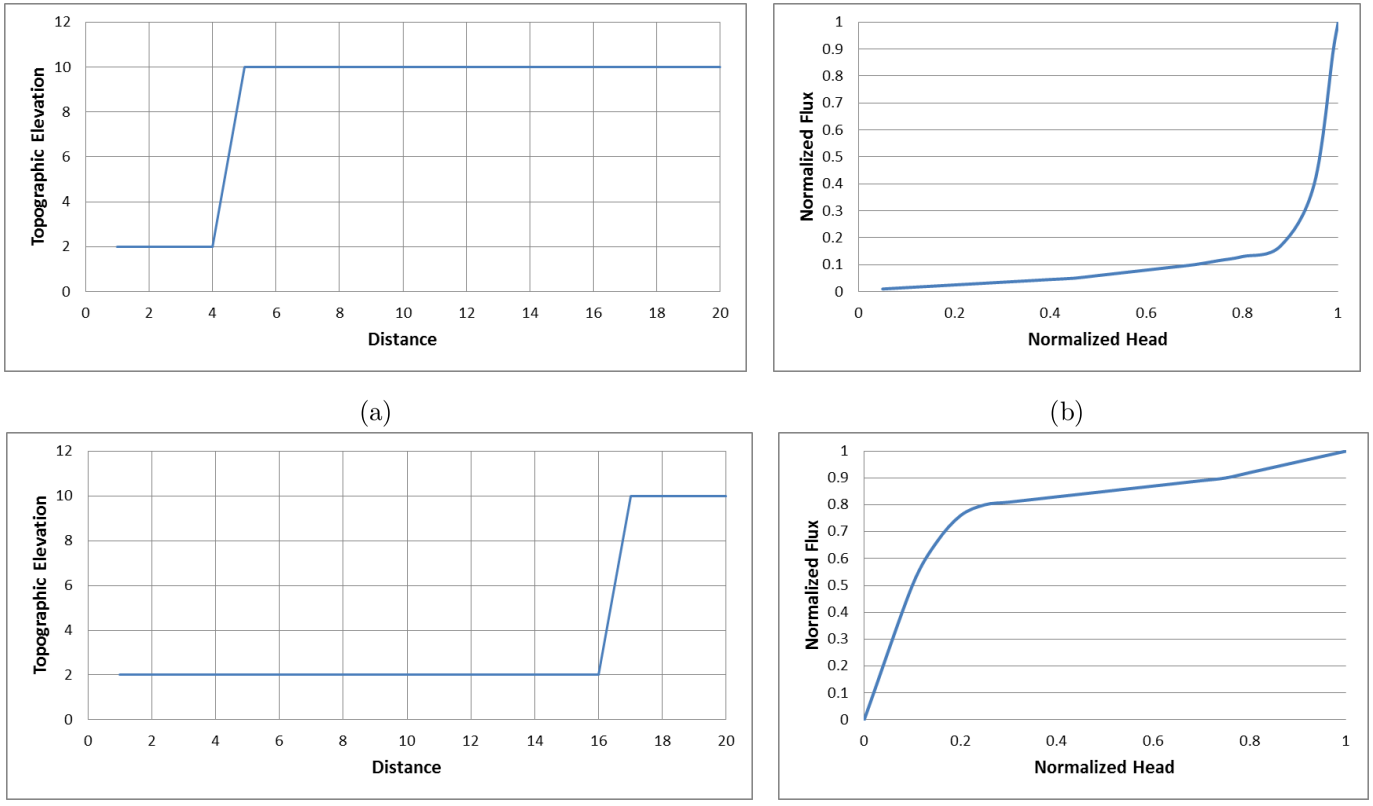

Figure 4.16: Example topographies with corresponding UFR; (a) Incised plain topography, (b) Incised plain UFR, (c) Valley topography, (d) Valley UFR

To understand the β term with respect to physical parameters, all of the simulation results, post-processing data, and regression analysis data were considered with respect to the physical parameters of the terrains. Based on the results discussed previously, it would appear that UFR shape and form is insensitive to physical parameters such as topographic indices, hydraulic conductivity and maximum potential evapotranspiration. This may be the result of the normalization method which accounts for these physical parameters. The conditions that appear to influence β term values the most are due to horizontal and vertical scale. The range of topographic elevations, specifically with respect to topographic elevation variance, controls UFR shape and form. Topographic elevation variance can indicate how planar a topographic surface is and as discussed previously, the more planar a topographic surface, the closer a UFR is to its point-scale approximation. The significance of a topography's variance on a UFR shape is not fully understood.

Some physical properties may alter the shape of UFRs and will require additional testing to discover the magnitude of their effects. These properties could include heterogeneous ET where the extinction depth for ET is correlated with topographic elevation and heterogeneous landcover such as vegetation. It is hypothesized that UFRs will maintain the power law relationships with variations in the amount ET and discharge occurring related to the variations in extinction depth and vegetation type. The tests performed in this thesis focused on ET and discharge as methods for water to leave the groundwater system in locations where the topographic surface is considered the upper boundary. In some situations, the land surface may be a body of water such as a wetland which could be considered a recharge area and not a discharge area. In this situation, a UFR may still be used to predict exchange fluxes between the groundwater and surface water systems. A modification of the UFR may be required which accounts for the wetland water surface to be treated as the normalized topographic surface. This may allow for the discharge UFR to only discharge when there is an increase to the surface water level. Many unique physical location situations are possible and UFRs may be capable of being adapted to represent each case. Further tests will need to be done to confirm the best approach for these situations.

4.4 Benchmarking - Modflow versus Raven

Results from benchmarking Raven and Modflow for groundwater flow are shown here. Figure 4.17 show the final water tables generated by Modflow and Raven following the transient simulation described in section 3.5.1. The water table plots from both simulations are overlain. The results from Modflow and Raven have an absolute mean error of 0.28m

and a relative mean error of 0.2%. Absolute error is calculated as the difference between the mean Modflow hydraulic head and mean Raven hydraulic head values. A maximum error of 0.31m was calculated for this test.

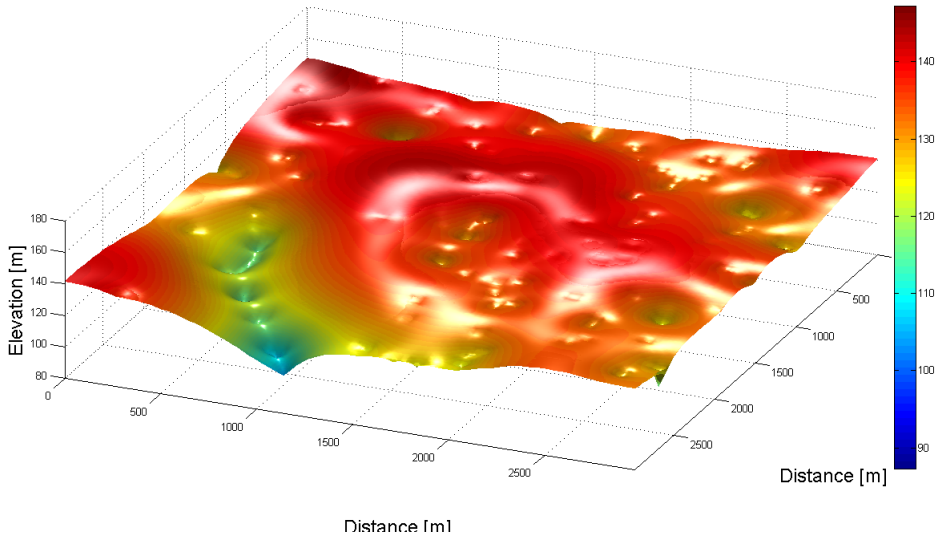

Figure 4.17: Benchmarking: Modflow and Raven transient simulation water table plot

In figure 4.18, it can be seen that Raven and Modflow generally calculate hydraulic head values that are 1:1 in comparison, however there are some values that deviate. An explanation for this may be the use of operator splitting in Raven. Flux rates such as evapotranspiration and discharge are calculated in the surface water component of the model before the groundwater component solves for lateral flow. This separation of the fluxes from the lateral solver in Raven but not in Modflow could be responsible for the discrepancy in compared results.

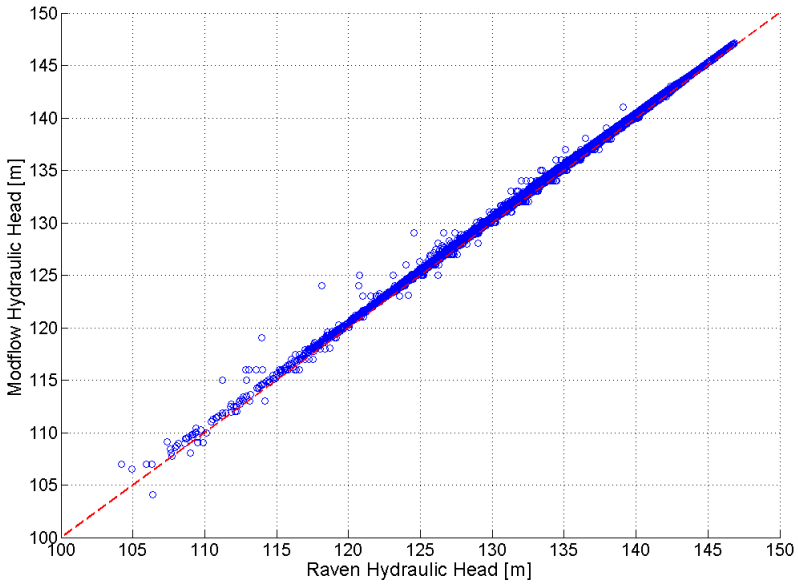

Figure 4.18: Scatter plot of heads from benchmarking for Modflow and Raven with a 1:1 trend line

4.5 Test Case 1 - Unstructured versus Structured Grid

Test case 1 was the first test of the unstructured groundwater component within Raven. Results from the coarse-scale unstructured simulation in Raven were compared to a fine-scale Modflow simulation using the same terrain and with the same parameters. The results can be seen in figure 4.19. Figure 4.19a shows the water table plot from Modflow. It follows the general topographic shape as it decreases in elevation on the east side of the plot. In figure 4.19b, the water table plot for Raven's results is shown as a disjointed surface with a single cell representing the hydraulic head for that unstructured grid. This preserves the average hydraulic head in each cell without any smoothing. Raven's water table at the coarse scale closely matches Modflow's (figure 4.19c). Raven when compared to Modflow has an absolute mean error of 0.0384 m and relative mean error of 0.027%. The error was calculated using the average hydraulic head from Modflow cells that were equivalent to the size of Raven's unstructured cells.

Figure 4.19c shows both Modflow's and Raven's water tables following the simulations. It may appear that the two are not showing similar results due to the coarse scale of the Raven groundwater cells, however the head in the coarse cells closely matches the averaged head for the coarse cell equivalent area of the Modflow simulation. Discrepancies between the fine scale and coarse scale heads is likely due to coarseness of the unstructured grid and because the exchange fluxes are calculated differently (traditional fluxes for Modflow and UFRs for Raven). Some error in the comparison may be due to the averaging of Modflow's head values as the unstructured grid used in Raven does not encompass the entirety of each fine-scale cell making area averaging less precise.

The results from the unstructured simulation show that Raven's unstructured groundwater flow methods can represent a simple system. Figure 4.20 shows the comparison of head values for the Modflow and Raven simulations. The Modflow cell heads are averaged to represent the Raven cell size in this comparison. The comparison of the head values follows the 1:1 trend line in the figure. There are some values that fall above the 1:1 trend line and some that fall below. These are likely due to errors in cells averaging. The plot shows (using whiskers) the range of the Modflow heads in all the cells contained within the upscaled Raven cell.

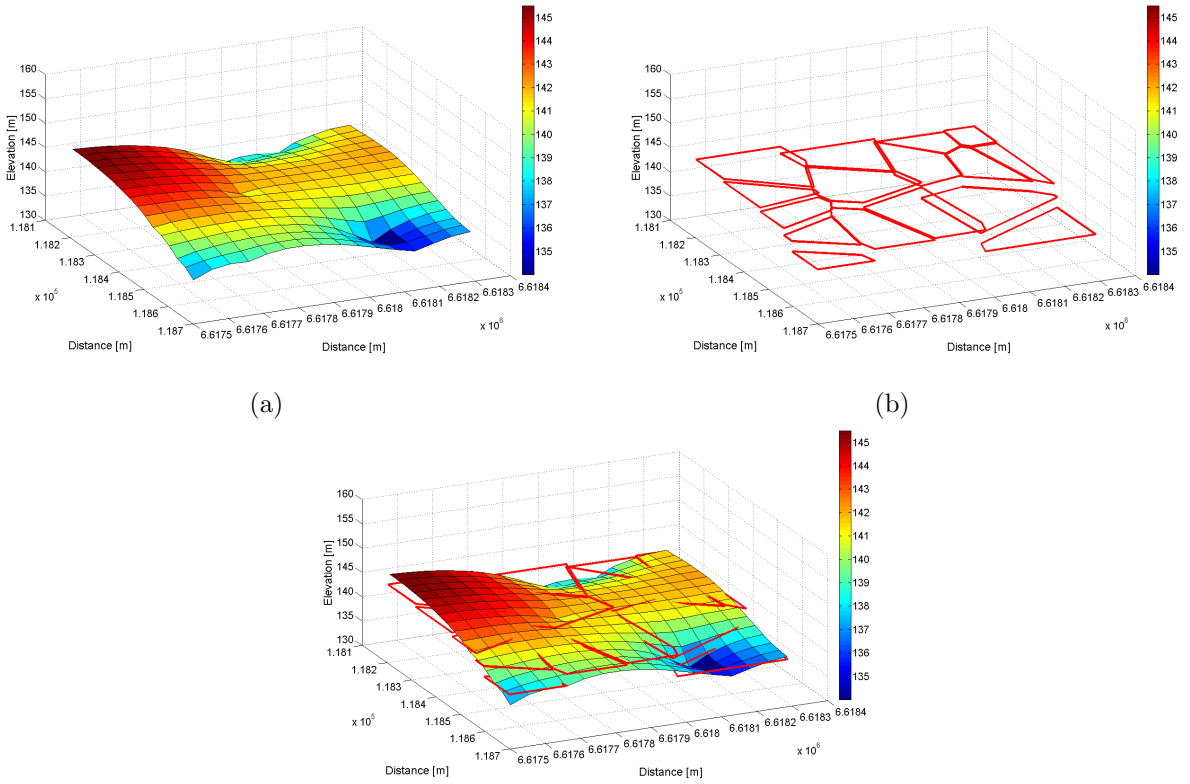

Figure 4.19: Water table plots from test case 1 showing (a) Modflow final water table, (b) Raven final water table, and (c) Modflow and Raven final water tables on same plot

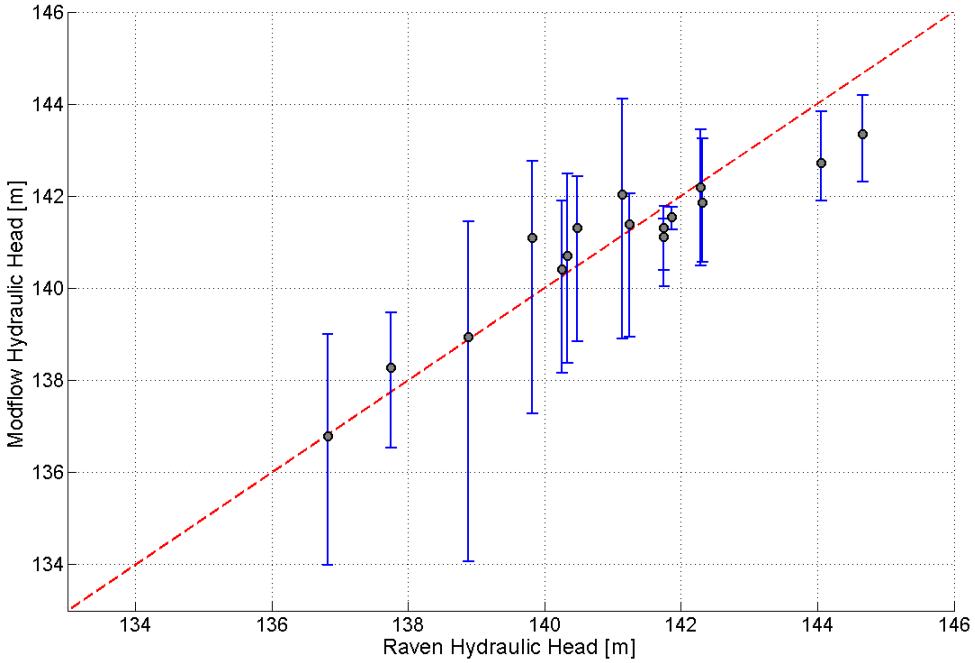

Figure 4.20: Whisker plot of heads from Modflow and Raven benchmarking with a 1:1 trend line (whiskers show max and min head values for upscaled cells from Modflow simulation

4.6 Test Case 2 - Real World Test Case

The simulation of the Grand River Watershed as a coupled surface water-groundwater unstructured basin scale model performed well. The water table produced by Raven for the unstructured groundwater system is shown in figure 4.21. This water table is the final water table of a 3 year simulation from January 1, 2004 to December 31, 2006.

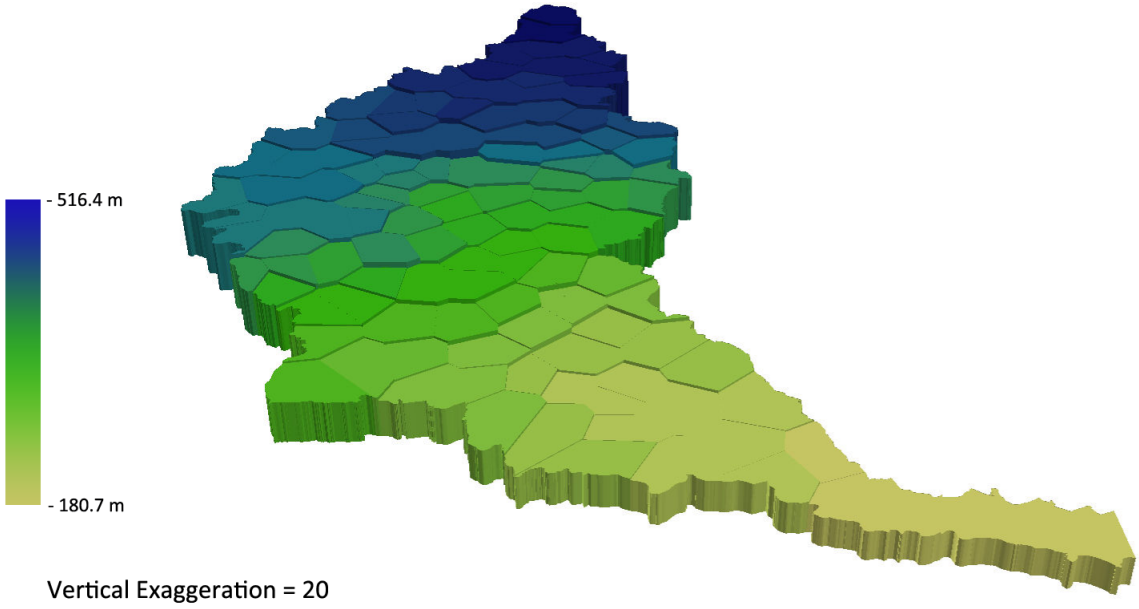

Figure 4.21: Water table for Grand River Watershed post calibration with vertical exaggeration of 20

The simulation was calibrated using 488 parameters and 13300 observations. The calibration parameters were stated in section 3.5.3. Data from 7 flow gauges and 16 groundwater monitoring wells were used as observations during calibration using PEST (Doherty, 2003) first and DDS (Tolson and Shoemaker, 2007) within Ostrich (Matott, 2015) second. Calibration was performed to both groundwater heads and hydrographs although no surface water parameters were included in the calibration. This was because the surface water model was roughly parameterized before the groundwater component was attached. Each streamflow gauge had daily flow measurements for the entire simulation length however the groundwater wells only had a year of observation data each. Well records were only complete for either 2004, 2005 or 2006 (each observation well only had

data for one of these years). Hydrograph and monitoring well observations were equally weighted for the calibration.

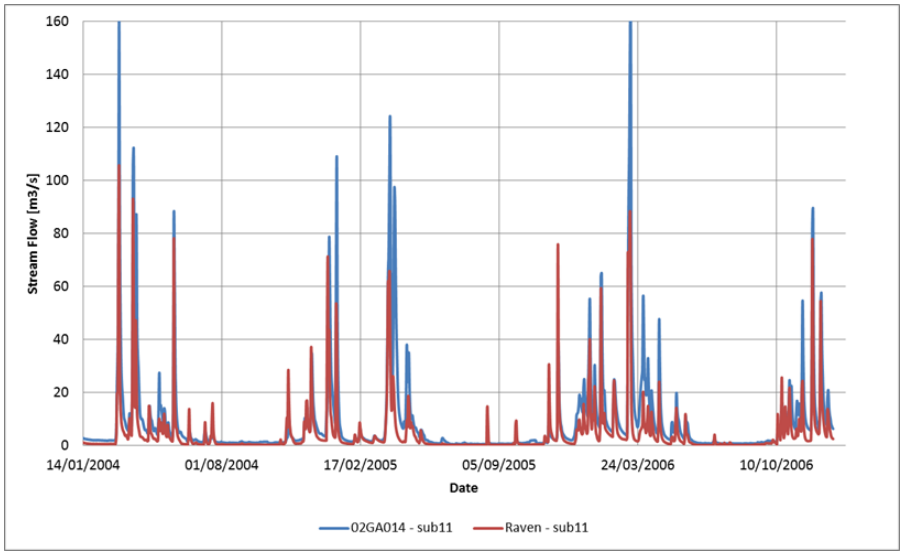

Figure 4.22: Hydrograph for subbasin 11 post calibration

Given the lack of surface water parameters used in the calibration, the results are promising. Figures 4.22 and 4.23 show hydrographs for subbasins 11 and 39, respectively. The general shape of the hydrographs match the observed data with some deviations explained by high baseflow and a failure to match the highest channel flows. Figure 4.24 shows the groundwater heads calculated by Raven compared to the observed heads for subbasins 1, 12, 53, 67, 68, 80, 92, 97, 98 and 120. This comparison shows that simulated and observed heads are close in value and general trend. It can be seen that Raven's unstructured groundwater component produces similar results to the observation data when calibrated.

Although the simulation results are not perfect, it is important to understand that this test is significant as the first real world test to use the unique upscaling methodology designed for this research. The use of UFRs in a coarse-scale coupled model with promising results suggests that UFRs may be applicable for use in other models. It is an important step forward to use coarse-scale modeling without the use of effective parameters and/or point-scale methods. With the continued exploration of UFR potential and the proper application of them in models, it may be possible to upscale without the loss of subgrid details.

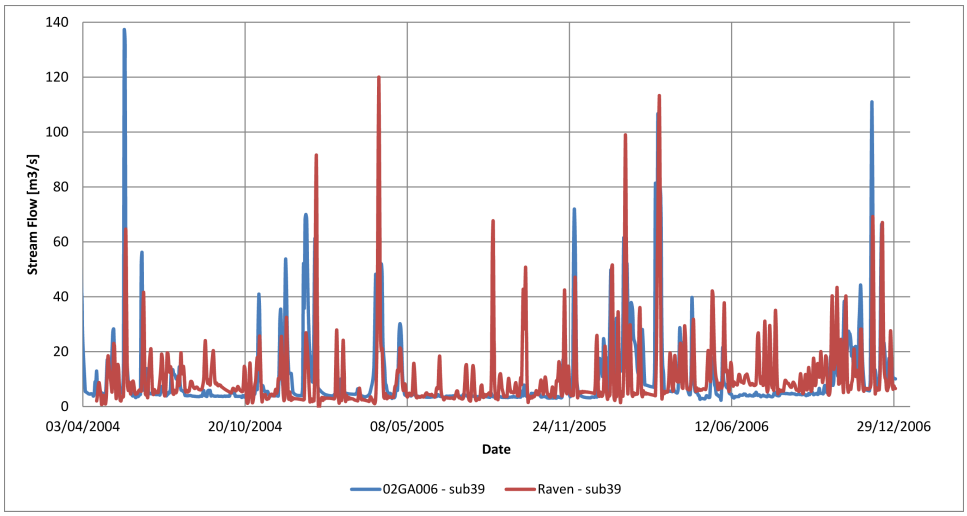

Figure 4.23: Hydrograph for subbasin 39 post calibration

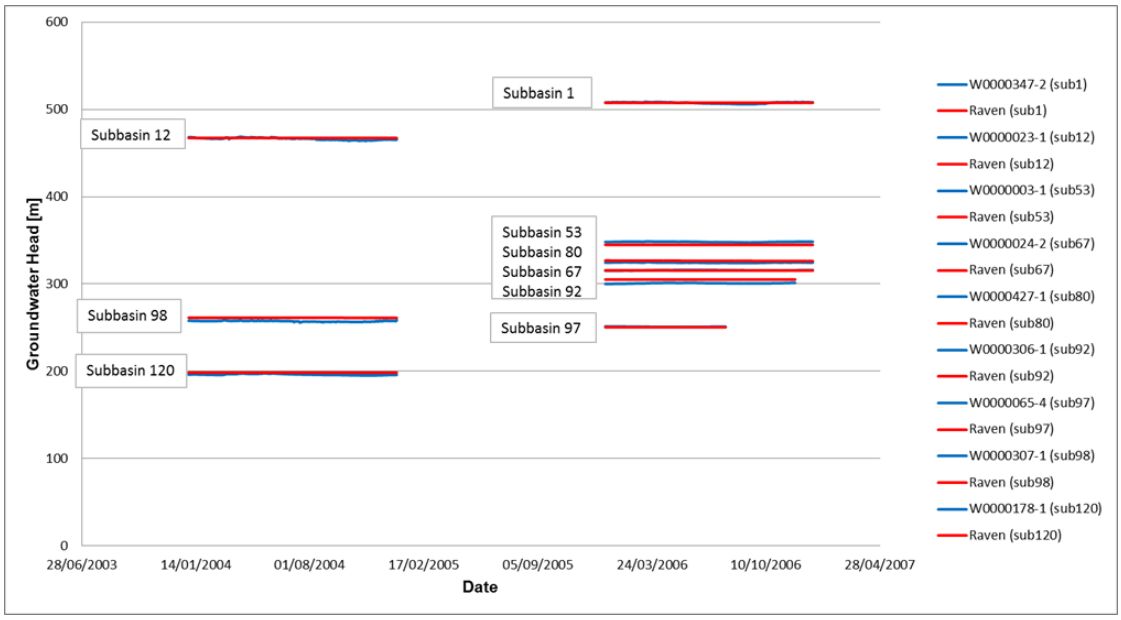

Figure 4.24: Groundwater head for subbasins 1, 12, 53, 67, 80, 92, 97, 98 and 120 post calibration

4.7 Additional Discussion

This research suggests that simply upscaling in the straightforward manner described in this thesis may make it possible to avoid or reduce many of the issues that currently exist when modelling GW-SW fluxes at regional scales. For example, the errors introduced to ET when upscaling as described by Kambhammettu et al. (2011) and Kambhammettu et al. (2013) would cease to be an issue as the UFRs would correctly produce the ET estimate without explicitly retaining the necessary subgrid elevation data to maintain accuracy. Additionally, as supported by Rihani et al. (2010), topographic slope affects ET fluxes, so the use of UFRs that incorporate slope effects would account for this terrain-specific property. Therefore, a UFR defining how average hydraulic head relates to average ET provides a straightforward approach for calculating ET without the need to use point-scale methods and the removal of dependence on point-scale methods prevents the introduction of unnecessary upscaling errors into a simulation. Based upon this, it may be beneficial to include a power law ET and/or drain module within Modflow to attend to subgrid topographic detail.

This research may be useful in several current models and studies. Recent work conducted by de Graaf et al. (2015) looked at the need to incorporate inter-watershed lateral flows to account for extra recharge during drought periods. de Graaf et al. (2015) investigated, at a global scale, the need for lateral groundwater flow to exist between separate basins. The inclusion of UFRs could help this work better represent the physical world at a regional/global scale while still explicitly modeling lateral flow with a high level of accuracy. Other work conducted by Milly et al. (2014) focused on exchange fluxes from the surface to the atmosphere. Other than the inclusion of ET in UFRs, no other UFRs have been generated that investigate other exchanges to atmospheric systems, but it should be possible to generate UFRs for a variety of processes. The LM3 model that Milly et al. (2014) built was an improvement on the LaD model which showed limitations in the way soil wetness and parameters were represented. The use of UFRs could further this research by permitting LM3 to represent the spatial heterogeneity of the soil while still calculating accurate exchange flux rates between the surface and atmospheric systems at coarse-scales. Condon and Maxwell (2015) recently looked at the importance of topography in groundwater flow. They investigated how topographic shape impacts flow systems across scales from local to regional. Since the study model was discretized using 1km cells, it would be beneficial to use UFRs to represent the exchange fluxes for these simulations.

These studies are just a few of the recent ones looking at the effect of topography and groundwater flow at large scales. Through this dissertation, it has been shown that UFRs are an effective upscaling method that functions well for multiple exchange flux processes

and that they can work using regular and unstructured grid systems. This makes UFRs a good choice to be included in the aforementioned studies. All of the previously mentioned studies used regular grids and are either conducted at a small spatial scale or use models like ParFlow to operate on upscaled cells (i.e., 1km resolution (Condon and Maxwell, 2015)). As discussed previously, this may not be the most ideal approach for conducting regional to global scale studies so the use of UFRs would be warranted to better approximate exchange flux rates and subsequently groundwater head.

Chapter 5

Conclusion

Fine scale Modflow models were here used to investigate the relationship between bulk aquifer storage and GW-SW exchange fluxes, specifically surface discharge (baseflow and seepage flow) and evapotranspiration, under both steady and transient conditions, and saturated and unsaturated conditions. The steady UFRs generated from this study indicate that relations between spatially averaged head and averaged exchange fluxes follow consistent, specific, and relatively simple trends; when properly normalized, these trends are independent of PET and hydraulic conductivity for homogeneous systems and mild heterogeneous systems. The power law relationships suggest that these UFRs may be a useful approximate representation of GW-SW storage-flux relationships for coarsely discretized models and that this representation is a better approximation than that of employing effective parameters. It is likely that generalizable relationships for specific terrain types can be extracted from the UFRs and that these could be used to better simulate regional scale GW-SW exchanges without significant loss of the influence of fine-scale detail that is commonly associated with coarse resolution models.

Through several studies investigating how UFRs are affected by saturation, transient conditions, heterogeneity, scale and terrain indices, a framework has been established that will allow for more predictability in the use of UFRs. This framework, as previously stated, indicates that UFRs yield similar results regardless of saturation, transient simulation and the occurrence of mild heterogeneity. However, it can been said that both horizontal and vertical scale/topographic variability affect the shape and form of a UFR. It has been shown that the magnitude of the β term of the power law relationship which defines a UFRs shape may be predicted with some understanding of the topographic elevation ranges in a basin or subbasin. This theory is undergoing further testing to determine at what level of certainty the β term may be predicted. The impact of additional terrain indices (e.g.,

normalized topographic mean, wetness index) on UFR shape and form are less clear due to the large number of potential parameters. While basic generalizable equations were able to be determined that could generate UFRs, those equations were not sophisticated enough to work for all terrains and cases. It is expected that these relationships can be determined for multiple terrain types which in turn will reduce the necessity of fine-scale models for specific terrains/locations. This is an important step forward to make UFRs more widely applicable.

UFRs have now been implemented in an unstructured groundwater model and in a unstructured coupled model. The use of UFRs in those transient groundwater models has shown that UFRs are capable of representing basic groundwater-surface water exchange fluxes. This application has many advantages for modelling; it may be possible to upscale to a coarse resolution model without the loss of subgrid details; the use of empirical relationships at coarse scales is more physically realistic; and when UFRs are used at coarse scales, the time of simulation is greatly reduced which makes calibration and uncertainty analyses possible even if it is only done to parameterize a fine-scale model.

5.1 Future Work

Ideally, UFRs will be terrain type specific but relatively scale independent so that regardless of a simulations resolution, a model can be setup to accommodate the discretization. This study also looked at the relationship between topography-controlled saturated surface area and averaged heads which may later aid in the understanding of upscaling effective recharge rates and/or direct runoff. UFRs may be directly incorporated into coarse low-resolution models as a surrogate for detailed simulation.

The next step in this research is to use these relationships to develop UFRs for specific terrain types (Reed et al., 2006; Sidle, 2006; Tetzlaff et al., 2008). An important step of this work would be the correlating of power law coefficient magnitudes to terrain characteristics so as to be able to generate UFRs for any terrain without having to perform fine scale simulations or having to include them in the calibration process.

APPENDICES

Appendix A

Appendix A: Raven Groundwater Input Files

A.1 Groundwater Discretization File

The groundwater system in Raven is discretized using the *.rvd file. Its features are described through the number of nodes, connections and information about the vertical discretization. Topographic information including the elevation of the surface, the top and bottom of each layer and the minimum topographic elevation in an upscaled cell. Each cell is described with the width of each face, its surface area and the area of the interface between cells. Additional details about the length between centroid of cells and the connected neighbouring cells is also included in this file.

Example Discretization File: model.rvd

```
* ------------------------------------------
* Raven GW Discretization file
* For groundwater grid discretization classes
* GW Demo Model
* Author: APS
* ------------------------------------------
* -----General Information--------------------
:Overview
*  ID,   #nodes, #layers, #horiz connections, #vert discretization, matrix format
   Unstr1,   16,       1,                 60,                    -1,             0
:EndOverview
* -----------Geometry -----------------------
```

```
:Basement
*  confined or unconfined(0=confined, 1=unconfined) [1 value per layer]
   0
:EndBasement
:Layers
* # of nodes/layer
  16
:EndLayers
:TopElevations
* Attributes, elevation
  :Units, m
  1 149.25
  2 152.4
  3 147.91
  4 142.88
  5 147
  6 141.47
  7 141.28
  8 145.08
  9 145.53
  10 146.82
  11 143.76
  12 151.21
  13 154.11
  14 152.4
  15 143.56
  16 139.83
:EndTopElevations
:BottomElevations
* Attributes, elevation
  :Units, m
  1 0
  2 0
  3 0
  4 0
  5 0
  6 0
  7 0
  8 0
  9 0
  10 0
  11 0
  12 0
  13 0
  14 0
```

```
  15 0
  16 0
:EndBottomElevations
:TopographicMinimum
* Attributes, elevation
  :Units, m
  1 148
  2 149
  3 142
  4 138
  5 142
  6 134
  7 134
  8 139
  9 138
  10 141
  11 138
  12 148
  13 149
  14 141
  15 140
  16 136
:EndTopographicMinimum
:CellArea
* Attributes, area
  :Units, m2
  1 8082.147
  2 11714.438
  3 19009.958
  4 12535.136
  5 29243.979
  6 29378.312
  7 44792.028
  8 41341.285
  9 30583.499
  10 38007.542
  11 28994.405
  12 39532.005
  13 15422.448
  14 15071.391
  15 14933.111
  16 10711.128
:EndCellArea
:NumberConnections
* Attributes, # of connections/node + 1
```

```
  1 4
  2 4
  3 6
  4 4
  5 6
  6 3
  7 6
  8 5
  9 4
  10 8
  11 6
  12 4
  13 4
  14 5
  15 4
  16 3
:EndNumberConnections
:Connections
* Attributes, Cell number, connecting cell #'s
  1,2,3,4
  2,1,3,7
  3,1,2,4,5,7
  4,1,3,5
  5,3,4,7,9,10
  6,7,8
  7,2,3,5,6,8
  8,6,7,10,11
  9,5,10,12
  10,5,8,9,11,12,13,14
  11,8,10,14,15,16
  12,9,10,13
  13,10,12,14
  14,10,11,13,15
  15,11,14,16
  16,11,15
:EndConnections
:VerticalConnections
* Attributes, Cell number, flag for horizontal or vertical connection
  1,0,0,0
  2,0,0,0
  3,0,0,0,0,0
  4,0,0,0
  5,0,0,0,0,0
  6,0,0
  7,0,0,0,0,0
```

```
  8,0,0,0,0
  9,0,0,0
  10,0,0,0,0,0,0,0,0
  11,0,0,0,0,0
  12,0,0,0
  13,0,0,0
  14,0,0,0,0
  15,0,0,0
  16,0,0
:EndVerticalConnections
:CL12
  1,46,70,64
  2,46,39,171
  3,70,39,64,64,99
  4,64,64,56
  5,64,56,107,94,133
  6,77,171
  7,171,99,107,77,121
  8,171,121,80,68
  9,94,80,137
  10,133,80,80,112,113,135,136
  11,68,112,121,71,103
  12,137,113,67
  13,135,67,37
  14,136,121,37,47
  15,71,47,47
  16,103,47
:EndCL12
:FaceWidth
* Attributes, area
  :Units, m
  1, 237.7296588, 80.52193902, 276.6657335
  2, 237.7296588, 690.4198499, 176.5996602
  3, 80.52193902, 690.4198499, 240.4115342, 408.5034014, 586.8134202
  4, 276.6657335, 240.4115342, 547.8571429
  5, 408.5034014, 547.8571429, 475.4034541, 632.618704, 250.2043318
  6, 1127.689694, 147.1257237,
  7, 176.5996602, 586.8134202, 475.4034541, 1127.689694, 727.6330301
  8, 147.1257237, 727.6330301, 708.0779185, 718.5934891
  9, 632.618704, 726.1953412, 278.0570068
  10, 250.2043318, 708.0779185, 726.1953412, 269.5812465, 492.3285497, 60.24917267, 114.9278215
  11, 718.5934891, 269.5812465, 145.1115486, 536.8138757, 144.997497
  12, 278.0570068, 492.3285497, 684.1866199
  13, 60.24917267, 684.1866199, 610.5643045
  14, 114.9278215, 145.1115486, 610.5643045, 622.6316523
```

```
  15, 536.8138757, 622.6316523, 576.1639133
  16, 144.997497, 576.1639133
:EndFaceWidth
:InterfaceArea
* Attributes, area
  :Units, m2
  1,36230,11910,39530
  2,36230,102120,24950
  3,11910,102120,34350,60050,82905
  4,39530,34350,80535
  5,60050,80535,67165,92065,36735
  6,159320,21345
  7,24950,82905,67165,159320,105565
  8,21345,105565,103960,103305
  9,92065,106620,42045
  10,36735,103960,106620,38755,74445,9285,17515
  11,103305,38755,22115,77065,20275
  12,42045,74445,105440
  13,9285,105440,93050
  14,17515,22115,93050,89385
  15,77065,89385,80565
  16,20275,80565
:EndInterfaceArea
:End
```

A.2 Groundwater Stress Period Properties File

The Stress Period Properities file includes details on evaportranspiration, drains, recharge, hydraulic conductivity and storage for each cell. These can be customized to vary for each cell and for specific time periods.

Example Stress Period Properties File: model.rvg

```
* ------------------------------------------
* Raven GW Stress Period Properties File
* For groundwater classes
* GW Demo Model
* Author: APS
* ------------------------------------------
* -----Process Properties---------------------
:GWSPProperties GW_P
  :StressPeriod 1
    :ETProperties
      :NumberRecords 16
      :Parameters, ID, ET_CELL, PET_MAX, EXTINCTION_DEPTH,
      :Units,      ??,      ??,    mm/d,                m,
      1 1 5 3
      2 2 5 3
      3 3 5 3
      4 4 5 3
      5 5 5 3
      6 6 5 3
      7 7 5 3
      8 8 5 3
      9 9 5 3
      10 10 5 3
      11 11 5   3
      12 12 5 3
      13 13 5 3
      14 14 5 3
      15 15 5 3
      16 16 5 3
    :EndETProperties
    :DrainProperties
      :NumberRecords 16
      :Parameters, ID, D_CELL, DRAIN_ELEVATION, CONDUCTANCE,
      :Units,      ??,     ??,               m,        m2/d,
      1 1 149.25 33000
      2 2 152.4 33000
      3 3 147.91 33000
```

```
    4 4 142.88 33000
    5 5 147.0 33000
    6 6 141.47 33000
    7 7 141.28 33000
    8 8 145.08 33000
    9 9 145.53 33000
    10 10 146.82 33000
    11 11 143.76 33000
    12 12 151.21 33000
    13 13 154.11 33000
    14 14 152.4 33000
    15 15 143.56 33000
    16 16 139.83 33000
  :EndDrainProperties
  :Recharge
    :NumberRecords 16
    :Parameters,  R_CELL, RECHARGE,
    :Units,         ??,     mm/d,
    1 1 10
    2 2 10
    3 3 10
    4 4 10
    5 5 10
    6 6 10
    7 7 10
    8 8 10
    9 9 10
    10 10 10
    11 11 10
    12 12 10
    13 13 10
    14 14 10
    15 15 10
    16 16 10
  :EndRecharge
  :HydraulicConductivity
:NumberRecords 16
:Isotropic
:Parameters, K_Cell, CONDUCTIVITY_X, CONDUCTIVITY_Y, CONDUCTIVITY_Z,
:Units,          ??,        m/d,         m/d,        m/d,
1 1 .364000000
2 2 .364000000
3 3 .364000000
4 4 .364000000
5 5 .364000000
```

```
  6 6 .364000000
  7 7 .364000000
  8 8 .364000000
  9 9 .364000000
  10 10 .364000000
  11 11 .364000000
  12 12 .364000000
  13 13 .364000000
  14 14 .364000000
  15 15 .364000000
  16 16 .364000000
:EndHydraulicConductivity
:Storage
  :NumberRecords 16
  :Parameters, SS_Cell, SS,
  :Units,           ??, 1/m,
      1 1  1.8100000E-01
      2 2  1.8100000E-01
      3 3  1.8100000E-01
      4 4  1.8100000E-01
      5 5  1.8100000E-01
      6 6  1.8100000E-01
      7 7  1.8100000E-01
      8 8  1.8100000E-01
      9 9  1.8100000E-01
      10 10  1.8100000E-01
      11 11  1.8100000E-01
      12 12  1.8100000E-01
      13 13  1.8100000E-01
      14 14  1.8100000E-01
      15 15  1.8100000E-01
      16 16  1.8100000E-01
:EndStorage
  :EndStressPeriod
:EndGWSPProperties
```

A.3 Groundwater Exchange Flux File

The Exchange Flux file details the implementation of UFRs for each cell. By specifying the coefficient and exponent for a UFR type, UFRs can be used in Raven to represent exchange fluxes at coarse scales.

Example Exchange Flux File: model.rve

```
* ------------------------------------------
* Raven GW exchange flux file
* For groundwater to surface water exchange classes
* GW Demo Model
* Author: APS
* ------------------------------------------
* -----Exchange Relationships--------
:RelationshipCount 3
:Cell 1
:Evapotranspiration
:Relationship_Type PowerLaw
.99990000, 15.070000
:EndEvapotranspiration
:Drain
:Relationship_Type PowerLaw
.9999000, 31.49000
:EndDrain
:SaturatedArea
:Relationship_Type PowerLaw
0.9999, 21.93
:EndSaturatedArea
:EndCell
:Cell 2
:Evapotranspiration
:Relationship_Type PowerLaw
.99990000, 15.070000
:EndEvapotranspiration
:Drain
:Relationship_Type PowerLaw
.9999000, 31.49000
:EndDrain
:SaturatedArea
:Relationship_Type PowerLaw
0.9999, 21.93
:EndSaturatedArea
:EndCell
:Cell 3
```

```
:Evapotranspiration
:Relationship_Type PowerLaw
.99990000, 15.070000
:EndEvapotranspiration
:Drain
:Relationship_Type PowerLaw
.9999000, 31.49000
:EndDrain
:SaturatedArea
:Relationship_Type PowerLaw
0.9999, 21.93
:EndSaturatedArea
:EndCell
```

A.4 Groundwater Overlap File

The Overlap file (or Vertical Exchange Flux file) tells Raven how surface water and groundwater cells relate spatially. Therefore when exchange fluxes occur, the correct amount calculated by the operator splitting within the surface water model is directed to the appropriate groundwater cell.

Example Overlap File: model.rvv

```
* ------------------------------------------
* Raven GW vertical exchange flux input file
* For groundwater to surface water exchange classes
* GW Demo Model
* Author: APS
* ------------------------------------------
* -----Grid to HRU Overlap Information--------
:HRUs 16
:GWCells 16
:OverlapArea
:Parameters, HRU #, % of HRU area covered by cell in order.......
1,1,0,0,0,0,0,0,0,0,0,0,0,0,0,0
2,0,1,0,0,0,0,0,0,0,0,0,0,0,0,0
3,0,0.139509,0.812593,0,0.047898,0,0,0,0,0,0,0,0,0,0
4,0.231382,0,0.014435,0.63454,0.115127,0,0,0,0.004516,0,0,0,0,0,0,0
5,0,0,0.095739,0.145865,0.727703,0,0,0,0.028733,0.001959,0,0,0,0,0,0
6,0,0,0,0,0,0,0.967349,0,0.032651,0,0,0,0,0,0,0
7,0,0.057662,0.085663,0,0.075097,0.157239,0.4526,0.171739,0,0,0,0,0,0,0,0
8,0,0,0,0,0,0,0,0,0.976916,0,0,0.023084,0,0,0,0
9,0,0,0,0,0,0.013806,0,0,0,0.861024,0.121569,0,0.0036,0,0,0,0
10,0,0,0,0,0,0.036172,0,0,0,0.064572,0.064594,0.75138,0.003579,0.041795,0.008594,0.029187,0,0
11,0,0,0,0,0,0,0,0,0.138867,0,0.02311,0.645653,0,0,0.06363,0.065332,0.063408
12,0,0,0,0,0,0,0,0,0,0.004296,0,0,0.81044,0.17998,0.005284,0,0
13,0,0,0,0,0,0,0,0,0,0,0,0,0,0.99961,0.00039,0,0
14,0,0,0,0,0,0,0,0,0,0,0,0,0,0.058283,0.912781,0.028936,0
15,0,0,0,0,0,0,0,0,0,0,0,0,0.03862,0,0,0.123078,0.746005,0.092297
16,0,0,0,0,0,0,0,0,0,0,0,0,0,0,0,0.000636,0.999364
:EndOverlapArea
```

Appendix B

Appendix B: Additional Figures

B.1 Additional Figures

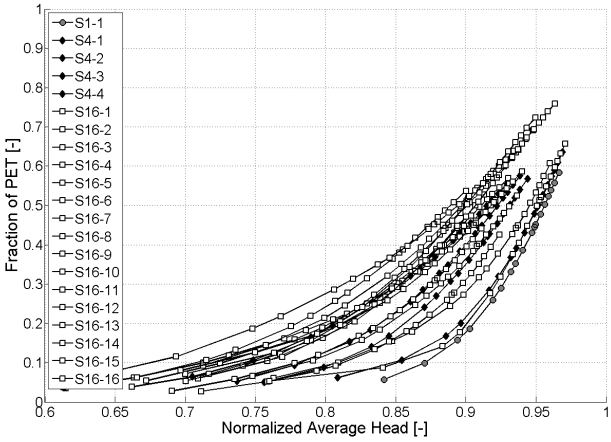

(a)

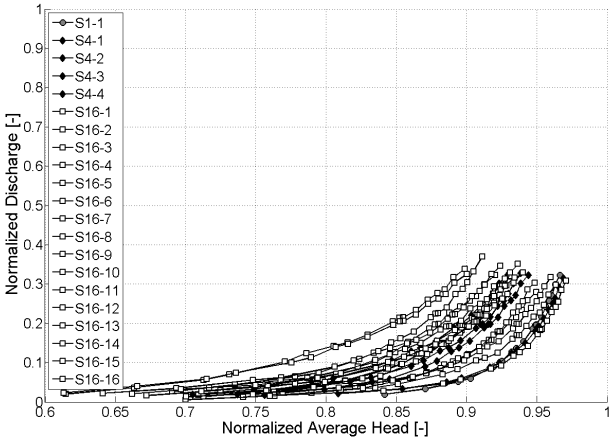

(b)

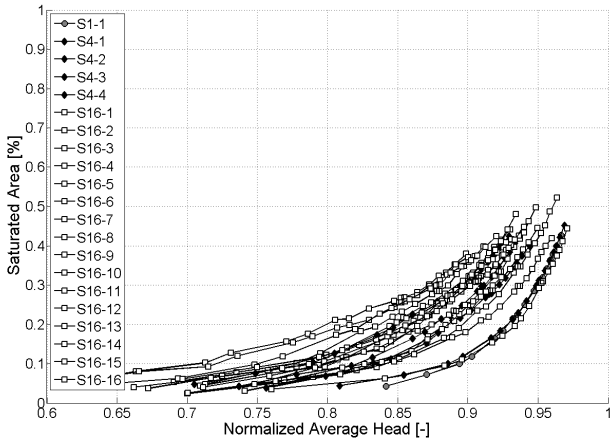

(c)

Figure B.1: UFRs for (a) ET, (b) discharge and (c) saturated area for 16 cells, 4 cells and 1 cell

References

Anderson, M., W. Woessner, and R. Hunt (2015). *Applied Groundwater Modeling: Simulation of Flow and Advective Transport*. San Diego, CA: Academic Press.

Barthel, R. (2014). A call for more fundamental science in regional hydrgeology. *Hydrgeology Journal 22*, 507–510.

Beckers, J. and E. Frind (2000). Calibration of the oro moraine multi-aquifer system: role of geology and objective function. *IAHS 265*, 164–170.

Bensoussan, A., J.-L. Lions, and G. Papanicolau (1978). *Asymptotic Analysis for Periodic Structures*. New York, NY: Elsevier.

Beven, K. (1984). Infiltration into a class of veritcally non-uniform soils. *Journal of Hydrological Science 29*, 425–434.

Beven, K. (1995). Linking parameters across scales: Subgrid parameterizations and scale dependent hydrological models. *Hydrological Processes 9*, 507–525.

Beven, K. (2013). Macropores and water flow in soils revisited. *Water Resources Research 49*, 3071–3092.

Beven, K. and M. Kirkby (1979). A physically-based, variable contributing area model of basin hydrology. *Hydrological Science Bulletin 24*(1), 43–69.

Blöschl, G. and M. Sivapalan (1995). Scale issues in hydrological modelling: A review. *Hydrological Processes 9*, 251–290.

Botte, G., J. Ritter, and R. White (2000). Comparison of finite difference and control volume methods for solving differential equations. *Computers and Chemical Engineering 24*, 2633–2654.

Bradford, R. and M. Acreman (2003). Applying modflow to wet grassland in-field habitats: a case study from pevensey levels, uk. *Hydrology and Earth System Sciences Discussions 7*, 43–55.

Bradley, C. (2002). Simulation of the annual water table dynamics of a floodplain wetland, narborough bog, uk. *Journal of Hydrology 261*, 150–172.

Brunner, P. and C. Simmons (2012). Hydrogeosphere: A fully integrated, physically based hydrological model. *Ground Water 50*(2), 170–176.

Burnash, R., R. Ferral, and R. McGuire (1973). A generalized streamflow simulation system: Conceptual modeling for digital computers. Technical report, US National Weather Service, Sacramento, California.

Camporese, M., C. Paniconi, M. Putti, and S. Orlandini (2010). Surface-subsurface flow modeling with path-based runoff routing, boundary condition-based coupling,and assimilation of multisource observation data. *Water Resources Research 46*, W02512.

Cardenas, M. (2008). Surface water-groundwater interface geomorphology leads to scaling of residence times. *Geophysical Research Letters 35*, L08402.

Chen, J., L. Durlofsky, M. Gerritsen, and X. Wen (2003). A coupled local-global upscaling approach for simulating in highly heterogeneous formations. *Advances in Water Resources 26*, 1041–1060.

Clark, M., A. Slater, D. Rupp, R. Woods, J. Vrugt, H. Gupta, T. Wagerner, and L. Hay (2008). Framework for understanding structural errors (fuse): A modular framework to diagnose differences between hydrological models. *Water Resources Research 44*, W00B02.

Clarke, R. (1973). A review of some mathematical models used in hydrology, with observations on their calibration and use. *Journal of Hydrology 19*, 1–20.

Condon, L. and R. Maxwell (2015). Evaluating the relationship between topography and groundwater using outputs from a continental scale integrated hydrology model. *Water Resources Research 51*, 6602–6621.

Craig, J. and the Raven Developement Team (2013). Raven users and developement manual v0.9, draft technical report. *Department of Civil & Environmental Engineering, University of Waterloo 0.9*, 1–115.

Crawford, N. and R. Linsley (1966). *Digital simulation in hydrology: Stanford watershed model IV*. Ph. D. thesis, Stanford University, Stanford, CA.

Dagan, G. (1989). *Flow and Transport in Porous Media*. New York: Springer-Verlag.

de Graaf, I., E. Sutanudjaja, L. van Beek, and M. Bierkens (2015). A high-resolution global-scale groundwater model. *Hydrology and Earth System Science 19*, 823–837.

del Pilar Alvarez, M., M. Trovatto, M. Harnández, and N. González (2012). Groundwater flow model, recharge estimation and sustainability in an arid region of patagonia, argentina. *Environmental Earth Science 66*, 2097–2108.

Desbarats, A. (1992). Spatial averaging of hydraulic conductivity in three-dimensional heterogeneous porous media. *Mathematical Geology 24*, 249–267.

Dickinson, R., A. Henderson-Sellers, and P. Kennedy (1993). Biosphere-atmosphere transfer scheme (bats) version 1e as coupled to the ncar community climate model. *NCAR Technical Note NCAR/TN-387+STR 1*, 1–40.

Diersch, H. (2005). *FEFLOW finite element subsurface flow and transport simulation system - Reference Manual*. Berlin, Germany: WASY Gmbh.

Doherty, J. (2003). Groundwater model calibration using pilot points and regularisation. *Groundwater 41*(2), 170–177.

Dooge, J. (1982). *Physical Hydrology* (2 ed.). London: Prentice-Hall Incorporated.

Dooge, J. (1986). Looking for hydrologic laws. *Water Resources Research 22*, 44S–58S.

Dupuit, J. (1863). *Études Théoriques et Practiques sur le Mouvement des Eaux dans les Canaux Decouverts et à Travers les Terrains Perméables* (2nd edition ed.). Paris, France: Dunod.

Durlofsky, L. (1992). Numerical calculation of equivalent grid block permeability tendors for heterogeneous porous media. *Water Resources Research 27*, 699–708.

Dutta, D. and K. Nakayama (2009). Effects of spatial grid resolution on river flow and surface inundation simulation by physically based distributed modelling approach. *Hydrological Processes 23*, 534–545.

Fan, Y., G. Miguez-Macho, C. Weaver, R. Walko, and A. Robock (2007). Incorporating water table dynamics in climate modeling: 1. water table observations and equilibrium water table simulations. *Journal of Geophysical Research 112*, D10125.

Farago, I. (2008). Additive and iterative operator splitting methods and their numerical investigation. *Journal of Computers and Mathematics with Applications 55*(10), 2266–2279.

Forchheimer, P. (1886). Über die ergiebigkeit von brunnen-anlagen und sickerschlitzen. *Zeitschrift des Architectenund Ingenieurs Vereins zu Hannover 32*, 539–564.

Freeze, R. (1972). Role of subsurface flow in generating surface runoff: 1. base flow contribution to channel flow. *Water Resources Research 8*, 609–623.

Freeze, R. and R. Harlan (1969). Blueprint for a physically-based, digitally-simulated hydrologic response model. *Journal of Hydrology 9*, 237–258.

Frei, S., G. Lischeid, and J. Fleckenstein (2010). Effects of micro-topography on surface-subsurface exchange and runoff generation in a virtual riparian wetland - a modeling study. *Advances in Water Resources 33*, 1388–1401.

Furman, A. (2008). Modeling coupled surface-subsurface flow processes: A review. *Vadose Zone Journal 7*, 741–756.

Gelhar, L. (1986). Stochastic subsurface hydrology from theory to applications. *Water Resources Research 22*, 135S–145S.

Gleeson, T. and A. Manning (2008). Regional groundwater flow in mountainous terrain: Three-dimensional simulations of topographic and hydrogeologic controls. *Water Resources Research 44*, W10403.

Gleeson, T., L. Marklund, L. Smith, and A. Manning (2011). Classifying the water table at regional to continental scales. *Geophysical Research Letters 38*, L05401.

Gunston, H. and C. Batchelor (1983). A comparison of the priestley-taylor and penman methods for estimating reference crop evapotranspiration in tropical countries. *Agricultural Water Management 6*(1), 65–77.

Günter, A., J. Seibert, and S. Uhlenbrook (2004). Modeling spatial patterns of saturated areas: An evaluation of different terrain indices. *Water Resources Research 40*(5), 1–19.

Gupta, V., L. Bastidas, S. Sorooshian, W. Shuttleworth, and Z. Yang (1999). Parameter estimation of a land surface scheme using multicriteria methods. *Journal of Geophysical Research 104*(D16), 19491–19503.

Haitjema, H. and S. Mitchell-Bruker (2005). Are water tables a subdued replica of the topography. *Ground Water 43*(6), 781–786.

Harbaugh, A. (2005). Modflow-2005: The us geological survey modular groundwater model - the ground-water flow process. Technical Report US Geological Survey Open-File Report 6-A16, US Geological Survey.

Harman, C., M. Sivapalan, and P. Kumar (2009). Power law catchment-scale recessions arising from heterogeneous linear small-scale dynamics. *Water Resources Research 45*, W09404.

Hoffman, J. (2001). *Numerical Methods for Engineers and Scientists* (2 ed.). New York, NY: CRC Press.

Howes, D. and E. Kenk (1997). Terrain classification system for british columbia (version 2), a system for the classification of surficial materials, landforms and geological processes of british columbia. Technical Report MOE Manual 10, Ministry of Environment/ Ministry of Crown Lands.

Iorgulescu, I. and A. Musy (1997). Generalization of topmodel for a power law transmissivity profile. *Hydrological Processes 11*, 1353–1355.

Jana, R. and B. Mohanty (2012a). On topographic controls of soil hydraulic parameter scaling at hillslope scales. *Water Resources Research 48*, W02518.

Jana, R. and B. Mohanty (2012b). A topography-based scaling algorithm for soil hydraulic parameters at hillslope scales: Field testing. *Water Resources Research 48*, W02519.

Jencso, K. and B. McGlynn (2011). Hierarchial controls on runoff generation: Topographically driven hydrologic connectivity, geology, and vegetation. *Water Resources Research 47*, W11527.

Jones, J., E. Sudicky, A. Brookfield, and Y.-J. Park (2006). An assessment of the tracer-based approach to quantifying groundwater contributions to streamflow. *Water Resources Research 42*, W02407.

Jyrkama, M. and J. Sykes (2006). *The Impact of Climate Change on Groundwater*, Chapter 28, pp. 1320. CRC Press.

Jyrkama, M., J. Sykes, and S. Normani (2002). Recharge estimation for transient groundwater modeling. *Groundwater 40*(6), 638–648.

Kambhammettu, B., J. King, and W. Schmid (2013). Grid-size dependency of evapotranspiration simulations in shallow aquifers: An optimal approach. *Journal of Hydrologic Engineering 19*(10), 1–26.

Kambhammettu, B., W. Schmid, J. King, and B. Creel (2011). Effects of elevation resolution on evapotranspiration simulations using modflow. *Groundwater 50*(3), 367–375.

Kampf, S. and S. Burges (2007). A framework for classifying and comparing distributed hillslope and catchment hydrologic models. *Water Resources Research 43*, W05423.

Kavvas, M. (1999). On the coarse-graining of hydrologic processes with increasing scales. *Journal of Hydrology 217*, 191–202.

Kavvas, M., Z.-Q. Chen, L. Tan, S.-T. Soong, A. Terakawa, J. Yoshitani, and K. Fukani (1998). A regional-scale land surface parameterization based an areally-averaged hydrological conservation equations. *Hydrological Sciences Journal 43*(4), 611–631.

Kavvas, M., S. Kure, Z.-Q. Chen, N. Ohara, and S. Jang (2013). Wehy-hcm for modelling interactive atmospheric-hydrologic processes at watershed scale. i: Model description. *Journal of Hydrologic Engineering 18*(10), 1262–1271.

Kollet, S. and R. Maxwell (2006). Integrated surface-groundwater flow modeling: A free-surface overland flow boundary condition in a parallel groundwater flow model. *Advances in Water Resources 29*, 945–958.

Kollet, S. and R. Maxwell (2008). Capturing the influence of groundwater dynamics on land surface processes using an integrated, distributed watershed model. *Water Resources Research 44*, W02402.

Koren, V., F. Moreda, S. Reed, M. Smith, and Z. Zhang (2006). Evaluation of a grid-based distibuted hydrological model over a large area. In *Predictions in Ungauged Basins: Promise and Progress (Proceedings of symposium S7)*. IAHS Publication 303.

Kure, S., S. Jang, N. Ohara, M. Kavvas, and Z.-Q. Chen (2013). Wehy-hcm for modelling interactive atmospheric-hydrologic processes at watershed scale. ii: Model application to ungauged and sparsely gauged watersheds. *Journal of Hydrologic Engineering 18*(10), 1272–1281.

Lamb, R., K. Beven, and S. Myrabø(1997). Discharge and water table predictions using a generalised topmodel formulation. *Hydrological Processes 11*(9), 1145–1167.

Li, H., W. Kinzelbach, P. Brunner, W. Li, and X. Dong (2008). Topography representation methods for improving evaporation simulation in groundwater modelling. *Journal of Hydrology 356*, 199–208.

Liang, X., Z. Xie, and M. Huang (2003). A new parameterization for surface and groundwater interactions and its impact on water budgets with the variable infiltration capacity (vic) land surface model. *Journal of Geophysical Research 108*(D16), 8613.

Loague, K., C. Heppner, B. Mirus, B. Ebel, Q. Ran, A. Carr, S. BeVille, and J. VanderKwaak (2006). Physics-based hydrologic-response simulation: foundation for hydroecology and hydrogeomorphology. *Hydrological Processes 20*, 1231–1237.

LP DAAC (2012, January). Aster global digital elevation model v002. https://lpdaac.usgs.gov.

Luo, Y., S. Peng, S. Khan, Y. Cui, Y. Wang, and Y. Feng (2009). A comparative study of groundwater evapotranspiration functions. In *Proceedings of the 18th World IMACS and MODSIM09 Congress on Modeling and Simulation*, Cairns, Australia, pp. 3095–3101.

Marklund, L. and A. Wörman (2011). The use of spectral analysis-based exact solutions to characterize topography-controlled groundwater flow. *Hydrogeology Journal 19*, 1531–1543.

Matheron, G. (2011). *Elements pout une Theorie des Milieux Poreux*. Paris: Masson.

Matott, L. (2015). Ostrich - an optimization software toolkit for research involving computational heuristics; documentation and users guide, version 16.02.10. `http://www.groundwater.buffalo.edu`.

Maxwell, R. and S. Kollet (2008). Interdependence of groundwater dynamics and land-energy feedbacks under climate change. *Nature Science 1*, 665–669.

McGuire, K., J. McDonnell, M. Weiler, C. Kendall, B. McGlynn, J. Welker, and J. Seibert (2005). The role of topography on catchment-scale water residence time. *Water Resources Research 41*, W05002.

Milly, P., S. Malyshev, E. Shevliakova, K. Dunne, K. Findell, T. Gleeson, Z. Liang, P. Phillipps, R. Stouffer, and S. Swenson (2014). An enhanced model of land water and energy for global hydrologic and earth-system studies. *Journal of Hydrometeorology 15*, 1739–1760.

Mohanty, B. and Z. Mousli (2000). Saturated hydraulic conductivity and soil water retention properties across a soil-slope transition. *Water Resources Research 36*(11), 3311–3324.

Montgomery, D., E. Peck, and G. Vining (2012). *Introduction to Linear Regression Analysis*. Danvers, MA: John Wiley and Sons.

Morita, M. and B. Yen (2000). Numerical methods for conjunctive two-dimensional surface and three-dimensional sub-surface flows. *International Journal of Numerical Methods in Fluids 32*, 921–957.

Neuman, S. (1990). Universal upscaling of hydraulic conductivities and dispersivities in geologic media. *Water Resources Research 26*, 1749–1758.

Osman, Y. and M. Bruen (2002). Modelling stream-aquifer seepage in an alluvial aquifer: an improved loosing-stream package for modflow. *Journal of Hydrology 264*, 69–86.

Panday, S. and P. Huyakorn (2004). A fully coupled physically-based spatially-distributed model for evaluating surface/subsurface flow. *Advances in Water Research 27*, 361–382.

Panday, S., C. Langevin, R. Niswonger, M. Ibaraki, and J. Hughes (2013). Modflow-usg version 1: An unstructured grid version of modflow for simulating groundwater flow and tightly coupled processes using a control volume finite-difference formulation. Technical Report Book 6, chapter A45, US Geological Survey Techniques and Methods.

PGMN (2015, August). Provincial groundwater monitoring network. https://www.ontario.ca/data/provincial-groundwater-monitoring-network.

Press, W., S. Teukolsky, W. Vetterling, and B. Flannery (1992). *Numerical Recipes in C: The Art of Scientific Computing* (2nd ed.). Cambridge: Cambridge University Press.

Racz, A., A. Fisher, C. Schmidt, B. Lockwood, and M. Los Huertos (2012). Spatial and temporal infiltration dynamics during managed aquifer recharge. *Ground Water 50*(4), 1–9.

Reed, P., R. Brooks, K. Davis, D. DeWalle, K. Dressler, C. Duffy, H. Lin, D. Miller, R. Najjar, K. Salvage, T. Wagener, and B. Yarnal (2006). Bridging river basin scales and processes to assess human climate impacts and the terrestrial hydrological system. *Water Resources Research 42*, W07418.

Rigon, R., G. Bertoldi, and T. Over (2005). Geotop: A distributed hydrological model with coupled water and energy budgets. *Journal of Hydrometeorology 7*, 371–388.

Rihani, J., R. Maxwell, and F. Chow (2010). Coupling groundwater and land surface processes: Idealized simulations to identify effects of terrain and subsurface heterogeneity on land surface energy fluxes. *Water Resources Research 46*, W12523.

Rupp, D. and J. Selker (2005). Drainage of a horizontal boussinesq aquifer with a power law hydraulic conductivity profile. *Water Resources Research 41*, W11422.

Rushton, K. (2007). Representation in regional models of saturated river-aquifer interaction for gaining/losing rivers. *Journal of Hydrology 334*, 262–281.

Rushton, K. and L. Tomlinson (1979). Possible mechanisms for leakage between aquifers and rivers. *Journal of Hydrology 40*, 49–65.

Saleh, F., N. Flipo, F. Habets, A. Ducharne, L. Oudin, P. Viennot, and E. Ledoux (2011). Modeling the impact of in-stream water level fluctuation on stream-aquifer interactions at the regional scale. *Journal of Hydrology 400*, 490–500.

Salvucci, G. and D. Entekhabi (1995). Hillslope and climatic controls on hydrologic fluxes. *Water Resources Research 31*(7), 1725–1739.

Sanford, W. (2002). Recharge and groundwater models: an overview. *Hydrogeology Journal 10*, 110–120.

Selker, J., J. Duan, and J.-Y. Parlange (1999). Green and ampt infiltration into soils of variable pore size with depth. *Water Resources Research 35*(5), 1685–1688.

Sellers, P., Y. Mintz, Y. Sud, and A. Dalcher (1986). A simple biosphere model (sib) for use within general circulation models. *Journal of Atmospheric Sciences 43*, 505–531.

Shafii, M. (2015). Grand river suface water model setup using raven, university of waterloo. Personal Communication.

Shah, S., M. Nachabe, and M. Ross (2007). Extinction depth and evapotranspiration from groundwater under selected land covers. *Ground Water 45*(3), 329–338.

Sidle, R. (2006). Field observations and process understanding in hydrology: essential components in scaling. *Hydrological Processes 20*, 1439–1445.

Simms, R. (2013). The effects of soil heterogeneity on the performance of horizontal ground loop heat exchangers. Masc thesis, University of Waterloo.

Singh, V. and D. Woolhiser (2002). Mathematical modeling of watershed hydrology. *Journal of Hydrologic Engineering 7*(4), 270–292.

Sivapalan, M. (2005). Pattern, process and function: Elements of a unified theory of hydrology at the catchment scale. In *Encyclopedia of Hydrological Science*. Wiley.

Snowdon, A. (2009). Improved numerical methods for distributed hydrological models. Masc thesis, University of Waterloo.

Snowdon, A. and J. Craig (2015). Effective groundwater-surface water exchange at watershed scales. *Hydrological Processes*.

Sophocleous, M. (2002). Interactions between groundwater and surface water: the state of science. *Hydrogeology Journal 10*, 52–67.

Soulsby, C., C. Neal, H. Laudon, D. Burns, P. Merot, M. Bonell, S. Dunn, and D. Tetzlaff (2008). Catchment data for process conceptualization: simply not enough? *Hydrological Processes 22*, 2057–2061.

Strack, O. (1984). Three-dimensional streamlines in dupuit-forchheimer models. *Water Resources Research 20*(7), 812–822.

Sulis, M., S. Meyerhoff, C. Paniconi, R. Maxwell, M. Putti, and S. Kollet (2010). A comparison of two physics-based numerical models for simulating surface water-groundwater interactions. *Advances in Water Resources 33*(4), 456–467.

Swain, E. (1992). Incorporating hydraulic structures in an open-channel model. In *Proceedings, 1992 National Hydraulic Engineering Conference, American Society of Civil Engineers*, New York, NY, pp. 1118–1123.

Swain, E. and E. Wexler (1996). A coupled surface-water and groundwater flow model (modbranch) for simulation of stream-aquifer interaction. Technical Report Modeling Techniques, Book 6, Chapter A6, US Geological Survey, Denver, Colorado.

Tetzlaff, D., S. Carey, H. Laudon, and K. McGuire (2010). Catchment process and heterogeneity at multiple scales - benchmarking observations, conceptualization and prediction. *Hydrological Processes 24*, 2203–2208.

Tetzlaff, D., J. McDonnell, S. Uhlenbrook, K. McGuire, P. Bogaart, F. Naef, A. Baird, S. Dunn, and C. Soulsby (2008). Conceptualizing catchment processes: simply too complex? *Hydrological Processes 22*, 1727–1730.

Tetzlaff, D., C. Soulsby, S. Waldron, I. Malcolm, R. Bacon, S. Dunn, A. Lilly, and A. Youngson (2007). Conceptualization of runoff processes using a geographical information system and tracers in a nested mesoscale catchment. *Hydrological Processes 21*, 1289–1307.

Therrien, R., R. Mclaren, E. Sudicky, and S. Panday (2006). *Hydrogeosphere*. Waterloo, Canada: Groundwater Simulations Group, University of Waterloo.

Tolson, B. and C. Shoemaker (2007). Dynamically dimensioned search algorithm for computationally efficient watershed model calibration. *Water Resources Research 43*, W01413.

Troch, P., G. Carrillo, I. Heidbüchel, S. Rajagopal, M. Switanek, T. Volkmann, and M. Yaeger (2008). Dealing with landscape heterogenity in watershed hydrology: A review of recent progress toward new hydrological theory. *Geography Compass 3*, 375–392.

Van der Vorst, H. (1992). Bi-cgstab: A fast and smoothly converging variant of bi-cg for the solution of nonsymmetric linear systems. *SIAM Journal of Science and Statistical Computing 13*(2), 631–644.

Van Genuchten, M. (1980). A closed-form equation for predicting the hydraulic conductivity of unsaturated soils. *Soil Science Society of America 44*, 892–898.

Van Nieuwenhuyse, B., M. Antoine, G. Wyseure, and G. Govers (2011). Pattern-process relationships in surface hydrology: hydrological connectivity expressed in landscape metrics. *Hydrological Processes 25*, 3760–3773.

VanderKwaak, J. and E. Sudicky (1999). Application of a physically-based numerical model of surface and subsurface water flow and solute transport. In *ModelCARE99, International Conference on Calibration and Reliability in Groundwater Modelling*, Volume 2, Zurich.

Vermeulen, P., C. Stroet, and A. Heemink (2006). Limitations to upscaling of groundwater flow models dominated by surface water interaction. *Water Resources Research 42*, W10406.

Wallender, W. and M. Grismer (2002). Irrigation hydrology: Crossing scales. *Journal of Irrigation and Drainage Engineering 128*(4), 203–211.

Walton, W. (1970). *Groundwater Resources Evaluation*. New York, N.Y.: McGraw-Hill.

Wang, S., J. Shao, X. Song, Y. Zhang, Z. Huo, and X. Zhou (2008). Application of modflow and geographic information system to groundwater flow simulation in north china plain, china. *Environmental Geology 55*, 1449–1462.

Warren, J. and H. Price (1961). Flow in heterogeneous porous media. *Society of Petroleum Engineering Journal 1*, 153–169.

Wen, X.-H. and J. Gómez-Hernaández (1996). Upscaling hydraulic conductivities in heterogeneous media: An overview. *Journal of Hydrology 183*, ix–xxxii.

Wheatcraft, S. and S. Tyler (1988). An explanation of scale-dependent dispersivity in heterogeneous aquifers using concepts of fractal geometry. *Water Resources Research 24*, 566–578.

Wiener, O. (1912). Die theorie des mischkorpers fur das feld der statona-ren stromung i. die mittelwertsatze fur kraft, polarisation und energie. *Abh. Math. Phys. Kl. Koenigl. Saech. Ges. Wiss. 32*, 509–604.

Winter, T. (2001). Ground water and surface water: the linkage tightens, but challenges remain. *Hydrological Processes 15*, 3605–3606.

Wood, E. (1995). Scaling bahaviour of hydrological fluxes and variables: Empirical studies using a hydrological model and remote sensing data. *Hydrological Processes 9*, 331–346.

Wood, E., D. Lettenmaier, and V. Zartarian (1992). A land-surface hydrology parameterization with subgrid variability for general circulation models. *Journal of Geophysical Research 97*(D3), 2717–2728.

Yang, X. and X. You (2013). Estimating parameters of van genuchten model for soil water retention curve by intelligent algorithms. *Applied Mathematics and Information Sciences 7*, 1977–1983.

Zhao, R. (1977). Flood forecasting method for humid regions of china. Technical report, East China College of Hydraulic Engineering, Nanjing, China.